Nearshore Macroalgae Cultivation for Carbon Sequestration by Biomass Harvesting: Evaluating Potential and Impacts with An Earth System Model

Jiajun Wu[1], Wanxuan Yao[2], David Peter Keller[3], and Andreas Oschlies[3]

[1]GEOMAR Helmholtz Centre for Ocean Research Kiel
[2]GEOMAR Helmholtz Centre for Ocean Research
[3]Helmholtz-Zentrum für Ozeanforschung Kiel, GEOMAR

March 04, 2024

Abstract

This study introduces an ocean-based carbon dioxide removal (CDR) approach: Nearshore Macroalgae Aquaculture for Carbon Sequestration (N-MACS). By cultivating macroalgae in nearshore ocean surface areas, N-MACS aims to sequester CO2 with subsequent carbon storage. Utilizing an Earth System Model with intermediate complexity (EMIC), we explore the CDR potential of N-MACS alongside its impacts on the global carbon cycle, marine biogeochemistry and marine ecosystems. Our investigations unveil that coastal N-MACS could potentially sequester 0.7 to 1.1 GtC yr-1. However, it also significantly suppresses marine phytoplankton net primary productivity because of nutrient removal and canopy shading, counteracting approximately 30% of the N-MACS CDR capacity. This suppression of surface NPP, in turn, reduces carbon export out of the euphotic zone to the ocean interior, leading to elevated dissolved oxygen levels and diminished denitrification in present-day oxygen minimum zones. Effects due to harvesting-induced phosphorus removal continue for centuries even beyond the cessation of N-MACS.

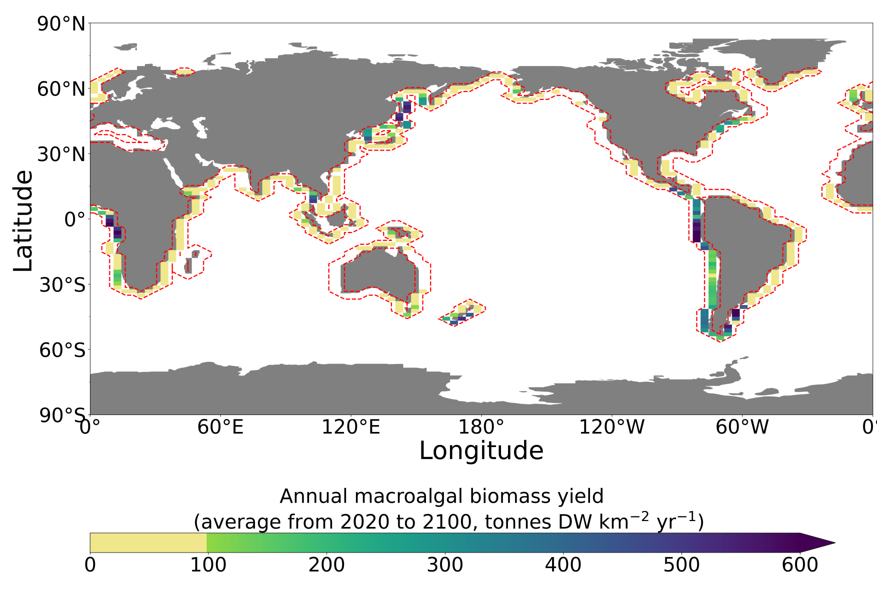

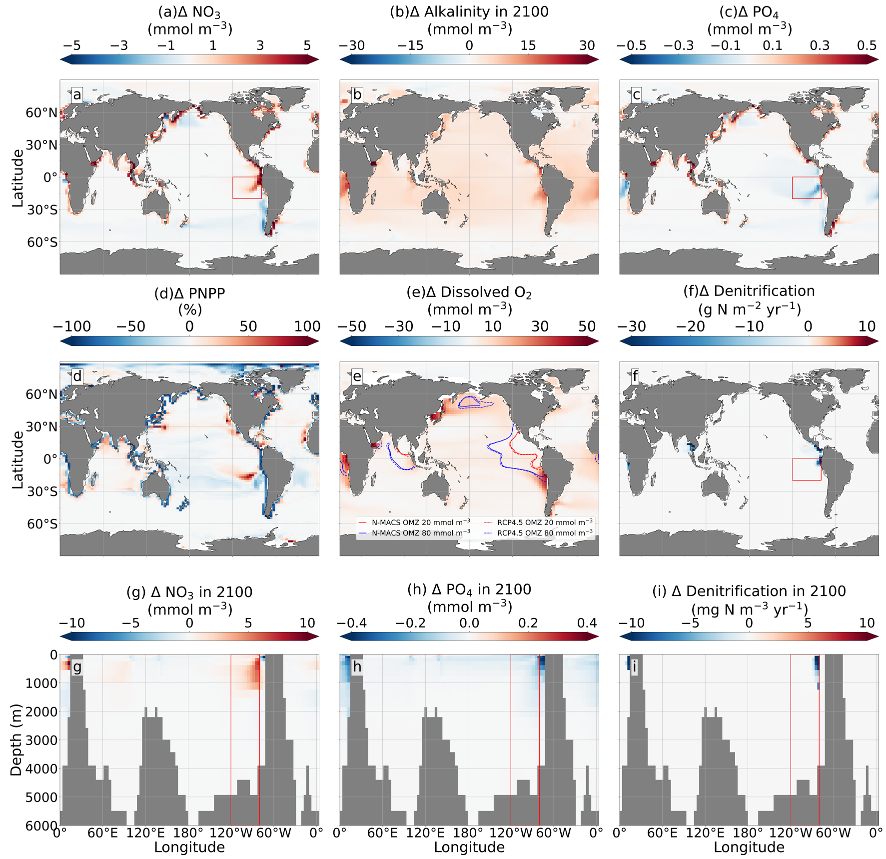
(a)Δ NO3
(mmol m−3)
−5 −3 −1 1 3 5
(b)Δ Alkalinity in 2100
(mmol m−3)
−30 −15 0 15 30
(c)Δ PO4
(mmol m−3)
−0.5 −0.3 −0.1 0.1 0.3 0.5
a
b
c
60°N
30°N
0°
30°S
60°S
Latitude
(d)Δ PNPP
(%)
−100 −50 0 50 100
(e)Δ Dissolved O2
(mmol m−3)
−50 −30 −10 10 30 50
(f)Δ Denitrification
(g N m−2 yr−1)
−30 −20 −10 0 10
d
e
f
N-MACS OMZ 20 mmol m−3
N-MACS OMZ 80 mmol m−3
RCP4.5 OMZ 20 mmol m−3
RCP4.5 OMZ 80 mmol m−3
(g) Δ NO3 in 2100
(mmol m−3)
−10 −5 0 5 10
(h) Δ PO4 in 2100
(mmol m−3)
−0.4 −0.2 0.0 0.2 0.4
(i) Δ Denitrification in 2100
(mg N m−3 yr−1)
−10 −5 0 5 10
g
h
i
Depth (m)
0
1000
2000
3000
4000
5000
6000
0° 60°E 120°E 180° 120°W 60°W 0°
Longitude

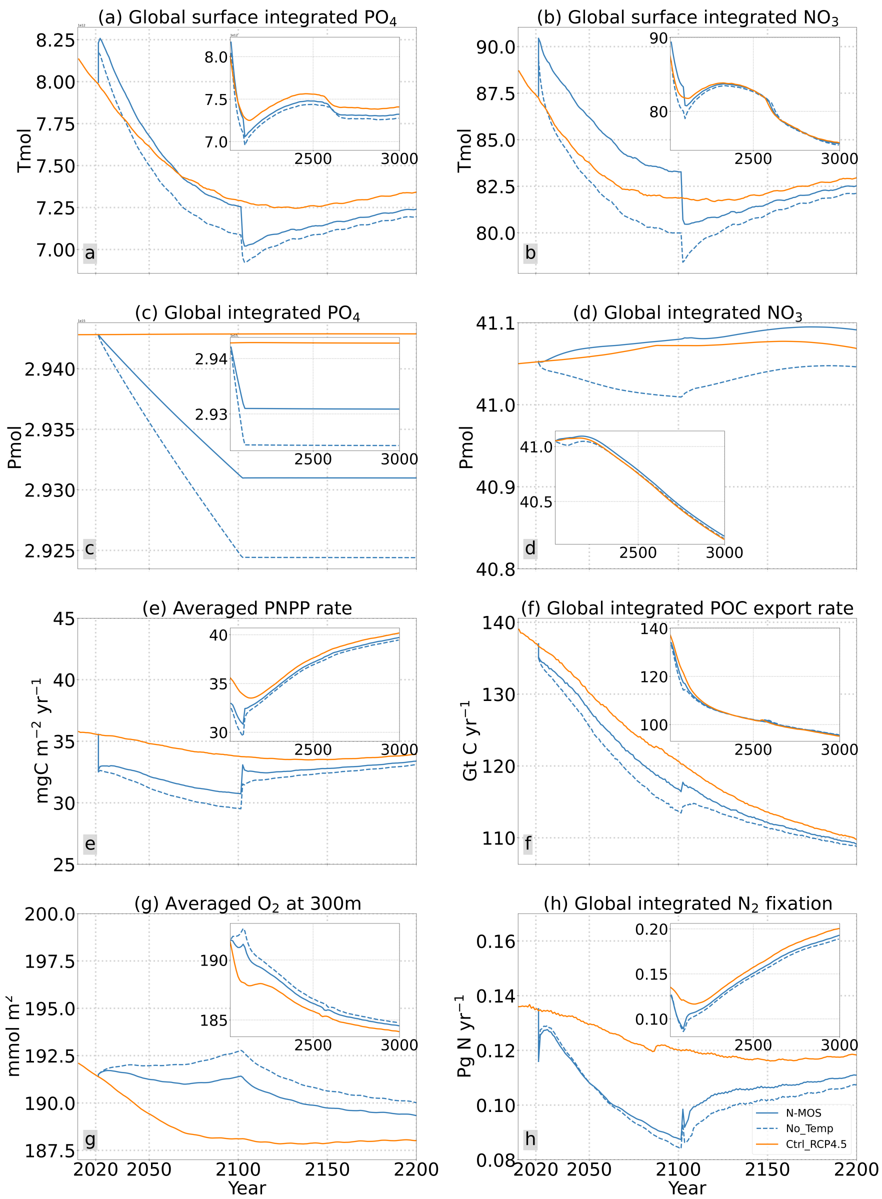
(a) Global surface integrated PO_4
(b) Global surface integrated NO_3
(c) Global integrated PO_4
(d) Global integrated NO_3
(e) Averaged PNPP rate
(f) Global integrated POC export rate
(g) Averaged O_2 at 300m
(h) Global integrated N_2 fixation
Tmol
Pmol
mgC m^{-2} yr^{-1}
Gt C yr^{-1}
mmol m^2
Pg N yr^{-1}
Year
N-MOS
No_Temp
Ctrl_RCP4.5

Nearshore Macroalgae Cultivation for Carbon Sequestration by Biomass Harvesting: Evaluating Potential and Impacts with An Earth System Model

Jiajun Wu[1,3], Wanxuan Yao[1], David. P. Keller[1], Andreas Oschlies[1,2]

[1]GEOMAR Helmholtz Centre for Ocean Research Kiel, Wischhofstr. 1-3, 24148 Kiel, Germany
[2]Kiel University, Christian-Albrechts-Platz 4, 24118 Kiel, Germany
[3]Alfred Wegener Institute Helmholtz Center for Marine and Polar Research, Am Handelshafen 12, 27570 Bremerhaven, Germany

Key Points:

- Offshore marcoalgae cultivation for CDR has a global potential of gigatonnes scale.
- Partition of marine net primary production shifts from phytoplankton to macroalgae due to shading and nutrient robbing.
- Open ocean net primary production reduces the oxygen deficit zones.

Corresponding author: Jiajun Wu, `jwu@geomar.de`

Abstract

This study introduces an ocean-based carbon dioxide removal (CDR) approach: Nearshore Macroalgae Aquaculture for Carbon Sequestration (N-MACS). By cultivating macroalgae in nearshore ocean surface areas, N-MACS aims to sequester CO_2 with subsequent carbon storage. Utilizing an Earth System Model with intermediate complexity (EMIC), we explore the CDR potential of N-MACS alongside its impacts on the global carbon cycle, marine biogeochemistry and marine ecosystems. Our investigations unveil that coastal N-MACS could potentially sequester 0.7 to 1.1 GtC yr^{-1}. However, it also significantly suppresses marine phytoplankton net primary productivity because of nutrient removal and canopy shading, counteracting approximately 30% of the N-MACS CDR capacity. This suppression of surface NPP, in turn, reduces carbon export out of the euphotic zone to the ocean interior, leading to elevated dissolved oxygen levels and diminished denitrification in present-day oxygen minimum zones. Effects due to harvesting-induced phosphorus removal continue for centuries even beyond the cessation of N-MACS.

Plain Language Summary

Our study explores the Nearshore Macroalgae Aquaculture for Carbon Sequestration (N-MACS) as a potential marine carbon dioxide removal strategy. This approach uses ocean-based seaweed farming to capture carbon dioxide —-the main greenhouse gas causing global warming-— and permanently stores it post harvesting through biomass processing and carbon storage. Our simulations indicate that N-MACS has the potential to remove substantial quantities of carbon dioxide every year. Nonetheless, harvesting will also remove oceanic nutrients and decrease open ocean primary production. At the same time, N-MACS can relieve the oxygen scarcity and mitigate surface ocean acidification. Those impacts on the oceanic ecosystem and marine biogeochemistry could potentially persist for centuries, upon the cessation of N-MACS.

1 Introduction

The IPCC's Sixth Assessment Report (IPCC (2022)) stipulates global net-zero CO_2 emissions by the early 2050s to restrict global warming to 1.5°C, recognizing Carbon Dioxide Removal (CDR) as essential to counterbalance residual emissions. Ocean-based CDR approaches are gaining traction due to the ocean's inherent carbon sequestration capacity (IPCC, 2022; Keller et al., 2021; GESAMP, 2019). As the Earth's largest dynamic carbon reservoir (Falkowski et al., 2000; Sarmiento & Gruber, 2013), the ocean's expanse and natural carbon absorption capacity, combined with measures like ocean fertilization, ocean alkalinity enhancement, can substantially augment carbon sequestration efforts (Buesseler et al., 2004; Bach et al., 2019).

Macroalgae offer an avenue for ocean-based CDR due to their notable net primary production rates and high carbon-to-nutrient ratios, facilitating effective carbon sequestration (N'Yeurt et al., 2012; Fernand et al., 2017; Gao et al., 2022). The global potential carbon export by macroalgae has been estimated as 1.4 GtC per year (Krause-Jensen & Duarte, 2016; Ortega et al., 2019; Barrón & Duarte, 2015). Cultivation technologies for macroalgae are well-established (e.g., Buck and Buchholz (2004); Goecke et al. (2020); Zhang et al. (2016)), with a global harvest reaching 34.7 million tonnes wet weight (WW) in 2019 (FAO, 2018; Cai et al., 2021). Macroalgae cultivation for ocean-CDR has been considered recently (Wu et al., 2023; Fernand et al., 2017). Based on geographic location, macroalgae-based CDR can be categorized into two categories: open-ocean cultivation with deep-ocean carbon storage (Wu et al., 2023; Bach et al., 2021), and nearshore cultivation for harvesting, followed by subsequent carbon storage achieved outside of the ocean such as biochar and Bioenergy with Carbon Capture and Storage (BECCS, Roberts et al. (2015); Bird et al. (2011); Fernand et al. (2017); Gattuso et al. (2021); Capron et al. (2020); Borchers et al. (2022); Chen et al. (2015)).

Prior to the large-scale implementation of ocean-based CDR strategies, comprehensive evaluations are essential to understand their potential and impacts on the marine environment (IPCC, 2022; Gattuso et al., 2021). Particularly, numerical simulations with Earth system models are pivotal as they, in contrast to field experiments pose, have no direct environmental impact (Oschlies et al., 2010; Keller et al., 2014; Keller, Lenton, Scott, et al., 2018; Siegel et al., 2021). Several modelling studies have examined macroalgae-based CDR strategies, revealing CDR capacities ranging from Mega (10^6) to Giga (10^9) tonnes depending on location and species. These studies, referenced as Wu et al. (2023); Bach et al. (2019) for open-ocean and Arzeno-Soltero et al. (2023); Berger et al. (2023) for nearshore areas, also underscore the constraints posed by marine physical and biogeochemical feedbacks on CDR capacity and efficiency. Furthermore, they highlight the potentially significant impacts on the global carbon cycle, marine biogeochemistry, and ecosystems through the alteration of ocean nutrient distributions and primary production patterns.

Here we evaluate 'Nearshore Macroalgae Aquaculture for Carbon Sequestration' (hereinafter N-MACS), operating under the assumption that the harvested carbon content will be sequestered from atmosphere and hence achieving CDR. The evaluation employs an Earth System Model of intermediate complexity, encompassing an explicit macroalgae component, to rigorously assess implications and carbon sequestration efficacy of N-MACS from 2020 to 3000, with N-MACS deployment from 2020 to 2100. Our objectives are to: a) examine the idealised large-scale CDR potential of N-MACS, and b) evaluate its effects on the global carbon cycle and marine biogeochemistry, including termination effects and millennial long-term effects.

2 Methods

We employ the University of Victoria Earth System Climate Model version 2.9 (UVic; Keller et al. (2012); Weaver et al. (2001)), an intermediate complexity Earth system model coupling a three-dimensional ocean circulation model (Pacanowski, 1996) including a dynamic thermodynamic sea ice module (Bitz & Lipscomb, 1999), a terrestrial model (Meissner et al., 2003; Weaver et al., 2001) and a one-layer atmospheric energy-moisture model (Fanning & Weaver, 1996). The horizontal resolution is 3.6° longitude × 1.8° latitude, and the ocean component has 19 vertical layers with thicknesses ranging from 50 m near the surface to 500 m in the deep ocean. The ocean biogeochemistry module includes nutrients (nitrogen and phosphate), one general phytoplankton type, and one diazotrophic phytoplankton (i.e., nitrogen fixers), one general macroalgae (see below section), one type of zooplankton, dissolved inorganic carbon, oxygen, and total alkalinity (Keller et al., 2012; Eby et al., 2013).

Upon spinning up the model under pre-industrial conditions, we employed CMIP5 forcing data for the historical period (Eby et al., 2013). From 2005 to 2100, we aligned the inputs of CO_2 emissions, land-use changes, volcanic radiative forcing, and sulfate aerosols with the RCP4.5 scenario. For the period post-2300, CO_2 emissions are projected to decline linearly, reaching zero by 3000, with other forcings maintained at constant levels. RCP4.5 is a moderate emissions trajectory with a radiative forcing of 4.5 W/m^2 by 2100 (Thomson et al., 2011; Meinshausen et al., 2011).

N-MACS is an extension of the Macroalgae Open-ocean Mariculture and Sinking (MOS) framework developed by (Wu et al., 2023), featuring an idealized generic model of the Phaeophyceae (brown algae) *Sacharina* integrated with UVic. Macroalgae growth is controlled by multiple limiting factors (erosion, nutrient availability, light, and temperature) with a fixed C:N:P stoichiometric molar ratio of 400:20:1. Initial seed biomass is deployed in each surface ocean grid box with adequate nutrients to be converted into seed biomass. The initial plantlet biomass in each N-MACS grid cell is equivalent to 0.02 mmol N m^{-3}, sourced directly from the grid box's inorganic N, P, and C pools without extra nutrient or carbon input. A constant maximum biomass yield of 3,300 tDW km^{-2} is set, focusing on large-scale impacts rather than optimizing farming strategies. Once biomass in a grid cell reaches this limit, macroalgae growth halts until end-of-season harvesting. In temperate zones, seeding starts on May 1st and harvesting occurs on October 31st in the northern hemisphere, while in the southern hemisphere, seeding begins on November 1 with harvesting on April 30, aligning with macroalgae growth phases. The model annually selects grid boxes with ample nutrients for reseeding, implying no further reseeding post-harvest in nutrient-depleted regions (detailed in Section 3.1, Wu et al. (2023)). Additionally, surface layer macroalgae create canopy shading effects on phytoplankton communities. Potential grazers like amphipods and gastropods (Jacobucci et al., 2008; Chikaraishi et al., 2007) are modeled within the UVic's zooplankton compartment (Keller et al., 2012). Further macroalgae model specifics, including parameters, functions, and cultivation strategies, are delineated in Wu et al. (2023, Sect. 2).

2.1 Experimental design

Our study contains a control run (Ctrl_RCP4.5) and two N-MACS simulations: the standard N-MACS simulation with all growth constraints, and a sensitivity simulation (No_Temp) with temperature constraint removed to examine the uncertainty in temperature-dependant growth rate in the modeled macroalgae. In both N-MACS simulations, macroalgae farms are limited to ocean surface zones directly along coasts between 60°S and 60°N, with grid boxes 200 to 400 km wide, aligning with Exclusive Economic Zones (EEZs) extending to 200 nautical miles from sovereign state coasts (Froehlich et al., 2019; Feng et al., 2017). It's presumed that all macroalgae production is promptly harvested post cultivation for biochar conversion or BECCS feedstock on land, indicating permanent carbon sequestration from the biomass with no nutrient return to the ocean. Meanwhile, natural macroalgae habitats are globally distributed along coastlines with species exhibiting varied temperature sensitivities (Duarte et al., 2022). The No_Temp simulation investigates the theoretical maximum coastal macroalgae biomass production with species optimally adapted to local temperatures. N-MACS CDR capacity is defined as the total carbon in harvested biomass, while its CDR efficacy is defined by the changes in combined oceanic and macroalgae carbon reservoir relative to the harvested macroalgal biomass carbon content. Our focus is on the the cultivation process outcomes, excluding possible carbon leakages in post-harvest CDR applications like biochar or BECCS (Chen et al., 2015; Fernand et al., 2017; Bird et al., 2011).

3 Results & Discussions

3.1 Macroalgae model validation

The employed macroalgae model was validated against literature data and used in idealized open-ocean cultivation simulations by Wu et al. (2023). Given the notable nutrient availability differences between nearshore regions and open oceans, we compare the productivity of simulated nearshore macroalgae with relevant observational and modeling data.

Fig.1 illustrates the N-MACS distribution and its mean annual biomass yield from 2020 to 2100. Simulations indicate a total N-MACS footprint of about 24 million km^2, with 14 to 15 million km^2 yielding significant productivity (over 100 tonnes DW $km^{-2}yr^{-1}$; Tab.1). These values are lower than other model-based estimates ranging from 48 to 100 million km^2 (Froehlich et al., 2019; Lehahn et al., 2016; Berger et al., 2023), hence presenting a more conservative N-MACS productivity. The reduced macroalgae farming areas in our model result from several factors: suboptimal UVic simulation of nutrient concentrations in nearshore regions without land run-off (Eby et al., 2009; Keller et al., 2012; Tivig et al., 2021), unique parameters for chosen brown algae species in our dynamic growth model (Froehlich et al., 2019), consistent nutrient feedback consideration unlike earlier assessments (Froehlich et al., 2019; Lehahn et al., 2016), and the assumption that farms are located within EEZs (Lehahn et al., 2016). Despite these differences, the N-MACS distribution pattern aligns with those in Lehahn et al. (2016, Fig. 3. A), Berger et al. (2023, Figure 4), Duarte et al. (2022, greenish pattern of Figure 1(a)), and Froehlich et al. (2019, Figure 1). While the total N-MACS area remains steady over time, regions of significant productivity (significant N-MACS areas) expand during the initial deployment decade (Fig.S11), resulting from dynamic nutrient cycling. Here, N-MACS suppresses phytoplankton due to canopy shading (Fig.S3), creating a nutrient surplus within its habitat that fertilizes N-MACS (see Sect.3.3).

In productive N-MACS regions, simulated macroalgae productivity averages 165 tonnes DW km^{-2} yr^{-1}, rising to 223 tonnes DW km^{-2} yr^{-1} in No_Temp (Tab.1). Farmed seaweed productivity, including the modeled *Saccharina* species, varies significantly depending on species, cultivation techniques, and environmental conditions. Reported *Saccharina* yields in Europe range from 4 to 450 tonnes DW km^{-2} yr^{-1} (Peteiro et al., 2014; Buck & Buchholz, 2004), while in northeast Asia, yields can reach 2,400-3,000 tonnes DW km^{-2} yr^{-1} (Yokoyama et al., 2007; Zhang et al., 2011).

Although N-MACS farms were initially established in all ocean grid boxes adjacent to land between 60°S and 60°N in year 2020, sustainable biomass harvests are mainly found in four regions with high nutrient availability: the Eastern Boundary Upwelling Systems in the nearshore Pacific regions of South America and the Atlantic coasts of Africa (Chavez & Messié, 2009; Fréon et al., 2009), the northeast Pacific and the Southern Ocean (Tab.S1). This is consistent with the findings of Berger et al. (2023), Arzeno-Soltero et al. (2023), and Duarte et al. (2021).

In the sensitivity study (No_Temp), where temperature no longer affects macroalgae growth, the N-MACS distribution mirrors the base case, albeit with increased biomass productivity in mid to high latitudinal coastal regions (Tab.1, Fig.S2). By employing local macroalgae species better adapted to specific temperature ranges, optimization of macroalgae cultivation and enhancement of the CDR potential of nearshore macroalgae-based strategies may be achievable.

Table 1. Summary table of N-MACS simulations. Significant N-MACS area is area with ≥100 tonnes DW per km^2 per year. The changes are N-MACS variations relative to Ctrl_RCP4.5.

	Unit	**N-MACS**	**No_Temp**
Total yield	Gt DW	188.96	293.40
N-MACS total area	10^6 km^2	24.34	23.65
Significant N-MACS area		14.29	15.97
Total carbon fixation in N-MACS	GtC	56.7	88.0
Annual carbon fixation (avg. 2020 to 2100)	GtC yr^{-1}	0.7	1.1
Annual unit area carbon fixation	tC km^{-2} yr^{-1}	29.1	46.5
Change of global climate system in 2100 (3000 in parentheses)			
Surface averaged temperature (SAT)	°C	-0.07 (-0.08)	-0.12 (-0.13)
Atmospheric CO_2 concentration	ppm	-14.2 (-12.0)	-22.6 (-18.3)
Change of global carbon reservoirs in 2100 (3000 in parentheses)			
Atmosphere		-30.1 (-25.5)	-47.9 (-38.9)
Ocean (including carbon fixation by N-MACS)	GtC	35.9 (31.4)	57.1 (48.8)
Land		-5.8 (-5.9)	-9.2 (-9.9)
Change of integrated marine biogeochemical parameters in 2100 (3000 in parentheses)			
POM export at 2km depth	GtC yr^{-1}	-4.151 (0.37)	-7.245 (0.58)
PO_4 (full depth)	Tmol	-11.64 (-11.91)	-18.10 (-18.49)
NO_3 (full depth)	Tmol	7.68 (15.78)	-62.51 (-6.01)
Phytoplankton NPP	GtC yr^{-1}	-0.36 (-0.52)	-0.50 (-0.82)

∗ DW: dry weight; POM: particle organic matter; tC: tonnes of carbon (10^3 Kg);
GtC: Giga (10^9) tonnes of carbon; Tmol: Tera moles (10^{12} moles).

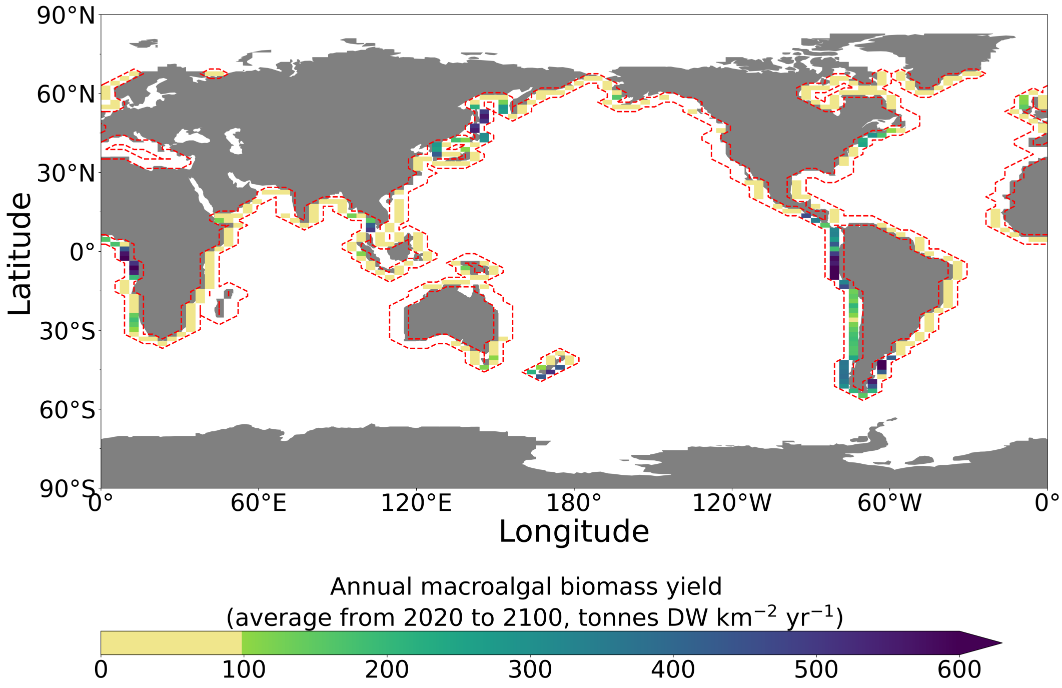

Figure 1. Annual macroalgae biomass yield (averaged from year 2020 to year 2100). Dashed red lines outline the initial seeding locations in year 2020. Regions with high macroalgae productivity include: Coasts of North Western Pacific (near northern China, Japan and Korean Peninsula), South Eastern Pacific (coasts of South America), South Eastern Atlantic (mid-south Africa coast), coast of New Zealand, and South Eastern of Australia. Yellowish areas indicate relatively lower yield ($\leq$100 tonnes DW per km^2 per year).

3.2 CDR capacity and impacts on carbon cycle

The CDR capacity of the N-MACS approach can be quantified as the carbon contained (and securely stored) within the harvested macroalgae biomass. From 2020 to 2100, the N-MACS simulation demonstrates a total sequestration of 56.7 GtC (equivalent to 207.9 GtCO_2). In the No_Temp simulation, this capacity increases to 88 GtC due to elevated macroalgal productivity. The atmospheric CO_2 sequestration in N-MACS/No_Temp scenarios translates to a reduction in global-mean surface air temperature (SAT) by 0.07°C/0.12°C (Tab.1, Fig.S1). While this reduction in SAT alone does not enable the RCP 4.5 emission scenario to align with the Paris Agreement, the annual carbon removal (equivalent to 2.60/4.03 Gt CO_2eq) is, for example, on par with the 2022 annual CO_2 emissions from the global building sector (2.94 Gt CO_2, IEA (2023)).

The simulated global average unit-area CDR capacity is 29.1 to 46.5 tC km^{-2} within N-MACS occupied regions (106.8 to 170.7 tCO_2 km^{-2}, Tab.1). Conversely, the global dynamic seaweed growth model of Arzeno-Soltero et al. (2023) suggested that macroalgae farming, particularly in the equatorial Pacific, could yield about 1 GtC for 1 million km^2 of EEZ waters, translating to 1,000 tC km^{-2} yr^{-1}. These differences stem from model differences and experiment setups. Their model, incorporating four types of macroalgae species with high carbon content and yield, operates independently from dynamic nutrient changes, which we find often limits N-MACS growth, and runs for one year. Our estimation is also lower than the globally averaged per-unit-area CDR capacity of 57 tC km^{-2} yr^{-1} in Wu et al. (2023), where the identical macroalgae model of N-MACS is applied to open-ocean regions. This difference primarily arises from the diverse distribution of macroalgae farms across varying nutrient fields, as depicted by Wu et al. (2023) for open-ocean regions, contrasted with the current N-MACS in nearshore areas. The discrepancy is exacerbated by the coarse grid resolution in UVic, likely underestimating coastal productivity (Keller et al., 2012; Tivig et al., 2021). Nevertheless, the annually averaged carbon sequestration of N-MACS is estimated at 0.7 to 1.1 GtC yr^{-1} (2.6 to 4.0 $GtCO_2$ yr^{-1}), surpassing the 0.37 GtC yr^{-1} reported by Berger et al. (2023), something again attributable to the different dynamic macroalgae growth and Earth system modeling approaches.

The net increase in the oceanic carbon reservoir, consisting of water-column carbon content and the harvested macroalgae in the N-MACS (No_Temp) simulations, is 35.9 (57.1) GtC in 2100 (Tab.1), equivalent to the N-MACS induced air-sea carbon flux in the model (Fig.S6, Fig.S7). However, the increase in the oceanic plus macroalgae carbon reservoir is approximately two-thirds of the harvested macroalgae carbon, corresponding to 63.3% (64.9%) of the net carbon removed by harvesting the macroalgae. The disparity between the increase in the ocean plus macroalgae carbon pool and the carbon harvested in the form of macroalgal biomass is largely caused by backfluxes from the ocean into the atmosphere due to diminished atmospheric pCO_2 (Oschlies, 2009) and partially by the reduced phytoplankton net primary production (PNPP) from canopy shading and nutrient competition effects introduced by N-MACS (see Sect.3.3). This efficiency is somewhat higher than the CDR efficiency of 58% in Berger et al. (2023), who employed a dynamic macroalgae growth model in conjunction with a high-resolution ocean biogeochemical model with prescribed atmospheric CO_2, i.e. without back-fluxes from the ocean into the atmosphere due to diminished atmospheric pCO_2, for 5-year simulations.

Meanwhile, the increase in the oceanic plus macroalgae carbon reservoir induced by N-MACS until 2100 leads to a corresponding decline in the terrestrial carbon reservoir of 5.8 to 9.2 GtC (see Tab. 1) via an atmospheric carbon climate feedback. This response illustrates the Earth system's endeavor to maintain equilibrium, with carbon cycling between terrestrial and oceanic reservoirs, primarily mediated by atmospheric interactions. This finding aligns with other studies, suggesting that ocean-based CDR could potentially weaken terrestrial carbon sinks, especially through the reduction of the CO_2 fertilization effect on terrestrial photosynthesis (Keller, Lenton, Littleton, et al., 2018).

During the implementation phase, an enhancement of approximately 29% (37%) in the air-to-sea downward carbon flux was observed within the macroalgae-occupied areas in N-MACS (No_Temp)(Fig.S5), aligning with the 52% enhancement reported by Berger et al. (2023). The lesser degree of carbon flux enhancement observed in our simulation within the macroalgae-occupied areas is attributed to 1) the canopy shading effect on phytoplankton in our model, reducing PNPP and subsequent carbon flux into the ocean (Fig.2d & Fig. S3); and 2) the dynamic atmospheric pCO_2 in our model compared to prescribed fixed pCO_2 in Berger et al. (2023), as well as different biogeochemical properties of macroalgae and phytoplankton in the two models. Our results further highlight the potential challenges inherent in the measurement, reporting, and verification processes when assessing carbon flux enhancements. Additionally, a slight decrease in DIC in mid and deep waters is evident in Fig.S4a, stemming from reduced water column remineralization due to the diminished downward particulate organic carbon (POC) export (see Sect.3.3).

3.3 Impacts on global marine biogeochemistry

In our simulations, the 80-year implementation of N-MACS has significantly impacted global marine biogeochemistry. This includes ocean surface nutrient distributions, surface ocean alkalinity, and dissolved oxygen concentrations at mid-depth (Fig. 2). Additionally, simulated net primary production and the distributions of ordinary phytoplankton and diazotrophs are also affected by N-MACS deployment. Notably, some of these impacts persist until the year 3000, despite the cessation of N-MACS in 2100 (see below).

The N-MACS macroalgae model delineates two primary impacts of macroalgae on phytoplankton: nutrient competition and canopy shading (Wu et al., 2023, Sect.2.2.3). Harvesting macroalgae not only sequesters carbon but also extracts nutrients within the harvested biomass, leading to an immediate drop in global PNPP post N-MACS initiation in 2020, with a gradual reduction during N-MACS deployment till 2100 (Fig.3e). This PNPP decline predominantly occurs along coast-adjacent N-MACS areas (Fig.2d). Additionally, certain open-ocean regions beyond coastal farms exhibit a PNPP increase, notably in the Indian Ocean, eastern Atlantic near Africa, and eastern equatorial Pacific. This is attributed to nutrient leakage from N-MACS areas (see Fig.2d; further details in the subsequent paragraph). N-MACS implementation suppresses oceanic nitrogen fixers, diazotrophs, due to canopy shading and phosphate competition by macroalgae (Fig.S9). Although certain regions exhibit heightened diazotroph biomass due to increased phosphate levels (Fig.S10a&c), the overall nitrogen fixation relative to DNPP diminishes during N-MACS deployment (Fig.3h). Zooplankton, assumed capable of grazing on macroalgae (Wu et al., 2023), primarily feed on phytoplankton due to a lower macroalgae grazing preference, hence their biomass trends closely with those of phytoplankton (not shown).

Fig.3a illustrates a notable increase in surface ocean PO_4 concentrations (top 50m) following N-MACS initiation, followed by a decrease. Three primary factors underlie this PO_4 rise. Firstly, the suppression of phytoplankton by macroalgae leads to a decreased organic carbon export out of the euphotic zone. Secondly, macroalgae cannot fully utilize the *in-situ* PO_4 due to the limited growth rate and maximum macroalgae biomass (Wu et al., 2023). Lastly, the higher stoichiometric N:P ratio of 20:1 in macroalgae, compared to the Redfield ratio of 16:1 in phytoplankton, entails less PO_4 consumption per nitrogen unit for growth. This explains the increases in surface PO_4 levels in N-MACS regions shown in Fig.2c (Fig.S8c for No_Temp). Nitrate concentrations in N-MACS regions also rise due to phytoplankton inhibition and unexhausted available nitrate from macroalgae growth (Fig.2a). These disparities consequently induce lateral nutrient leakage from N-MACS areas, fertilizing the aforementioned downstream area of coastal N-MACS farms. Here, augmented PNPP consumes the displaced nutrients, driving a regional PO_4 concentration reduction (Fig.2c).

A reduction in surface PNPP within N-MACS regions triggers a decline in particulate organic matter (POM) export to ocean depths, as observed at 2000 m in Fig. 3f and Tab.1. This decline subsequently diminishes oxygen consumption via aerobic remineralization of organic carbon, thus elevating the oxygen concentration across middle and bottom waters (Fig.S4d, Fig.S12d). Notable increases in dissolved oxygen concentrations at 300m depth are apparent in the northwestern Pacific, eastern equatorial Pacific, and southern Atlantic near the South American continent (Fig.2e & Fig.3). Specifically, oxygen minimum zones (OMZs) in the North Pacific and equatorial Atlantic Ocean have shrunk compared to Ctrl_RCP4.5. The increased oxygen levels inhibit denitrification in the subsurface and the upwelling system in the eastern equatorial Pacific (Fig.2f&i, Bange et al. (2019); Ravishankara et al. (2009)), and diminished remineralization of organic carbon curtails nutrient regeneration, reducing nutrient upwelling (Fig.2g&h). This results in elevated NO_3 but reduced PO_4 compared to the Ctrl_RCP4.5 in the open ocean of the eastern equatorial Pacific (Fig.2a, c, d & f). Another factor contributing to the reduced PO_4 in the source waters of the upwelling regions is the decreased PNPP in the N-MACS areas, which lessens export and thereby reduces the PO_4 source from POM remineralization (Fig.2d,Fig.3f). Furthermore, the aforementioned decreased denitrification increases the NO_3 supply in the upwelling system to the surface, especially in oxygen-depleted regions off Peru where reduced POM remineralization leads to lesser denitrification and nitrogen loss. However, in the No_Temp simulation, amplified macroalgae growth utilizes upwelled NO_3 before export to the open ocean, mitigating the NO_3 increase in the eastern equatorial Pacific (Fig.S8a).

Despite the reduction in mid-depth denitrification (Fig.2i), which also diminishes alkalinity production, the surface alkalinity in N-MACS increases about 1% or 10 to 20 mmol m^{-3} by 2100 (Fig.2b), due to reduced $CaCO_3$ generation from the PNPP reduction induced by continuous phosphate removal by N-MACS (Fig.S12, Schmittner et al. (2008, Eq.2)). Post N-MACS discontinuation in 2100, which effectively terminates canopy shading and nutrient competition effects, results in a marked resurgence in PNPP and thereby also a decreases in global surface nutrient concentrations (Fig3a, b&e). Additionally, diazotroph biomass, DNPP, and nitrogen fixation recover (Fig.S9, Fig3h). The export of PNPP and POC as well as the subsurface oxygen consumption via organic carbon remineralization also recovers (Fig3g). Additionally, the air-sea CO_2 flux reverts to baseline levels after cessation of the carbon sequestration by macroalgal harvest from the ocean (Fig.S6, S7).

By year 3000, the average surface temperature in the N-MACS/No_Temp simulations is slightly lower by -0.08/-0.13 °C, respectively, compared to Ctrl_RCP4.5, maintaining the temperature reduction achieved by N-MACS in 2100 (Tab.1). After N-MACS termination in year 2100 and until year 3000, both oceanic and terrestrial carbon reservoirs shrink, with oceanic plus macroalgae carbon storage decreasing by 4.5 GtC in N-MACS and 8.3 GtC in No_Temp, and terrestrial carbon storage declining by 0.1 GtC and 0.7 GtC in N-MACS and No_Temp scenarios respectively. This leads to a 4.6 / 9.0 GtC or 2.2 / 4.3 ppm atmospheric CO_2 increase (Tab.1). Decreased global temperatures slow photosynthesis and soil respiration, in combination yielding a small reduction in the terrestrial carbon pool. The decrease in the oceanic carbon pool mainly arises from the PNPP reduction as a consequence of permanent phosphate removal during the operation of N-MACS. This enduring PO_4 removal leads to long-term alterations in marine biogeochemistry, as shown by extended simulations until year 3000 (Fig.3). Though only 0.4% of total oceanic phosphate is removed by 2100 (Fig.3c), it induces a persistent reduction in PNPP, DNPP, and nitrogen fixation (Fig.3a&h, S10b&d). This prevents PNPP and DNPP recovery to RCP4.5 levels from 2100 to 3000 (Fig. 3 e), leading to increased oxygen due to overall POC export reduction (Fig.3d&g, Fig.S12).

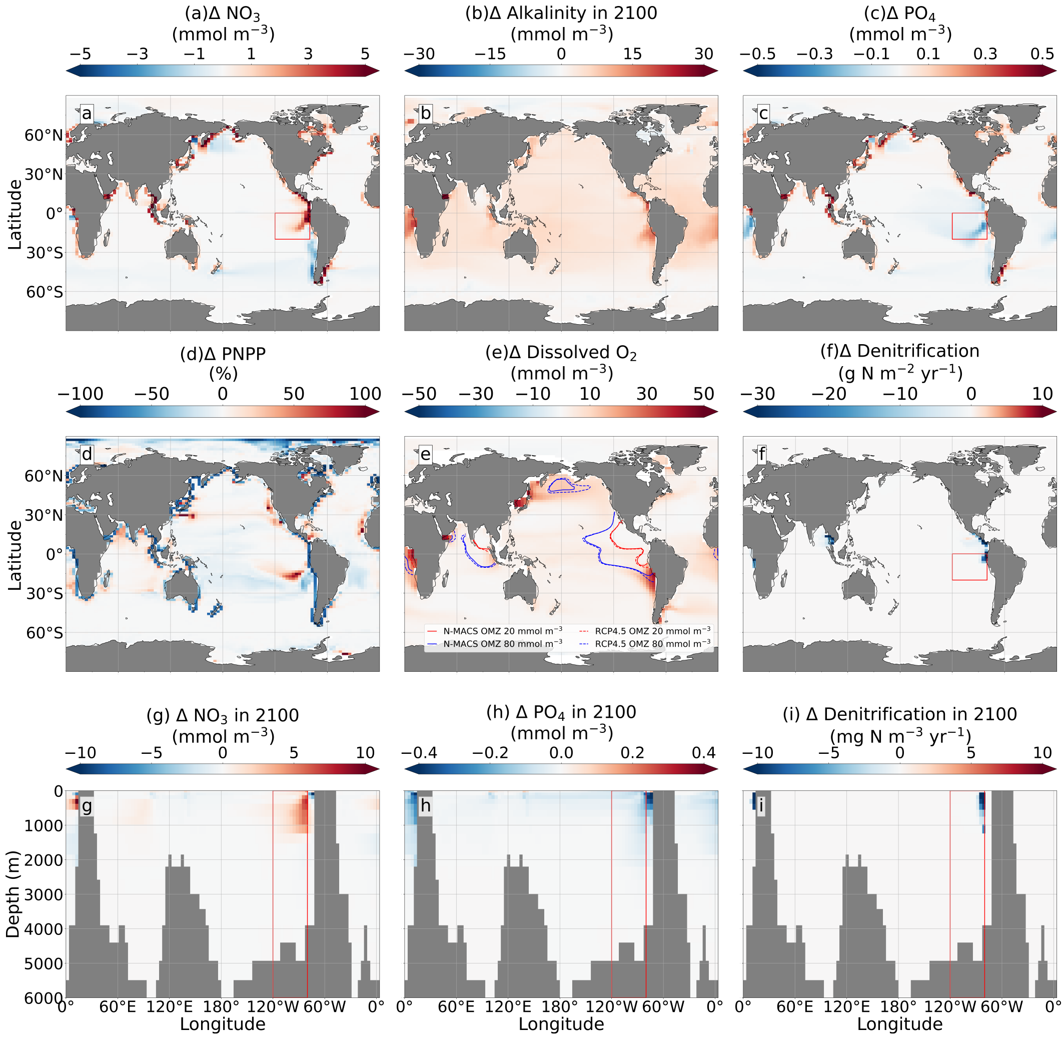

Figure 2. Differences in simulated oceanic properties in year 2100 after continuous N-MACS deployment from 2020 to 2100, with respect to Ctrl_RCP4.5 without N-MACS deployment (data averaged over this period, except for **d** and **e** representing data in 2100): **a**: Surface-layer nitrate (top 50m); **b**: Surface-layer alkalinity; **c**: Surface-layer phosphate; **d**: Phytoplankton net primary production (PNPP); **e**: Dissolved oxygen concentrations and oxygen minimum zones (OMZs) at a depth of 300m; **f**: Oceanic denitrification rates. Subfigures **g, h & i** represent latitudinally averaged data from 20°S to 0°, relative to the Ctrl_RCP4.5 scenario depicted in subfigures **a, c, & f** (highlighted by red rectangular regions between latitudes 20°S to 0° and longitudes 80°W to 120°W): **g**: Phosphate concentrations, **h**: Nitrate concentrations, **i**: Annual denitrification rates.

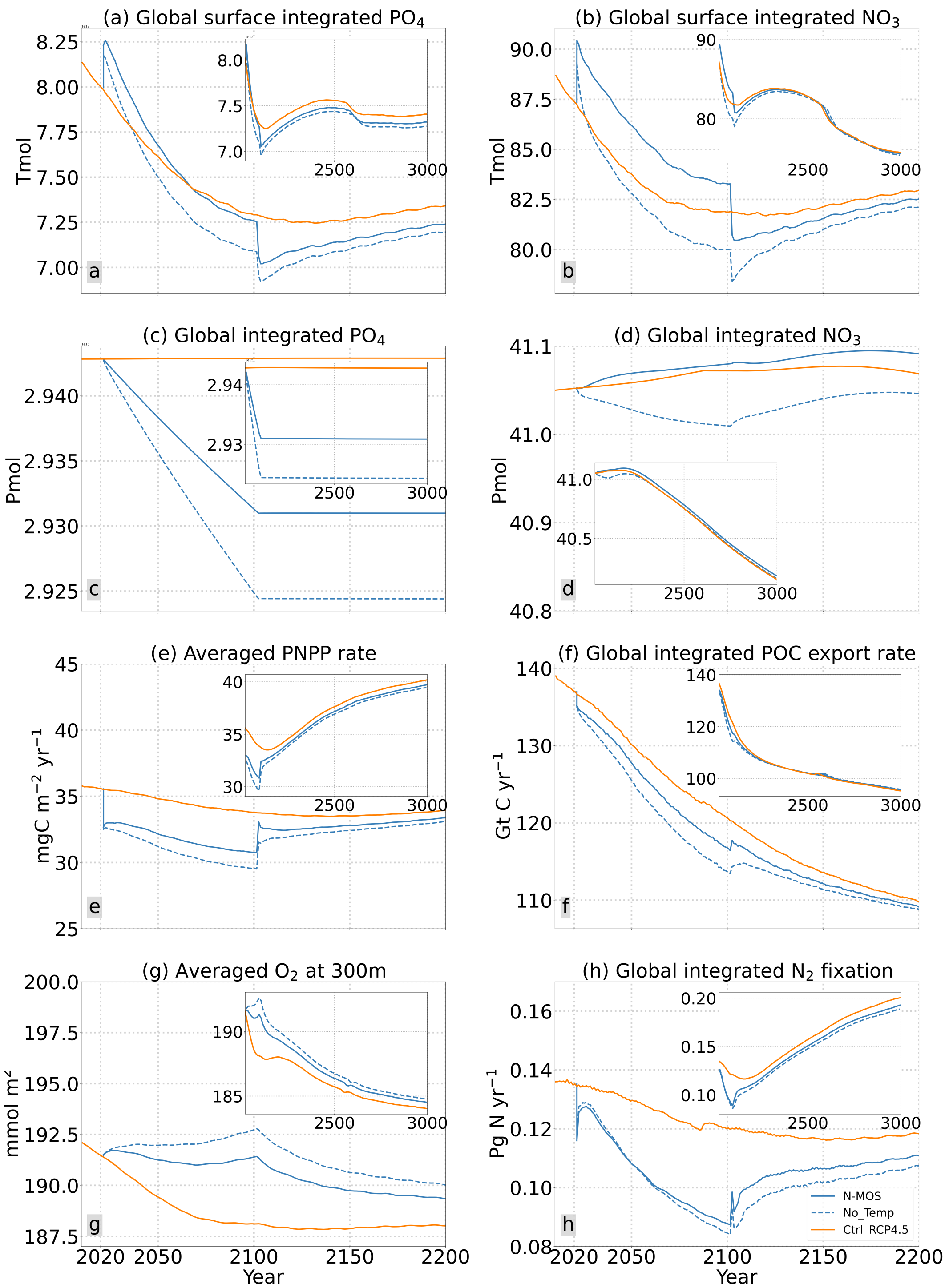

Figure 3. Temporal evolution of globally integrated nutrients, Phytoplankton Net Primary Production (PNPP), and Particulate Organic Carbon (POC) Export at 2,000m depth: Comparison of N-MACS (solid blue), No_Temp (dashed blue), and Ctrl_RCP4.5 Baseline Simulation (orange). Insets in each panel extend the timeline to the year 3000. **a & c**: Permanent removal of PO_4 from the surface, **b & d**: Surface NO_3 levels and global NO_3 trends (increase in N-MACS, decrease in No_Temp). **e**: Surface PNPP (see also Fig.2d). **f**: The export of POC at 2,000m depth. **g**: The averaged O_2 concentration at 300m depth. **h**: Globally integrated Nitrogen fixation.

4 Conclusion & Outlook

Our analysis highlights the substantial annual gigatonne-scale CO_2 sequestration potential of N-MACS, though with marine biogeochemical and global carbon cycle feedbacks reducing the additional air-sea CO_2 flux by 35% compared to carbon removal via harvesting. Large-scale N-MACS deployment considerably alters marine biogeochemistry and ecosystems, suppressing PNPP, elevating dissolved oxygen concentrations, reducing denitrification, and decreasing surface ocean alkalinity. Terminating N-MACS in 2100 triggers a transient rebound in surface PNPP and a decrease in the air-sea CO_2 flux, yet long-term effects like nutrient depletion and increased oxygen levels persist for centuries. Promising regions for macroalgae production include the upwelling systems in South America, Africa's Atlantic coasts, the Northeast Pacific, and the Southern Ocean.

Our simulations have certain limitations: Given that the UVic operates on a coarse grid resolution ($1.8° \times 3.6°$), it inadequately represents the physical and biogeochemical processes of the coastal ecosystem in the marine ecosystem model (Keller et al., 2012). While not significantly impacting our current global and millennial scale simulations, it may affect coastal macroalgae farming simulations when considering nutrient fluxes in coastal areas (e.g., Van Der Molen et al. (2018)). Possible improvements to our model include a consideration of a wider range of macroalgae species (Arzeno-Soltero et al., 2023; Duarte et al., 2022), explicit accounting of iron limitation (Paine et al., 2023; Anton et al., 2018), dynamic cellular stoichiometry, and current impacts on macroalgae frond erosion (Frieder et al., 2022; Broch & Slagstad, 2012). Acknowledging both remineralization-resistant particulate and dissolved organic carbon release from macroalgae and subsequent deep-water may be crucial for comprehending the CDR capacity (Pedersen et al., 2021; Ortega et al., 2019; Duarte & Krause-Jensen, 2017; Wada & Hama, 2013). Further considerations include macroalgae halocarbon emissions (Baker et al., 2001; Leedham et al., 2013; Jia et al., 2022) and alterations in ocean surface albedo and local ecosystem (Bach et al., 2021; Boyd et al., 2022). Herein it's assumed that no nutrients from the harvested biomass are returned to the ocean, which significantly impacts the simulated biogeochemistry. Thus, evaluating nutrient extraction and return strategies is imperative if N-MACS is pursued as a sustainable CDR approach.

Governance and societal facets need consideration in macroalgae-based CDR, particularly due to potential spatial competition between macroalgae cultivation and fisheries, especially along the Peruvian coast (Gattuso et al., 2021; Ricart et al., 2022; Merk et al., 2022). A Comprehensive Life Cycle Analysis (LCA) considering energy consumption biomass conversion efficiency, and financial cost is pivotal (Fernand et al., 2017; Melara et al., 2020; Capron et al., 2020; Hughes et al., 2012; Aitken et al., 2014).

5 Open Research

The data files used in this paper are available through GEOMAR at (Wu, 2024).

Acknowledgments

Jiajun Wu acknowledges funding from sea4soCiety (FKZ: 03F0896G) of the German Marine Research Alliance (DAM) research mission "Marine carbon sinks in decarbonization pathways" (CDRmare). Wanxuan Yao acknowledges funding from German Federal Ministry of Education and Research under grant agreement 03F0898E. Jiajun Wu and Wanxuan Yao acknowledge the National Key Research and Development Program of China (No. 2020YFA0608304). Andreas Oschlies and David P. Keller acknowledge funding from the EU Horizon 2020 research and innovation program under grant agreement No.869357 (project OceanNETs).

References

Aitken, D., Bulboa, C., Godoy-Faundez, A., Turrion-Gomez, J. L., & Antizar-Ladislao, B. (2014, July). Life cycle assessment of macroalgae cultivation and processing for biofuel production. *Journal of Cleaner Production*, *75*, 45–56. Retrieved 2023-05-18, from `https://linkinghub.elsevier.com/retrieve/pii/S0959652614003138` doi: 10.1016/j.jclepro.2014.03.080

Anton, A., Hendriks, I. E., Marbà, N., Krause-Jensen, D., Garcias-Bonet, N., & Duarte, C. M. (2018). Iron Deficiency in Seagrasses and Macroalgae in the Red Sea Is Unrelated to Latitude and Physiological Performance. *Frontiers in Marine Science*, *5*. Retrieved 2023-07-11, from `https://www.frontiersin.org/articles/10.3389/fmars.2018.00074`

Arzeno-Soltero, I. B., Saenz, B. T., Frieder, C. A., Long, M. C., DeAngelo, J., Davis, S. J., & Davis, K. A. (2023, June). Large global variations in the carbon dioxide removal potential of seaweed farming due to biophysical constraints. *Communications Earth & Environment*, *4*(1), 1–12. Retrieved 2023-06-21, from `https://www.nature.com/articles/s43247-023-00833-2` (Number: 1 Publisher: Nature Publishing Group) doi: 10.1038/s43247-023-00833-2

Bach, L. T., Gill, S. J., Rickaby, R. E. M., Gore, S., & Renforth, P. (2019, October). CO2 Removal With Enhanced Weathering and Ocean Alkalinity Enhancement: Potential Risks and Co-benefits for Marine Pelagic Ecosystems. *Frontiers in Climate*, *1*, 7. Retrieved 2023-05-18, from `https://www.frontiersin.org/article/10.3389/fclim.2019.00007/full` doi: 10.3389/fclim.2019.00007

Bach, L. T., Tamsitt, V., Gower, J., Hurd, C. L., Raven, J. A., & Boyd, P. W. (2021, May). Testing the climate intervention potential of ocean afforestation using the Great Atlantic Sargassum Belt. *Nature Communications*, *12*(1), 2556. Retrieved 2023-05-18, from `https://www.nature.com/articles/s41467-021-22837-2` doi: 10.1038/s41467-021-22837-2

Baker, J., Sturges, W., Sugier, J., Sunnenberg, G., Lovett, A., Reeves, C., … Penkett, S. (2001, January). Emissions of CH3Br, organochlorines, and organoiodines from temperate macroalgae. *Chemosphere - Global Change Science*, *3*(1), 93–106. Retrieved 2023-05-18, from `https://linkinghub.elsevier.com/retrieve/pii/S1465997200000210` doi: 10.1016/S1465-9972(00)00021-0

Bange, H. W., Arévalo-Martínez, D. L., De La Paz, M., Farías, L., Kaiser, J., Kock, A., … Wilson, S. T. (2019, April). A Harmonized Nitrous Oxide (N2O) Ocean Observation Network for the 21st Century. *Frontiers in Marine Science*, *6*, 157. Retrieved 2023-05-18, from `https://www.frontiersin.org/article/10.3389/fmars.2019.00157/full` doi: 10.3389/fmars.2019.00157

Barrón, C., & Duarte, C. M. (2015, October). Dissolved organic carbon pools and export from the coastal ocean: DOC EXPORT COASTAL OCEAN. *Global Biogeochemical Cycles*, *29*(10), 1725–1738. Retrieved 2023-05-18, from `http://doi.wiley.com/10.1002/2014GB005056` doi: 10.1002/2014GB005056

Berger, M., Kwiatkowski, L., Ho, D. T., & Bopp, L. (2023, February). Ocean dynamics and biological feedbacks limit the potential of macroalgae carbon dioxide removal. *Environmental Research Letters*, *18*(2), 024039. Retrieved 2023-05-18, from `https://iopscience.iop.org/article/10.1088/1748-9326/acb06e` doi: 10.1088/1748-9326/acb06e

Bird, M. I., Wurster, C. M., De Paula Silva, P. H., Bass, A. M., & De Nys, R. (2011, January). Algal biochar – production and properties. *Bioresource Technology*, *102*(2), 1886–1891. Retrieved 2023-05-18, from `https://linkinghub.elsevier.com/retrieve/pii/S0960852410013179` doi: 10.1016/j.biortech.2010.07.106

Bitz, C. M., & Lipscomb, W. H. (1999, July). An energy-conserving thermodynamic model of sea ice. *Journal of Geophysical Research: Oceans*, *104*(C7), 15669–15677. Retrieved 2023-05-20, from http://doi.wiley.com/10.1029/1999JC900100 doi: 10.1029/1999JC900100

Borchers, M., Thrän, D., Chi, Y., Dahmen, N., Dittmeyer, R., Dolch, T., … Yeates, C. (2022, October). Scoping carbon dioxide removal options for Germany–What is their potential contribution to Net-Zero CO2? *Frontiers in Climate*, *4*, 810343. Retrieved 2023-05-18, from https://www.frontiersin.org/articles/10.3389/fclim.2022.810343/full doi: 10.3389/fclim.2022.810343

Boyd, P. W., Bach, L. T., Hurd, C. L., Paine, E., Raven, J. A., & Tamsitt, V. (2022, June). Potential negative effects of ocean afforestation on offshore ecosystems. *Nature Ecology & Evolution*, *6*(6), 675–683. Retrieved 2024-01-24, from https://www.nature.com/articles/s41559-022-01722-1 (Number: 6 Publisher: Nature Publishing Group) doi: 10.1038/s41559-022-01722-1

Broch, O. J., & Slagstad, D. (2012, August). Modelling seasonal growth and composition of the kelp Saccharina latissima. *Journal of Applied Phycology*, *24*(4), 759–776. Retrieved 2023-05-18, from http://link.springer.com/10.1007/s10811-011-9695-y doi: 10.1007/s10811-011-9695-y

Buck, B. H., & Buchholz, C. M. (2004, October). The offshore-ring: A new system design for the open ocean aquaculture of macroalgae. *Journal of Applied Phycology*, *16*(5), 355–368. Retrieved 2023-05-18, from http://link.springer.com/10.1023/B:JAPH.0000047947.96231.ea doi: 10.1023/B:JAPH.0000047947.96231.ea

Buesseler, K. O., Andrews, J. E., Pike, S. M., & Charette, M. A. (2004, April). The Effects of Iron Fertilization on Carbon Sequestration in the Southern Ocean. *Science*, *304*(5669), 414–417. Retrieved 2023-07-15, from https://www.science.org/doi/full/10.1126/science.1086895 (Publisher: American Association for the Advancement of Science) doi: 10.1126/science.1086895

Cai, J., Lovatelli, A., Aguilar-Manjarrez, J., Cornish, L., Dabbadie, L., Desrochers, A., … others (2021). Seaweeds and microalgae: an overview for unlocking their potential in global aquaculture development. *FAO Fisheries and Aquaculture Circular*(1229).

Capron, M. E., Stewart, J. R., De Ramon N'Yeurt, A., Chambers, M. D., Kim, J. K., Yarish, C., … Hasan, M. A. (2020, September). Restoring Pre-Industrial CO2 Levels While Achieving Sustainable Development Goals. *Energies*, *13*(18), 4972. Retrieved 2023-05-18, from https://www.mdpi.com/1996-1073/13/18/4972 doi: 10.3390/en13184972

Chavez, F. P., & Messié, M. (2009, December). A comparison of Eastern Boundary Upwelling Ecosystems. *Progress in Oceanography*, *83*(1-4), 80–96. Retrieved 2023-05-20, from https://linkinghub.elsevier.com/retrieve/pii/S0079661109000998 doi: 10.1016/j.pocean.2009.07.032

Chen, H., Zhou, D., Luo, G., Zhang, S., & Chen, J. (2015, July). Macroalgae for biofuels production: Progress and perspectives. *Renewable and Sustainable Energy Reviews*, *47*, 427–437. Retrieved 2023-05-18, from https://linkinghub.elsevier.com/retrieve/pii/S1364032115002397 doi: 10.1016/j.rser.2015.03.086

Chikaraishi, Y., Kashiyama, Y., Ogawa, N., Kitazato, H., & Ohkouchi, N. (2007, July). Metabolic control of nitrogen isotope composition of amino acids in macroalgae and gastropods: implications for aquatic food web studies. *Marine Ecology Progress Series*, *342*, 85–90. Retrieved 2023-05-18, from http://www.int-res.com/abstracts/meps/v342/p85-90/ doi: 10.3354/meps342085

Duarte, C. M., Bruhn, A., & Krause-Jensen, D. (2021, October). A seaweed aquaculture imperative to meet global sustainability targets. *Nature Sustainability*, *5*(3), 185–193. Retrieved 2023-05-18, from https://www.nature.com/

articles/s41893-021-00773-9 doi: 10.1038/s41893-021-00773-9

Duarte, C. M., Gattuso, J., Hancke, K., Gundersen, H., Filbee-Dexter, K., Pedersen, M. F., … Field, R. (2022, July). Global estimates of the extent and production of macroalgal forests. *Global Ecology and Biogeography*, *31*(7), 1422–1439. Retrieved 2023-05-18, from https://onlinelibrary.wiley.com/doi/10.1111/geb.13515 doi: 10.1111/geb.13515

Duarte, C. M., & Krause-Jensen, D. (2017, January). Export from Seagrass Meadows Contributes to Marine Carbon Sequestration. *Frontiers in Marine Science*, *4*. Retrieved 2023-05-18, from http://journal.frontiersin.org/article/10.3389/fmars.2017.00013/full doi: 10.3389/fmars.2017.00013

Eby, M., Weaver, A. J., Alexander, K., Zickfeld, K., Abe-Ouchi, A., Cimatoribus, A. A., … Zhao, F. (2013, May). Historical and idealized climate model experiments: an intercomparison of Earth system models of intermediate complexity. *Climate of the Past*, *9*(3), 1111–1140. Retrieved 2023-05-18, from https://cp.copernicus.org/articles/9/1111/2013/ doi: 10.5194/cp-9-1111-2013

Eby, M., Zickfeld, K., Montenegro, A., Archer, D., Meissner, K. J., & Weaver, A. J. (2009, May). Lifetime of Anthropogenic Climate Change: Millennial Time Scales of Potential CO2 and Surface Temperature Perturbations. *Journal of Climate*, *22*(10), 2501–2511. Retrieved 2023-05-20, from http://journals.ametsoc.org/doi/10.1175/2008JCLI2554.1 doi: 10.1175/2008JCLI2554.1

Falkowski, P., Scholes, R. J., Boyle, E., Canadell, J., Canfield, D., Elser, J., … Steffen, W. (2000, October). The Global Carbon Cycle: A Test of Our Knowledge of Earth as a System. *Science*, *290*(5490), 291–296. Retrieved 2023-05-29, from https://www.science.org/doi/10.1126/science.290.5490.291 doi: 10.1126/science.290.5490.291

Fanning, A. F., & Weaver, A. J. (1996, June). An atmospheric energy-moisture balance model: Climatology, interpentadal climate change, and coupling to an ocean general circulation model. *Journal of Geophysical Research: Atmospheres*, *101*(D10), 15111–15128. Retrieved 2023-05-20, from http://doi.wiley.com/10.1029/96JD01017 doi: 10.1029/96JD01017

FAO (Ed.). (2018). *Meeting the sustainable development goals* (No. 2018). Rome.

Feng, E. Y., Koeve, W., Keller, D. P., & Oschlies, A. (2017, December). Model-Based Assessment of the CO_2 Sequestration Potential of Coastal Ocean Alkalinization. *Earth's Future*, *5*(12), 1252–1266. Retrieved 2023-05-18, from http://doi.wiley.com/10.1002/2017EF000659 doi: 10.1002/2017EF000659

Fernand, F., Israel, A., Skjermo, J., Wichard, T., Timmermans, K. R., & Golberg, A. (2017, August). Offshore macroalgae biomass for bioenergy production: Environmental aspects, technological achievements and challenges. *Renewable and Sustainable Energy Reviews*, *75*, 35–45. Retrieved 2023-05-18, from https://linkinghub.elsevier.com/retrieve/pii/S1364032116307018 doi: 10.1016/j.rser.2016.10.046

Frieder, C. A., Yan, C., Chamecki, M., Dauhajre, D., McWilliams, J. C., Infante, J., … Davis, K. A. (2022, March). A Macroalgal Cultivation Modeling System (MACMODS): Evaluating the Role of Physical-Biological Coupling on Nutrients and Farm Yield. *Frontiers in Marine Science*, *9*, 752951. Retrieved 2023-05-18, from https://www.frontiersin.org/articles/10.3389/fmars.2022.752951/full doi: 10.3389/fmars.2022.752951

Froehlich, H. E., Afflerbach, J. C., Frazier, M., & Halpern, B. S. (2019, September). Blue Growth Potential to Mitigate Climate Change through Seaweed Offsetting. *Current Biology*, *29*(18), 3087–3093.e3. Retrieved 2023-05-18, from https://linkinghub.elsevier.com/retrieve/pii/S0960982219308863 doi: 10.1016/j.cub.2019.07.041

Fréon, P., Barange, M., & Arístegui, J. (2009, December). Eastern Boundary Upwelling Ecosystems: Integrative and comparative approaches. *Progress in Oceanography*, *83*(1-4), 1–14. Retrieved 2023-05-20, from `https://linkinghub.elsevier.com/retrieve/pii/S0079661109001323` doi: 10.1016/j.pocean.2009.08.001

Gao, G., Gao, L., Jiang, M., Jian, A., & He, L. (2022, January). The potential of seaweed cultivation to achieve carbon neutrality and mitigate deoxygenation and eutrophication. *Environmental Research Letters*, *17*(1), 014018. Retrieved 2023-05-18, from `https://iopscience.iop.org/article/10.1088/1748-9326/ac3fd9` doi: 10.1088/1748-9326/ac3fd9

Gattuso, J.-P., Williamson, P., Duarte, C. M., & Magnan, A. K. (2021, January). The Potential for Ocean-Based Climate Action: Negative Emissions Technologies and Beyond. *Frontiers in Climate*, *2*, 575716. Retrieved 2023-05-18, from `https://www.frontiersin.org/articles/10.3389/fclim.2020.575716/full` doi: 10.3389/fclim.2020.575716

GESAMP. (2019). High level review of a wide range of proposed marine geoengineering techniques. In P. W. Boyd & C. M. G. Vivian (Eds.), *Rep. stud. gesamp no. 98* (p. 144).

Goecke, F., Klemetsdal, G., & Ergon, . (2020, February). Cultivar Development of Kelps for Commercial Cultivation—Past Lessons and Future Prospects. *Frontiers in Marine Science*, *8*, 110. Retrieved 2023-05-18, from `https://www.frontiersin.org/article/10.3389/fmars.2020.00110/full` doi: 10.3389/fmars.2020.00110

Hughes, A. D., Black, K. D., Campbell, I., Davidson, K., Kelly, M. S., & Stanley, M. S. (2012, December). Does seaweed offer a solution for bioenergy with biological carbon capture and storage? *Greenhouse Gases: Science and Technology*, *2*(6), 402–407. Retrieved 2023-05-23, from `https://onlinelibrary.wiley.com/doi/10.1002/ghg.1319` doi: 10.1002/ghg.1319

IEA. (2023). *Co2 emissions in 2022.* Paris: International Energy Agency. Retrieved from `https://www.iea.org/reports/co2-emissions-in-2022` (License: CC BY 4.0)

IPCC. (2022). Summary for Policymakers. In P. Shukla et al. (Eds.), *Climate change 2022: Mitigation of climate change. contribution of working group iii to the sixth assessment report of the intergovernmental panel on climate change.* Cambridge, UK and New York, NY, USA: Cambridge University Press. doi: 10.1017/9781009157926.001

Jacobucci, G. B., Güth, A. Z., & Leite, F. P. P. (2008). Experimental evaluation of amphipod grazing over biomass of Sargassum filipendula (Phaeophyta) and its dominant epiphyte. *Nauplius.*

Jia, Y., Quack, B., Kinley, R. D., Pisso, I., & Tegtmeier, S. (2022, June). Potential environmental impact of bromoform from *Asparagopsis* farming in Australia. *Atmospheric Chemistry and Physics*, *22*(11), 7631–7646. Retrieved 2024-02-27, from `https://acp.copernicus.org/articles/22/7631/2022/` (Publisher: Copernicus GmbH) doi: 10.5194/acp-22-7631-2022

Keller, D. P., Brent, K., Bach, L. T., & Rickels, W. (2021, August). Editorial: The Role of Ocean-Based Negative Emission Technologies for Climate Mitigation. *Frontiers in Climate*, *3*, 743816. Retrieved 2023-05-18, from `https://www.frontiersin.org/articles/10.3389/fclim.2021.743816/full` doi: 10.3389/fclim.2021.743816

Keller, D. P., Feng, E. Y., & Oschlies, A. (2014, February). Potential climate engineering effectiveness and side effects during a high carbon dioxide-emission scenario. *Nature Communications*, *5*(1), 3304. Retrieved 2023-05-20, from `https://www.nature.com/articles/ncomms4304` doi: 10.1038/ncomms4304

Keller, D. P., Lenton, A., Littleton, E. W., Oschlies, A., Scott, V., & Vaughan, N. E. (2018, September). The Effects of Carbon Dioxide Removal on the Carbon

Cycle. *Current Climate Change Reports*, *4*(3), 250–265. Retrieved 2023-05-18, from http://link.springer.com/10.1007/s40641-018-0104-3 doi: 10.1007/s40641-018-0104-3

Keller, D. P., Lenton, A., Scott, V., Vaughan, N. E., Bauer, N., Ji, D., … Zickfeld, K. (2018, March). The Carbon Dioxide Removal Model Intercomparison Project (CDRMIP): rationale and experimental protocol for CMIP6. *Geoscientific Model Development*, *11*(3), 1133–1160. Retrieved 2023-05-18, from https://gmd.copernicus.org/articles/11/1133/2018/ doi: 10.5194/gmd-11-1133-2018

Keller, D. P., Oschlies, A., & Eby, M. (2012, September). A new marine ecosystem model for the University of Victoria Earth System Climate Model. *Geoscientific Model Development*, *5*(5), 1195–1220. Retrieved 2024-02-05, from https://gmd.copernicus.org/articles/5/1195/2012/gmd-5-1195-2012.html (Publisher: Copernicus GmbH) doi: 10.5194/gmd-5-1195-2012

Krause-Jensen, D., & Duarte, C. M. (2016, October). Substantial role of macroalgae in marine carbon sequestration. *Nature Geoscience*, *9*(10), 737–742. Retrieved 2024-01-18, from https://www.nature.com/articles/ngeo2790 doi: 10.1038/ngeo2790

Leedham, E. C., Hughes, C., Keng, F. S. L., Phang, S.-M., Malin, G., & Sturges, W. T. (2013, June). Emission of atmospherically significant halocarbons by naturally occurring and farmed tropical macroalgae. *Biogeosciences*, *10*(6), 3615–3633. Retrieved 2023-05-18, from https://bg.copernicus.org/articles/10/3615/2013/ doi: 10.5194/bg-10-3615-2013

Lehahn, Y., Ingle, K. N., & Golberg, A. (2016, July). Global potential of offshore and shallow waters macroalgal biorefineries to provide for food, chemicals and energy: feasibility and sustainability. *Algal Research*, *17*, 150–160. Retrieved 2023-05-18, from https://linkinghub.elsevier.com/retrieve/pii/S2211926416301151 doi: 10.1016/j.algal.2016.03.031

Meinshausen, M., Smith, S. J., Calvin, K., Daniel, J. S., Kainuma, M. L. T., Lamarque, J.-F., … Van Vuuren, D. P. (2011, November). The RCP greenhouse gas concentrations and their extensions from 1765 to 2300. *Climatic Change*, *109*(1-2), 213–241. Retrieved 2023-05-18, from http://link.springer.com/10.1007/s10584-011-0156-z doi: 10.1007/s10584-011-0156-z

Meissner, K. J., Weaver, A. J., Matthews, H. D., & Cox, P. M. (2003, December). The role of land surface dynamics in glacial inception: a study with the UVic Earth System Model. *Climate Dynamics*, *21*(7-8), 515–537. Retrieved 2023-05-18, from http://link.springer.com/10.1007/s00382-003-0352-2 doi: 10.1007/s00382-003-0352-2

Melara, A. J., Singh, U., & Colosi, L. M. (2020, November). Is aquatic bioenergy with carbon capture and storage a sustainable negative emission technology? Insights from a spatially explicit environmental life-cycle assessment. *Energy Conversion and Management*, *224*, 113300. Retrieved 2023-05-18, from https://linkinghub.elsevier.com/retrieve/pii/S0196890420308396 doi: 10.1016/j.enconman.2020.113300

Merk, C., Grunau, J., Riekhof, M.-C., & Rickels, W. (2022, November). The need for local governance of global commons: The example of blue carbon ecosystems. *Ecological Economics*, *201*, 107581. Retrieved 2023-07-19, from https://www.sciencedirect.com/science/article/pii/S0921800922002439 doi: 10.1016/j.ecolecon.2022.107581

N'Yeurt, A. D. R., Chynoweth, D. P., Capron, M. E., Stewart, J. R., & Hasan, M. A. (2012, November). Negative carbon via Ocean Afforestation. *Process Safety and Environmental Protection*, *90*(6), 467–474. Retrieved 2023-05-18, from https://linkinghub.elsevier.com/retrieve/pii/S0957582012001206 doi: 10.1016/j.psep.2012.10.008

Ortega, A., Geraldi, N. R., Alam, I., Kamau, A. A., Acinas, S. G., Logares, R., …

Duarte, C. M. (2019, September). Important contribution of macroalgae to oceanic carbon sequestration. *Nature Geoscience*, *12*(9), 748–754. doi: 10.1038/s41561-019-0421-8
Oschlies, A. (2009, August). Impact of atmospheric and terrestrial CO_2 feedbacks on fertilization-induced marine carbon uptake. *Biogeosciences*, *6*(8), 1603–1613. Retrieved 2023-09-06, from https://bg.copernicus.org/articles/6/1603/2009/ (Publisher: Copernicus GmbH) doi: 10.5194/bg-6-1603-2009
Oschlies, A., Pahlow, M., Yool, A., & Matear, R. J. (2010, February). Climate engineering by artificial ocean upwelling: Channelling the sorcerer's apprentice: OCEAN PIPE IMPACTS. *Geophysical Research Letters*, *37*(4). Retrieved 2023-05-20, from http://doi.wiley.com/10.1029/2009GL041961 doi: 10.1029/2009GL041961
Pacanowski, R. C. (1996). Documentation user's guide and reference manual (mom2, version 2). *GFDL Ocean Technical Report 3.2*, *329*.
Paine, E. R., Boyd, P. W., Strzepek, R. F., Ellwood, M., Brewer, E. A., Diaz-Pulido, G., … Hurd, C. L. (2023, June). Iron limitation of kelp growth may prevent ocean afforestation. *Communications Biology*, *6*(1), 1–9. Retrieved 2023-07-11, from https://www.nature.com/articles/s42003-023-04962-4 (Number: 1 Publisher: Nature Publishing Group) doi: 10.1038/s42003-023-04962-4
Pedersen, M., Filbee-Dexter, K., Frisk, N., Sárossy, Z., & Wernberg, T. (2021, February). Carbon sequestration potential increased by incomplete anaerobic decomposition of kelp detritus. *Marine Ecology Progress Series*, *660*, 53–67. Retrieved 2023-05-18, from https://www.int-res.com/abstracts/meps/v660/p53-67/ doi: 10.3354/meps13613
Peteiro, C., Sánchez, N., Dueñas-Liaño, C., & Martínez, B. (2014, February). Open-sea cultivation by transplanting young fronds of the kelp Saccharina latissima. *Journal of Applied Phycology*, *26*(1), 519–528. Retrieved 2023-05-18, from http://link.springer.com/10.1007/s10811-013-0096-2 doi: 10.1007/s10811-013-0096-2
Ravishankara, A. R., Daniel, J. S., & Portmann, R. W. (2009, October). Nitrous Oxide (N_2O): The Dominant Ozone-Depleting Substance Emitted in the 21st Century. *Science*, *326*(5949), 123–125. Retrieved 2023-05-18, from https://www.science.org/doi/10.1126/science.1176985 doi: 10.1126/science.1176985
Ricart, A. M., Krause-Jensen, D., Hancke, K., Price, N. N., Masqué, P., & Duarte, C. M. (2022, August). Sinking seaweed in the deep ocean for carbon neutrality is ahead of science and beyond the ethics. *Environmental Research Letters*, *17*(8), 081003. Retrieved 2023-05-18, from https://iopscience.iop.org/article/10.1088/1748-9326/ac82ff doi: 10.1088/1748-9326/ac82ff
Roberts, D. A., Paul, N. A., Dworjanyn, S. A., Bird, M. I., & De Nys, R. (2015, April). Biochar from commercially cultivated seaweed for soil amelioration. *Scientific Reports*, *5*(1), 9665. Retrieved 2023-05-18, from https://www.nature.com/articles/srep09665 doi: 10.1038/srep09665
Sarmiento, J. L., & Gruber, N. (2013). *Ocean Biogeochemical Dynamics.* Princeton University Press. Retrieved 2023-05-29, from http://www.jstor.org/stable/10.2307/j.ctt3fgxqx doi: 10.2307/j.ctt3fgxqx
Schmittner, A., Oschlies, A., Matthews, H. D., & Galbraith, E. D. (2008). Future changes in climate, ocean circulation, ecosystems, and biogeochemical cycling simulated for a business-as-usual CO2 emission scenario until year 4000 AD. *Global Biogeochemical Cycles*, *22*(1). Retrieved 2023-11-12, from https://onlinelibrary.wiley.com/doi/abs/10.1029/2007GB002953 (_eprint: https://onlinelibrary.wiley.com/doi/pdf/10.1029/2007GB002953) doi: 10.1029/2007GB002953
Siegel, D. A., DeVries, T., Doney, S. C., & Bell, T. (2021, October). Assessing the sequestration time scales of some ocean-based carbon dioxide reduction strate-

gies. *Environmental Research Letters*, *16*(10), 104003. Retrieved 2023-05-18, from https://iopscience.iop.org/article/10.1088/1748-9326/ac0be0 doi: 10.1088/1748-9326/ac0be0

Thomson, A. M., Calvin, K. V., Smith, S. J., Kyle, G. P., Volke, A., Patel, P., … Edmonds, J. A. (2011, November). RCP4.5: a pathway for stabilization of radiative forcing by 2100. *Climatic Change*, *109*(1-2), 77–94. Retrieved 2023-05-18, from http://link.springer.com/10.1007/s10584-011-0151-4 doi: 10.1007/s10584-011-0151-4

Tivig, M., Keller, D. P., & Oschlies, A. (2021, October). Riverine nitrogen supply to the global ocean and its limited impact on global marine primary production: a feedback study using an Earth system model. *Biogeosciences*, *18*(19), 5327–5350. Retrieved 2023-06-19, from https://bg.copernicus.org/articles/18/5327/2021/ (Publisher: Copernicus GmbH) doi: 10.5194/bg-18-5327-2021

Van Der Molen, J., Ruardij, P., Mooney, K., Kerrison, P., O'Connor, N. E., Gorman, E., … Capuzzo, E. (2018, February). Modelling potential production of macroalgae farms in UK and Dutch coastal waters. *Biogeosciences*, *15*(4), 1123–1147. Retrieved 2023-05-18, from https://bg.copernicus.org/articles/15/1123/2018/ doi: 10.5194/bg-15-1123-2018

Wada, S., & Hama, T. (2013, September). The contribution of macroalgae to the coastal dissolved organic matter pool. *Estuarine, Coastal and Shelf Science*, *129*, 77–85. Retrieved 2023-05-18, from https://linkinghub.elsevier.com/retrieve/pii/S0272771413002722 doi: 10.1016/j.ecss.2013.06.007

Weaver, A. J., Eby, M., Wiebe, E. C., Bitz, C. M., Duffy, P. B., Ewen, T. L., … Yoshimori, M. (2001, December). The UVic earth system climate model: Model description, climatology, and applications to past, present and future climates. *Atmosphere-Ocean*, *39*(4), 361–428. Retrieved 2023-05-18, from https://www.tandfonline.com/doi/full/10.1080/07055900.2001.9649686 doi: 10.1080/07055900.2001.9649686

Wu, J. (2024). *Supplementary data to Wu et al. (2024): Nearshore Macroalgae Cultivation for Carbon Sequestration by Biomass Harvesting: An Evaluation of Potential and Impacts Utilizing an Earth System Model [Data].* GEOMAR Helmholtz Centre for Ocean Research Kiel https://hdl.handle.net/20.500.12085/31ae24e4-98a6-452e-8b55-f27372f9b571.

Wu, J., Keller, D. P., & Oschlies, A. (2023, February). Carbon dioxide removal via macroalgae open-ocean mariculture and sinking: an Earth system modeling study. *Earth System Dynamics*, *14*(1), 185–221. Retrieved 2023-05-18, from https://esd.copernicus.org/articles/14/185/2023/ doi: 10.5194/esd-14-185-2023

Yokoyama, S., Jonouchi, K., & Imou, K. (2007). Energy production from marine biomass: fuel cell power generation driven by methane produced from seaweed. *International Journal of Marine and Environmental Sciences*, *1*(4), 24–27.

Zhang, J., Liu, T., Bian, D., Zhang, L., Li, X., Liu, D., … Xiao, L. (2016, December). Breeding and genetic stability evaluation of the new Saccharina variety "Ailunwan" with high yield. *Journal of Applied Phycology*, *28*(6), 3413–3421. Retrieved 2023-05-18, from http://link.springer.com/10.1007/s10811-016-0810-y doi: 10.1007/s10811-016-0810-y

Zhang, J., Liu, Y., Yu, D., Song, H., Cui, J., & Liu, T. (2011, April). Study on high-temperature-resistant and high-yield Laminaria variety "Rongfu". *Journal of Applied Phycology*, *23*(2), 165–171. Retrieved 2023-05-18, from http://link.springer.com/10.1007/s10811-011-9650-y doi: 10.1007/s10811-011-9650-y

Figure 1.

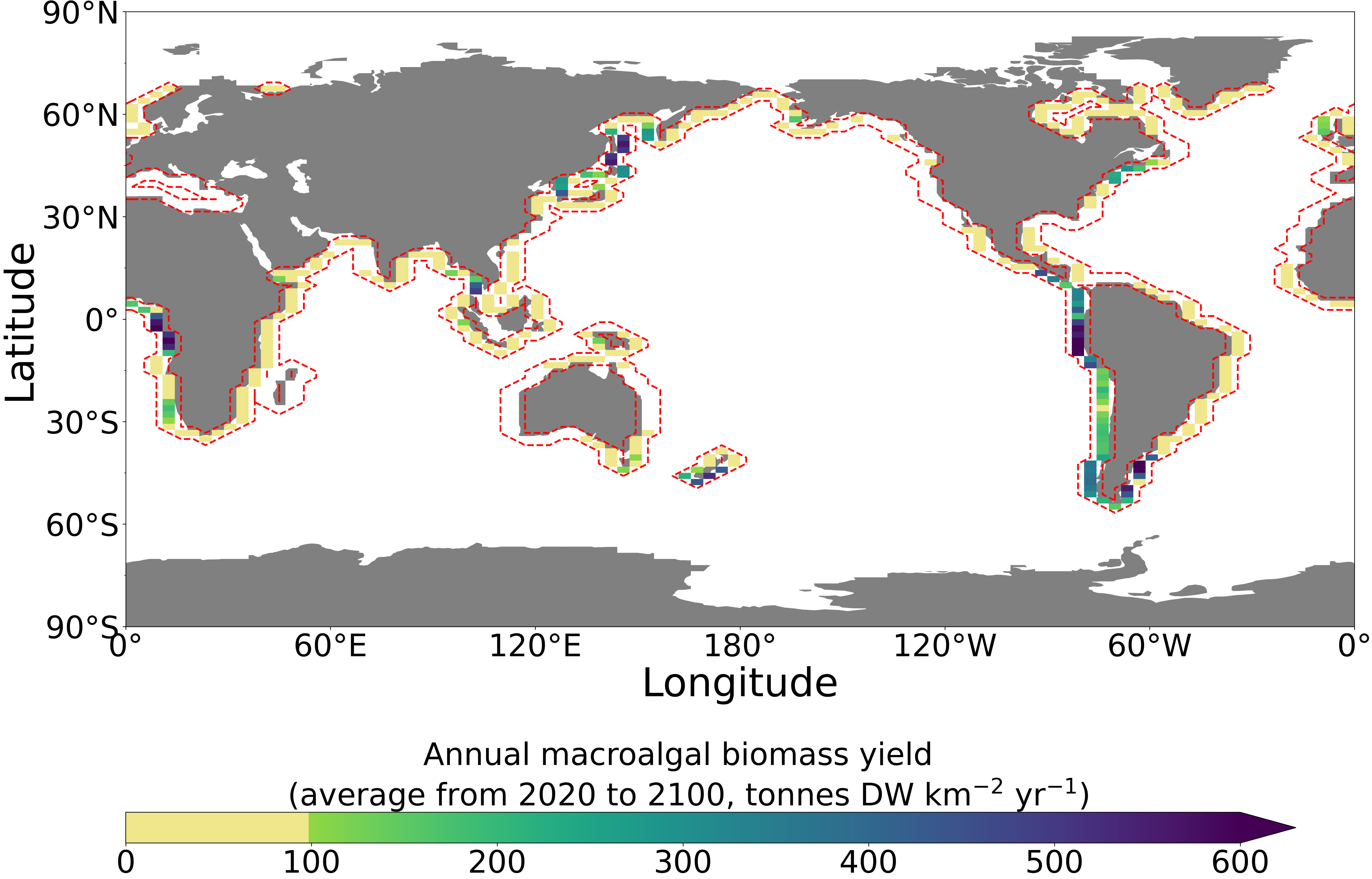

90°N
60°N
30°N
0°
30°S
60°S
90°S
Latitude
0°
60°E
120°E
180°
120°W
60°W
0°
Longitude
Annual macroalgal biomass yield
(average from 2020 to 2100, tonnes DW km^{-2} yr^{-1})
0
100
200
300
400
500
600

Figure 2.

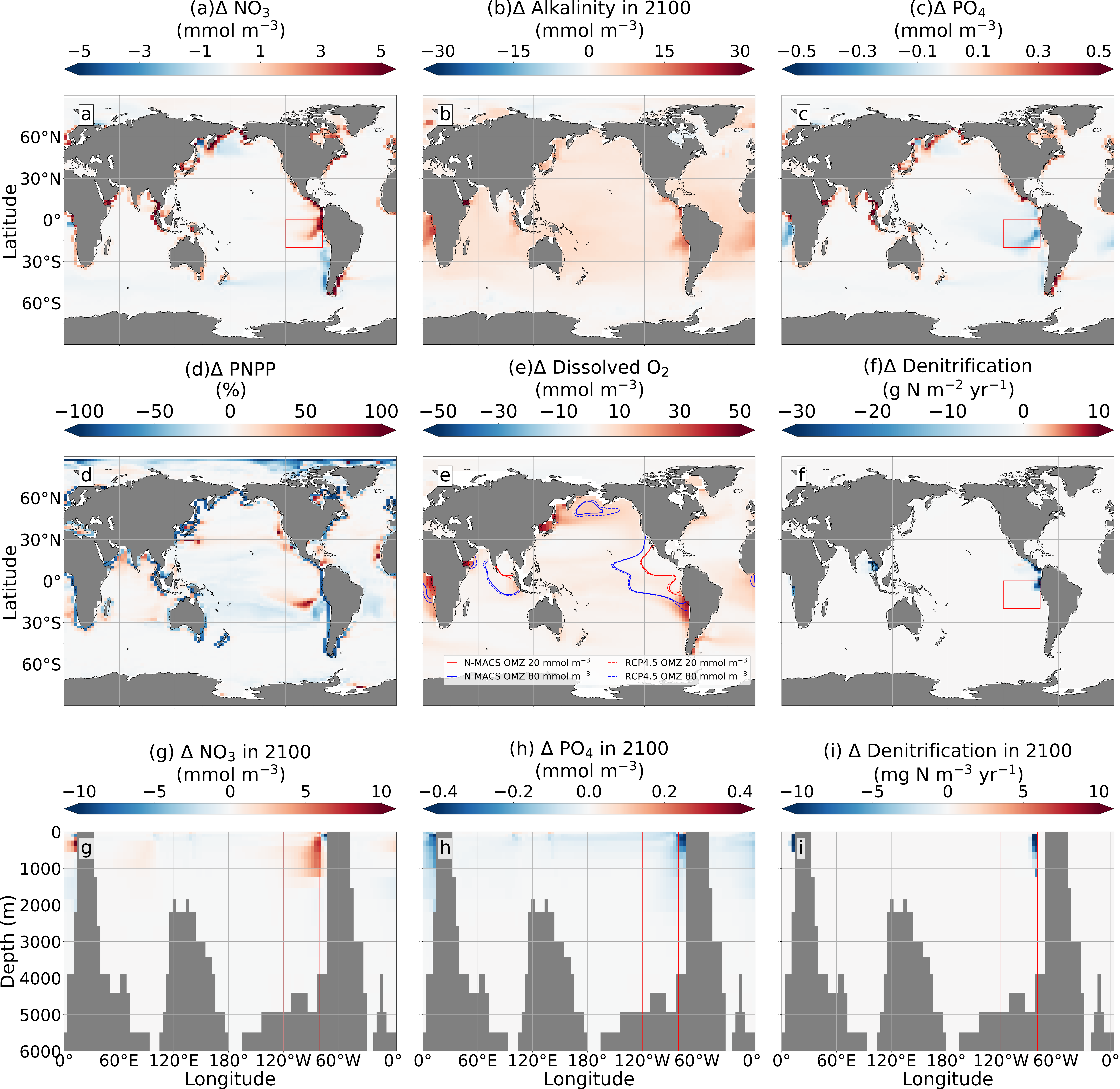

(a)Δ NO3 (mmol m−3)
(b)Δ Alkalinity in 2100 (mmol m−3)
(c)Δ PO4 (mmol m−3)
(d)Δ PNPP (%)
(e)Δ Dissolved O2 (mmol m−3)
(f)Δ Denitrification (g N m−2 yr−1)
N-MACS OMZ 20 mmol m−3
N-MACS OMZ 80 mmol m−3
RCP4.5 OMZ 20 mmol m−3
RCP4.5 OMZ 80 mmol m−3
(g) Δ NO3 in 2100 (mmol m−3)
(h) Δ PO4 in 2100 (mmol m−3)
(i) Δ Denitrification in 2100 (mg N m−3 yr−1)
Latitude
Depth (m)
Longitude

Figure 3.


(a) Global surface integrated PO4
Tmol
(b) Global surface integrated NO3
Tmol
(c) Global integrated PO4
Pmol
(d) Global integrated NO3
Pmol
(e) Averaged PNPP rate
mgC m−2 yr−1
(f) Global integrated POC export rate
Gt C yr−1
(g) Averaged O2 at 300m
mmol m2
(h) Global integrated N2 fixation
Pg N yr−1
Year
N-MOS
No_Temp
Ctrl_RCP4.5

Nearshore Macroalgae Cultivation for Carbon Sequestration by Biomass Harvesting: Evaluating Potential and Impacts with An Earth System Model

Jiajun Wu[1,3], Wanxuan Yao[1], David. P. Keller[1], Andreas Oschlies[1,2]

[1]GEOMAR Helmholtz Centre for Ocean Research Kiel, Wischhofstr. 1-3, 24148 Kiel, Germany
[2]Kiel University, Christian-Albrechts-Platz 4, 24118 Kiel, Germany
[3]Alfred Wegener Institute Helmholtz Center for Marine and Polar Research, Am Handelshafen 12, 27570 Bremerhaven, Germany

Key Points:

- Offshore marcoalgae cultivation for CDR has a global potential of gigatonnes scale.
- Partition of marine net primary production shifts from phytoplankton to macroalgae due to shading and nutrient robbing.
- Open ocean net primary production reduces the oxygen deficit zones.

Corresponding author: Jiajun Wu, jwu@geomar.de

Abstract

This study introduces an ocean-based carbon dioxide removal (CDR) approach: Nearshore Macroalgae Aquaculture for Carbon Sequestration (N-MACS). By cultivating macroalgae in nearshore ocean surface areas, N-MACS aims to sequester CO_2 with subsequent carbon storage. Utilizing an Earth System Model with intermediate complexity (EMIC), we explore the CDR potential of N-MACS alongside its impacts on the global carbon cycle, marine biogeochemistry and marine ecosystems. Our investigations unveil that coastal N-MACS could potentially sequester 0.7 to 1.1 GtC yr^{-1}. However, it also significantly suppresses marine phytoplankton net primary productivity because of nutrient removal and canopy shading, counteracting approximately 30% of the N-MACS CDR capacity. This suppression of surface NPP, in turn, reduces carbon export out of the euphotic zone to the ocean interior, leading to elevated dissolved oxygen levels and diminished denitrification in present-day oxygen minimum zones. Effects due to harvesting-induced phosphorus removal continue for centuries even beyond the cessation of N-MACS.

Plain Language Summary

Our study explores the Nearshore Macroalgae Aquaculture for Carbon Sequestration (N-MACS) as a potential marine carbon dioxide removal strategy. This approach uses ocean-based seaweed farming to capture carbon dioxide —-the main greenhouse gas causing global warming-— and permanently stores it post harvesting through biomass processing and carbon storage. Our simulations indicate that N-MACS has the potential to remove substantial quantities of carbon dioxide every year. Nonetheless, harvesting will also remove oceanic nutrients and decrease open ocean primary production. At the same time, N-MACS can relieve the oxygen scarcity and mitigate surface ocean acidification. Those impacts on the oceanic ecosystem and marine biogeochemistry could potentially persist for centuries, upon the cessation of N-MACS.

1 Introduction

The IPCC's Sixth Assessment Report (IPCC (2022)) stipulates global net-zero CO_2 emissions by the early 2050s to restrict global warming to 1.5°C, recognizing Carbon Dioxide Removal (CDR) as essential to counterbalance residual emissions. Ocean-based CDR approaches are gaining traction due to the ocean's inherent carbon sequestration capacity (IPCC, 2022; Keller et al., 2021; GESAMP, 2019). As the Earth's largest dynamic carbon reservoir (Falkowski et al., 2000; Sarmiento & Gruber, 2013), the ocean's expanse and natural carbon absorption capacity, combined with measures like ocean fertilization, ocean alkalinity enhancement, can substantially augment carbon sequestration efforts (Buesseler et al., 2004; Bach et al., 2019).

Macroalgae offer an avenue for ocean-based CDR due to their notable net primary production rates and high carbon-to-nutrient ratios, facilitating effective carbon sequestration (N'Yeurt et al., 2012; Fernand et al., 2017; Gao et al., 2022). The global potential carbon export by macroalgae has been estimated as 1.4 GtC per year (Krause-Jensen & Duarte, 2016; Ortega et al., 2019; Barrón & Duarte, 2015). Cultivation technologies for macroalgae are well-established (e.g., Buck and Buchholz (2004); Goecke et al. (2020); Zhang et al. (2016)), with a global harvest reaching 34.7 million tonnes wet weight (WW) in 2019 (FAO, 2018; Cai et al., 2021). Macroalgae cultivation for ocean-CDR has been considered recently (Wu et al., 2023; Fernand et al., 2017). Based on geographic location, macroalgae-based CDR can be categorized into two categories: open-ocean cultivation with deep-ocean carbon storage (Wu et al., 2023; Bach et al., 2021), and nearshore cultivation for harvesting, followed by subsequent carbon storage achieved outside of the ocean such as biochar and Bioenergy with Carbon Capture and Storage (BECCS, Roberts et al. (2015); Bird et al. (2011); Fernand et al. (2017); Gattuso et al. (2021); Capron et al. (2020); Borchers et al. (2022); Chen et al. (2015)).

Prior to the large-scale implementation of ocean-based CDR strategies, comprehensive evaluations are essential to understand their potential and impacts on the marine environment (IPCC, 2022; Gattuso et al., 2021). Particularly, numerical simulations with Earth system models are pivotal as they, in contrast to field experiments pose, have no direct environmental impact (Oschlies et al., 2010; Keller et al., 2014; Keller, Lenton, Scott, et al., 2018; Siegel et al., 2021). Several modelling studies have examined macroalgae-based CDR strategies, revealing CDR capacities ranging from Mega (10^6) to Giga (10^9) tonnes depending on location and species. These studies, referenced as Wu et al. (2023); Bach et al. (2019) for open-ocean and Arzeno-Soltero et al. (2023); Berger et al. (2023) for nearshore areas, also underscore the constraints posed by marine physical and biogeochemical feedbacks on CDR capacity and efficiency. Furthermore, they highlight the potentially significant impacts on the global carbon cycle, marine biogeochemistry, and ecosystems through the alteration of ocean nutrient distributions and primary production patterns.

Here we evaluate 'Nearshore Macroalgae Aquaculture for Carbon Sequestration' (hereinafter N-MACS), operating under the assumption that the harvested carbon content will be sequestered from atmosphere and hence achieving CDR. The evaluation employs an Earth System Model of intermediate complexity, encompassing an explicit macroalgae component, to rigorously assess implications and carbon sequestration efficacy of N-MACS from 2020 to 3000, with N-MACS deployment from 2020 to 2100. Our objectives are to: a) examine the idealised large-scale CDR potential of N-MACS, and b) evaluate its effects on the global carbon cycle and marine biogeochemistry, including termination effects and millennial long-term effects.

2 Methods

We employ the University of Victoria Earth System Climate Model version 2.9 (UVic; Keller et al. (2012); Weaver et al. (2001)), an intermediate complexity Earth system model coupling a three-dimensional ocean circulation model (Pacanowski, 1996) including a dynamic thermodynamic sea ice module (Bitz & Lipscomb, 1999), a terrestrial model (Meissner et al., 2003; Weaver et al., 2001) and a one-layer atmospheric energy-moisture model (Fanning & Weaver, 1996). The horizontal resolution is 3.6° longitude × 1.8° latitude, and the ocean component has 19 vertical layers with thicknesses ranging from 50 m near the surface to 500 m in the deep ocean. The ocean biogeochemistry module includes nutrients (nitrogen and phosphate), one general phytoplankton type, and one diazotrophic phytoplankton (i.e., nitrogen fixers), one general macroalgae (see below section), one type of zooplankton, dissolved inorganic carbon, oxygen, and total alkalinity (Keller et al., 2012; Eby et al., 2013).

Upon spinning up the model under pre-industrial conditions, we employed CMIP5 forcing data for the historical period (Eby et al., 2013). From 2005 to 2100, we aligned the inputs of CO_2 emissions, land-use changes, volcanic radiative forcing, and sulfate aerosols with the RCP4.5 scenario. For the period post-2300, CO_2 emissions are projected to decline linearly, reaching zero by 3000, with other forcings maintained at constant levels. RCP4.5 is a moderate emissions trajectory with a radiative forcing of 4.5 W/m^2 by 2100 (Thomson et al., 2011; Meinshausen et al., 2011).

N-MACS is an extension of the Macroalgae Open-ocean Mariculture and Sinking (MOS) framework developed by (Wu et al., 2023), featuring an idealized generic model of the Phaeophyceae (brown algae) *Sacharina* integrated with UVic. Macroalgae growth is controlled by multiple limiting factors (erosion, nutrient availability, light, and temperature) with a fixed C:N:P stoichiometric molar ratio of 400:20:1. Initial seed biomass is deployed in each surface ocean grid box with adequate nutrients to be converted into seed biomass. The initial plantlet biomass in each N-MACS grid cell is equivalent to 0.02 mmol N m^{-3}, sourced directly from the grid box's inorganic N, P, and C pools without extra nutrient or carbon input. A constant maximum biomass yield of 3,300 tDW km^{-2} is set, focusing on large-scale impacts rather than optimizing farming strategies. Once biomass in a grid cell reaches this limit, macroalgae growth halts until end-of-season harvesting. In temperate zones, seeding starts on May 1st and harvesting occurs on October 31st in the northern hemisphere, while in the southern hemisphere, seeding begins on November 1 with harvesting on April 30, aligning with macroalgae growth phases. The model annually selects grid boxes with ample nutrients for reseeding, implying no further reseeding post-harvest in nutrient-depleted regions (detailed in Section 3.1, Wu et al. (2023)). Additionally, surface layer macroalgae create canopy shading effects on phytoplankton communities. Potential grazers like amphipods and gastropods (Jacobucci et al., 2008; Chikaraishi et al., 2007) are modeled within the UVic's zooplankton compartment (Keller et al., 2012). Further macroalgae model specifics, including parameters, functions, and cultivation strategies, are delineated in Wu et al. (2023, Sect. 2).

2.1 Experimental design

Our study contains a control run (Ctrl_RCP4.5) and two N-MACS simulations: the standard N-MACS simulation with all growth constraints, and a sensitivity simulation (No_Temp) with temperature constraint removed to examine the uncertainty in temperature-dependant growth rate in the modeled macroalgae. In both N-MACS simulations, macroalgae farms are limited to ocean surface zones directly along coasts between 60°S and 60°N, with grid boxes 200 to 400 km wide, aligning with Exclusive Economic Zones (EEZs) extending to 200 nautical miles from sovereign state coasts (Froehlich et al., 2019; Feng et al., 2017). It's presumed that all macroalgae production is promptly harvested post cultivation for biochar conversion or BECCS feedstock on land, indicating permanent carbon sequestration from the biomass with no nutrient return to the ocean. Meanwhile, natural macroalgae habitats are globally distributed along coastlines with species exhibiting varied temperature sensitivities (Duarte et al., 2022). The No_Temp simulation investigates the theoretical maximum coastal macroalgae biomass production with species optimally adapted to local temperatures. N-MACS CDR capacity is defined as the total carbon in harvested biomass, while its CDR efficacy is defined by the changes in combined oceanic and macroalgae carbon reservoir relative to the harvested macroalgal biomass carbon content. Our focus is on the the cultivation process outcomes, excluding possible carbon leakages in post-harvest CDR applications like biochar or BECCS (Chen et al., 2015; Fernand et al., 2017; Bird et al., 2011).

3 Results & Discussions

3.1 Macroalgae model validation

The employed macroalgae model was validated against literature data and used in idealized open-ocean cultivation simulations by Wu et al. (2023). Given the notable nutrient availability differences between nearshore regions and open oceans, we compare the productivity of simulated nearshore macroalgae with relevant observational and modeling data.

Fig.1 illustrates the N-MACS distribution and its mean annual biomass yield from 2020 to 2100. Simulations indicate a total N-MACS footprint of about 24 million km^2, with 14 to 15 million km^2 yielding significant productivity (over 100 tonnes DW $km^{-2}yr^{-1}$; Tab.1). These values are lower than other model-based estimates ranging from 48 to 100 million km^2 (Froehlich et al., 2019; Lehahn et al., 2016; Berger et al., 2023), hence presenting a more conservative N-MACS productivity. The reduced macroalgae farming areas in our model result from several factors: suboptimal UVic simulation of nutrient concentrations in nearshore regions without land run-off (Eby et al., 2009; Keller et al., 2012; Tivig et al., 2021), unique parameters for chosen brown algae species in our dynamic growth model (Froehlich et al., 2019), consistent nutrient feedback consideration unlike earlier assessments (Froehlich et al., 2019; Lehahn et al., 2016), and the assumption that farms are located within EEZs (Lehahn et al., 2016). Despite these differences, the N-MACS distribution pattern aligns with those in Lehahn et al. (2016, Fig. 3. A), Berger et al. (2023, Figure 4), Duarte et al. (2022, greenish pattern of Figure 1(a)), and Froehlich et al. (2019, Figure 1). While the total N-MACS area remains steady over time, regions of significant productivity (significant N-MACS areas) expand during the initial deployment decade (Fig.S11), resulting from dynamic nutrient cycling. Here, N-MACS suppresses phytoplankton due to canopy shading (Fig.S3), creating a nutrient surplus within its habitat that fertilizes N-MACS (see Sect.3.3).

In productive N-MACS regions, simulated macroalgae productivity averages 165 tonnes DW km^{-2} yr^{-1}, rising to 223 tonnes DW km^{-2} yr^{-1} in No_Temp (Tab.1). Farmed seaweed productivity, including the modeled *Saccharina* species, varies significantly depending on species, cultivation techniques, and environmental conditions. Reported *Saccharina* yields in Europe range from 4 to 450 tonnes DW km^{-2} yr^{-1} (Peteiro et al., 2014; Buck & Buchholz, 2004), while in northeast Asia, yields can reach 2,400-3,000 tonnes DW km^{-2} yr^{-1} (Yokoyama et al., 2007; Zhang et al., 2011).

Although N-MACS farms were initially established in all ocean grid boxes adjacent to land between 60°S and 60°N in year 2020, sustainable biomass harvests are mainly found in four regions with high nutrient availability: the Eastern Boundary Upwelling Systems in the nearshore Pacific regions of South America and the Atlantic coasts of Africa (Chavez & Messié, 2009; Fréon et al., 2009), the northeast Pacific and the Southern Ocean (Tab.S1). This is consistent with the findings of Berger et al. (2023), Arzeno-Soltero et al. (2023), and Duarte et al. (2021).

In the sensitivity study (No_Temp), where temperature no longer affects macroalgae growth, the N-MACS distribution mirrors the base case, albeit with increased biomass productivity in mid to high latitudinal coastal regions (Tab.1, Fig.S2). By employing local macroalgae species better adapted to specific temperature ranges, optimization of macroalgae cultivation and enhancement of the CDR potential of nearshore macroalgae-based strategies may be achievable.

Table 1. Summary table of N-MACS simulations. Significant N-MACS area is area with ≥100 tonnes DW per km^2 per year. The changes are N-MACS variations relative to Ctrl_RCP4.5.

	Unit	**N-MACS**	**No_Temp**
Total yield	Gt DW	188.96	293.40
N-MACS total area	10^6 km^2	24.34	23.65
Significant N-MACS area		14.29	15.97
Total carbon fixation in N-MACS	GtC	56.7	88.0
Annual carbon fixation (avg. 2020 to 2100)	GtC yr^{-1}	0.7	1.1
Annual unit area carbon fixation	tC km^{-2} yr^{-1}	29.1	46.5
Change of global climate system in 2100 (3000 in parentheses)			
Surface averaged temperature (SAT)	°C	-0.07 (-0.08)	-0.12 (-0.13)
Atmospheric CO_2 concentration	ppm	-14.2 (-12.0)	-22.6 (-18.3)
Change of global carbon reservoirs in 2100 (3000 in parentheses)			
Atmosphere		-30.1 (-25.5)	-47.9 (-38.9)
Ocean (including carbon fixation by N-MACS)	GtC	35.9 (31.4)	57.1 (48.8)
Land		-5.8 (-5.9)	-9.2 (-9.9)
Change of integrated marine biogeochemical parameters in 2100 (3000 in parentheses)			
POM export at 2km depth	GtC yr^{-1}	-4.151 (0.37)	-7.245 (0.58)
PO_4 (full depth)	Tmol	-11.64 (-11.91)	-18.10 (-18.49)
NO_3 (full depth)	Tmol	7.68 (15.78)	-62.51 (-6.01)
Phytoplankton NPP	GtC yr^{-1}	-0.36 (-0.52)	-0.50 (-0.82)

∗ DW: dry weight; POM: particle organic matter; tC: tonnes of carbon (10^3 Kg);
GtC: Giga (10^9) tonnes of carbon; Tmol: Tera moles (10^{12} moles).

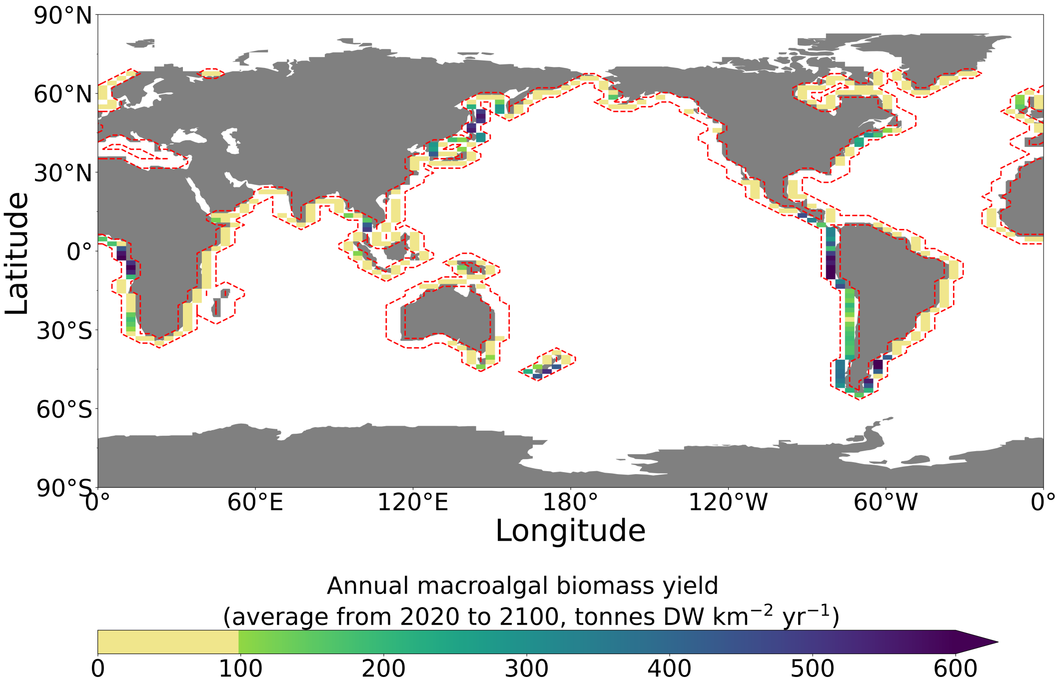

Figure 1. Annual macroalgae biomass yield (averaged from year 2020 to year 2100). Dashed red lines outline the initial seeding locations in year 2020. Regions with high macroalgae productivity include: Coasts of North Western Pacific (near northern China, Japan and Korean Peninsula), South Eastern Pacific (coasts of South America), South Eastern Atlantic (mid-south Africa coast), coast of New Zealand, and South Eastern of Australia. Yellowish areas indicate relatively lower yield ($\leq$100 tonnes DW per km^2 per year).

3.2 CDR capacity and impacts on carbon cycle

The CDR capacity of the N-MACS approach can be quantified as the carbon contained (and securely stored) within the harvested macroalgae biomass. From 2020 to 2100, the N-MACS simulation demonstrates a total sequestration of 56.7 GtC (equivalent to 207.9 GtCO_2). In the No_Temp simulation, this capacity increases to 88 GtC due to elevated macroalgal productivity. The atmospheric CO_2 sequestration in N-MACS/No_Temp scenarios translates to a reduction in global-mean surface air temperature (SAT) by 0.07°C/0.12°C (Tab.1, Fig.S1). While this reduction in SAT alone does not enable the RCP 4.5 emission scenario to align with the Paris Agreement, the annual carbon removal (equivalent to 2.60/4.03 Gt CO_2eq) is, for example, on par with the 2022 annual CO_2 emissions from the global building sector (2.94 Gt CO_2, IEA (2023)).

The simulated global average unit-area CDR capacity is 29.1 to 46.5 tC km^{-2} within N-MACS occupied regions (106.8 to 170.7 tCO_2 km^{-2}, Tab.1). Conversely, the global dynamic seaweed growth model of Arzeno-Soltero et al. (2023) suggested that macroalgae farming, particularly in the equatorial Pacific, could yield about 1 GtC for 1 million km^2 of EEZ waters, translating to 1,000 tC km^{-2} yr^{-1}. These differences stem from model differences and experiment setups. Their model, incorporating four types of macroalgae species with high carbon content and yield, operates independently from dynamic nutrient changes, which we find often limits N-MACS growth, and runs for one year. Our estimation is also lower than the globally averaged per-unit-area CDR capacity of 57 tC km^{-2} yr^{-1} in Wu et al. (2023), where the identical macroalgae model of N-MACS is applied to open-ocean regions. This difference primarily arises from the diverse distribution of macroalgae farms across varying nutrient fields, as depicted by Wu et al. (2023) for open-ocean regions, contrasted with the current N-MACS in nearshore areas. The discrepancy is exacerbated by the coarse grid resolution in UVic, likely underestimating coastal productivity (Keller et al., 2012; Tivig et al., 2021). Nevertheless, the annually averaged carbon sequestration of N-MACS is estimated at 0.7 to 1.1 GtC yr^{-1} (2.6 to 4.0 $GtCO_2$ yr^{-1}), surpassing the 0.37 GtC yr^{-1} reported by Berger et al. (2023), something again attributable to the different dynamic macroalgae growth and Earth system modeling approaches.

The net increase in the oceanic carbon reservoir, consisting of water-column carbon content and the harvested macroalgae in the N-MACS (No_Temp) simulations, is 35.9 (57.1) GtC in 2100 (Tab.1), equivalent to the N-MACS induced air-sea carbon flux in the model (Fig.S6, Fig.S7). However, the increase in the oceanic plus macroalgae carbon reservoir is approximately two-thirds of the harvested macroalgae carbon, corresponding to 63.3% (64.9%) of the net carbon removed by harvesting the macroalgae. The disparity between the increase in the ocean plus macroalgae carbon pool and the carbon harvested in the form of macroalgal biomass is largely caused by backfluxes from the ocean into the atmosphere due to diminished atmospheric pCO_2 (Oschlies, 2009) and partially by the reduced phytoplankton net primary production (PNPP) from canopy shading and nutrient competition effects introduced by N-MACS (see Sect.3.3). This efficiency is somewhat higher than the CDR efficiency of 58% in Berger et al. (2023), who employed a dynamic macroalgae growth model in conjunction with a high-resolution ocean biogeochemical model with prescribed atmospheric CO_2, i.e. without back-fluxes from the ocean into the atmosphere due to diminished atmospheric pCO_2, for 5-year simulations.

Meanwhile, the increase in the oceanic plus macroalgae carbon reservoir induced by N-MACS until 2100 leads to a corresponding decline in the terrestrial carbon reservoir of 5.8 to 9.2 GtC (see Tab. 1) via an atmospheric carbon climate feedback. This response illustrates the Earth system's endeavor to maintain equilibrium, with carbon cycling between terrestrial and oceanic reservoirs, primarily mediated by atmospheric interactions. This finding aligns with other studies, suggesting that ocean-based CDR could potentially weaken terrestrial carbon sinks, especially through the reduction of the CO_2 fertilization effect on terrestrial photosynthesis (Keller, Lenton, Littleton, et al., 2018).

During the implementation phase, an enhancement of approximately 29% (37%) in the air-to-sea downward carbon flux was observed within the macroalgae-occupied areas in N-MACS (No_Temp)(Fig.S5), aligning with the 52% enhancement reported by Berger et al. (2023). The lesser degree of carbon flux enhancement observed in our simulation within the macroalgae-occupied areas is attributed to 1) the canopy shading effect on phytoplankton in our model, reducing PNPP and subsequent carbon flux into the ocean (Fig.2d & Fig. S3); and 2) the dynamic atmospheric pCO_2 in our model compared to prescribed fixed pCO_2 in Berger et al. (2023), as well as different biogeochemical properties of macroalgae and phytoplankton in the two models. Our results further highlight the potential challenges inherent in the measurement, reporting, and verification processes when assessing carbon flux enhancements. Additionally, a slight decrease in DIC in mid and deep waters is evident in Fig.S4a, stemming from reduced water column remineralization due to the diminished downward particulate organic carbon (POC) export (see Sect.3.3).

3.3 Impacts on global marine biogeochemistry

In our simulations, the 80-year implementation of N-MACS has significantly impacted global marine biogeochemistry. This includes ocean surface nutrient distributions, surface ocean alkalinity, and dissolved oxygen concentrations at mid-depth (Fig. 2). Additionally, simulated net primary production and the distributions of ordinary phytoplankton and diazotrophs are also affected by N-MACS deployment. Notably, some of these impacts persist until the year 3000, despite the cessation of N-MACS in 2100 (see below).

The N-MACS macroalgae model delineates two primary impacts of macroalgae on phytoplankton: nutrient competition and canopy shading (Wu et al., 2023, Sect.2.2.3). Harvesting macroalgae not only sequesters carbon but also extracts nutrients within the harvested biomass, leading to an immediate drop in global PNPP post N-MACS initiation in 2020, with a gradual reduction during N-MACS deployment till 2100 (Fig.3e). This PNPP decline predominantly occurs along coast-adjacent N-MACS areas (Fig.2d). Additionally, certain open-ocean regions beyond coastal farms exhibit a PNPP increase, notably in the Indian Ocean, eastern Atlantic near Africa, and eastern equatorial Pacific. This is attributed to nutrient leakage from N-MACS areas (see Fig.2d; further details in the subsequent paragraph). N-MACS implementation suppresses oceanic nitrogen fixers, diazotrophs, due to canopy shading and phosphate competition by macroalgae (Fig.S9). Although certain regions exhibit heightened diazotroph biomass due to increased phosphate levels (Fig.S10a&c), the overall nitrogen fixation relative to DNPP diminishes during N-MACS deployment (Fig.3h). Zooplankton, assumed capable of grazing on macroalgae (Wu et al., 2023), primarily feed on phytoplankton due to a lower macroalgae grazing preference, hence their biomass trends closely with those of phytoplankton (not shown).

Fig.3a illustrates a notable increase in surface ocean PO_4 concentrations (top 50m) following N-MACS initiation, followed by a decrease. Three primary factors underlie this PO_4 rise. Firstly, the suppression of phytoplankton by macroalgae leads to a decreased organic carbon export out of the euphotic zone. Secondly, macroalgae cannot fully utilize the *in-situ* PO_4 due to the limited growth rate and maximum macroalgae biomass (Wu et al., 2023). Lastly, the higher stoichiometric N:P ratio of 20:1 in macroalgae, compared to the Redfield ratio of 16:1 in phytoplankton, entails less PO_4 consumption per nitrogen unit for growth. This explains the increases in surface PO_4 levels in N-MACS regions shown in Fig.2c (Fig.S8c for No_Temp). Nitrate concentrations in N-MACS regions also rise due to phytoplankton inhibition and unexhausted available nitrate from macroalgae growth (Fig.2a). These disparities consequently induce lateral nutrient leakage from N-MACS areas, fertilizing the aforementioned downstream area of coastal N-MACS farms. Here, augmented PNPP consumes the displaced nutrients, driving a regional PO_4 concentration reduction (Fig.2c).

A reduction in surface PNPP within N-MACS regions triggers a decline in particulate organic matter (POM) export to ocean depths, as observed at 2000 m in Fig. 3f and Tab.1. This decline subsequently diminishes oxygen consumption via aerobic remineralization of organic carbon, thus elevating the oxygen concentration across middle and bottom waters (Fig.S4d, Fig.S12d). Notable increases in dissolved oxygen concentrations at 300m depth are apparent in the northwestern Pacific, eastern equatorial Pacific, and southern Atlantic near the South American continent (Fig.2e & Fig.3). Specifically, oxygen minimum zones (OMZs) in the North Pacific and equatorial Atlantic Ocean have shrunk compared to Ctrl_RCP4.5. The increased oxygen levels inhibit denitrification in the subsurface and the upwelling system in the eastern equatorial Pacific (Fig.2f&i, Bange et al. (2019); Ravishankara et al. (2009)), and diminished remineralization of organic carbon curtails nutrient regeneration, reducing nutrient upwelling (Fig.2g&h). This results in elevated NO_3 but reduced PO_4 compared to the Ctrl_RCP4.5 in the open ocean of the eastern equatorial Pacific (Fig.2a, c, d & f). Another factor contributing to the reduced PO_4 in the source waters of the upwelling regions is the decreased PNPP in the N-MACS areas, which lessens export and thereby reduces the PO_4 source from POM remineralization (Fig.2d,Fig.3f). Furthermore, the aforementioned decreased denitrification increases the NO_3 supply in the upwelling system to the surface, especially in oxygen-depleted regions off Peru where reduced POM remineralization leads to lesser denitrification and nitrogen loss. However, in the No_Temp simulation, amplified macroalgae growth utilizes upwelled NO_3 before export to the open ocean, mitigating the NO_3 increase in the eastern equatorial Pacific (Fig.S8a).

Despite the reduction in mid-depth denitrification (Fig.2i), which also diminishes alkalinity production, the surface alkalinity in N-MACS increases about 1% or 10 to 20 mmol m^{-3} by 2100 (Fig.2b), due to reduced $CaCO_3$ generation from the PNPP reduction induced by continuous phosphate removal by N-MACS (Fig.S12, Schmittner et al. (2008, Eq.2)). Post N-MACS discontinuation in 2100, which effectively terminates canopy shading and nutrient competition effects, results in a marked resurgence in PNPP and thereby also a decreases in global surface nutrient concentrations (Fig3a, b&e). Additionally, diazotroph biomass, DNPP, and nitrogen fixation recover (Fig.S9, Fig3h). The export of PNPP and POC as well as the subsurface oxygen consumption via organic carbon remineralization also recovers (Fig3g). Additionally, the air-sea CO_2 flux reverts to baseline levels after cessation of the carbon sequestration by macroalgal harvest from the ocean (Fig.S6, S7).

By year 3000, the average surface temperature in the N-MACS/No_Temp simulations is slightly lower by -0.08/-0.13 °C, respectively, compared to Ctrl_RCP4.5, maintaining the temperature reduction achieved by N-MACS in 2100 (Tab.1). After N-MACS termination in year 2100 and until year 3000, both oceanic and terrestrial carbon reservoirs shrink, with oceanic plus macroalgae carbon storage decreasing by 4.5 GtC in N-MACS and 8.3 GtC in No_Temp, and terrestrial carbon storage declining by 0.1 GtC and 0.7 GtC in N-MACS and No_Temp scenarios respectively. This leads to a 4.6 / 9.0 GtC or 2.2 / 4.3 ppm atmospheric CO_2 increase (Tab.1). Decreased global temperatures slow photosynthesis and soil respiration, in combination yielding a small reduction in the terrestrial carbon pool. The decrease in the oceanic carbon pool mainly arises from the PNPP reduction as a consequence of permanent phosphate removal during the operation of N-MACS. This enduring PO_4 removal leads to long-term alterations in marine biogeochemistry, as shown by extended simulations until year 3000 (Fig.3). Though only 0.4% of total oceanic phosphate is removed by 2100 (Fig.3c), it induces a persistent reduction in PNPP, DNPP, and nitrogen fixation (Fig.3a&h, S10b&d). This prevents PNPP and DNPP recovery to RCP4.5 levels from 2100 to 3000 (Fig. 3 e), leading to increased oxygen due to overall POC export reduction (Fig.3d&g, Fig.S12).

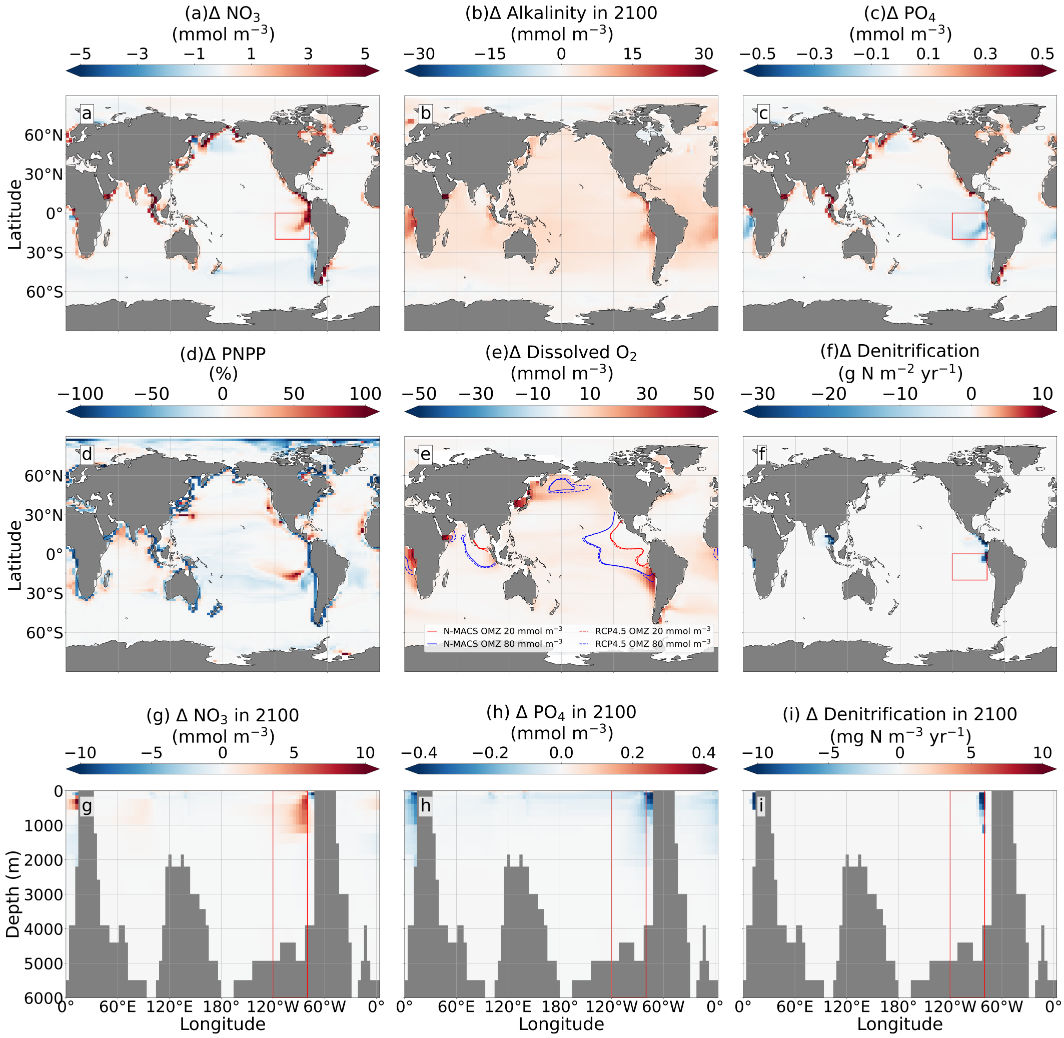

Figure 2. Differences in simulated oceanic properties in year 2100 after continuous N-MACS deployment from 2020 to 2100, with respect to Ctrl_RCP4.5 without N-MACS deployment (data averaged over this period, except for **d** and **e** representing data in 2100): **a**: Surface-layer nitrate (top 50m); **b**: Surface-layer alkalinity; **c**: Surface-layer phosphate; **d**: Phytoplankton net primary production (PNPP); **e**: Dissolved oxygen concentrations and oxygen minimum zones (OMZs) at a depth of 300m; **f**: Oceanic denitrification rates. Subfigures **g, h & i** represent latitudinally averaged data from 20°S to 0°, relative to the Ctrl_RCP4.5 scenario depicted in subfigures **a, c, & f** (highlighted by red rectangular regions between latitudes 20°S to 0° and longitudes 80°W to 120°W): **g**: Phosphate concentrations, **h**: Nitrate concentrations, **i**: Annual denitrification rates.

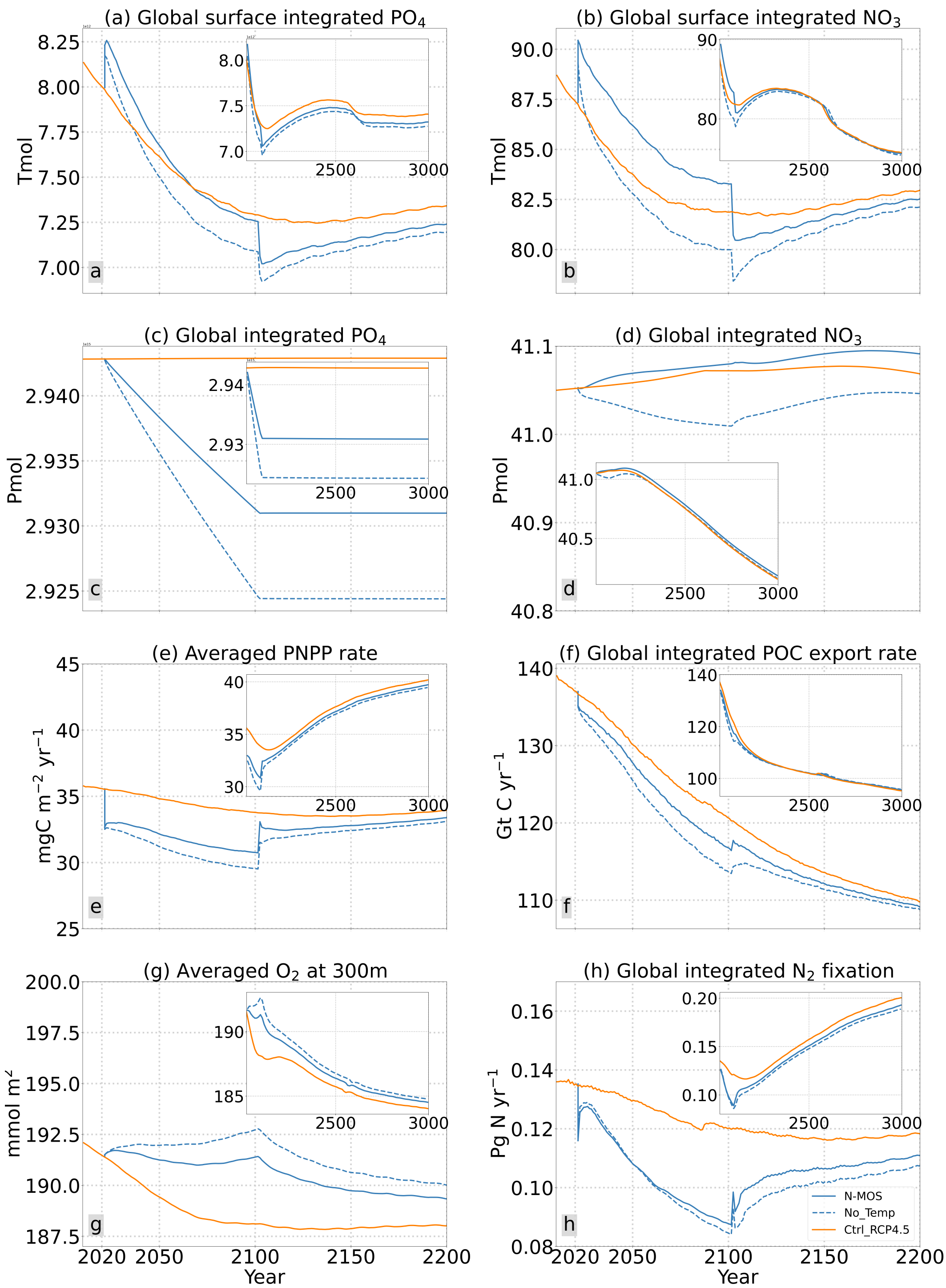

Figure 3. Temporal evolution of globally integrated nutrients, Phytoplankton Net Primary Production (PNPP), and Particulate Organic Carbon (POC) Export at 2,000m depth: Comparison of N-MACS (solid blue), No_Temp (dashed blue), and Ctrl_RCP4.5 Baseline Simulation (orange). Insets in each panel extend the timeline to the year 3000. **a & c**: Permanent removal of PO_4 from the surface, **b & d**: Surface NO_3 levels and global NO_3 trends (increase in N-MACS, decrease in No_Temp). **e**: Surface PNPP (see also Fig.2d). **f**: The export of POC at 2,000m depth. **g**: The averaged O_2 concentration at 300m depth. **h**: Globally integrated Nitrogen fixation.

4 Conclusion & Outlook

Our analysis highlights the substantial annual gigatonne-scale CO_2 sequestration potential of N-MACS, though with marine biogeochemical and global carbon cycle feedbacks reducing the additional air-sea CO_2 flux by 35% compared to carbon removal via harvesting. Large-scale N-MACS deployment considerably alters marine biogeochemistry and ecosystems, suppressing PNPP, elevating dissolved oxygen concentrations, reducing denitrification, and decreasing surface ocean alkalinity. Terminating N-MACS in 2100 triggers a transient rebound in surface PNPP and a decrease in the air-sea CO_2 flux, yet long-term effects like nutrient depletion and increased oxygen levels persist for centuries. Promising regions for macroalgae production include the upwelling systems in South America, Africa's Atlantic coasts, the Northeast Pacific, and the Southern Ocean.

Our simulations have certain limitations: Given that the UVic operates on a coarse grid resolution ($1.8° \times 3.6°$), it inadequately represents the physical and biogeochemical processes of the coastal ecosystem in the marine ecosystem model (Keller et al., 2012). While not significantly impacting our current global and millennial scale simulations, it may affect coastal macroalgae farming simulations when considering nutrient fluxes in coastal areas (e.g., Van Der Molen et al. (2018)). Possible improvements to our model include a consideration of a wider range of macroalgae species (Arzeno-Soltero et al., 2023; Duarte et al., 2022), explicit accounting of iron limitation (Paine et al., 2023; Anton et al., 2018), dynamic cellular stoichiometry, and current impacts on macroalgae frond erosion (Frieder et al., 2022; Broch & Slagstad, 2012). Acknowledging both remineralization-resistant particulate and dissolved organic carbon release from macroalgae and subsequent deep-water may be crucial for comprehending the CDR capacity (Pedersen et al., 2021; Ortega et al., 2019; Duarte & Krause-Jensen, 2017; Wada & Hama, 2013). Further considerations include macroalgae halocarbon emissions (Baker et al., 2001; Leedham et al., 2013; Jia et al., 2022) and alterations in ocean surface albedo and local ecosystem (Bach et al., 2021; Boyd et al., 2022). Herein it's assumed that no nutrients from the harvested biomass are returned to the ocean, which significantly impacts the simulated biogeochemistry. Thus, evaluating nutrient extraction and return strategies is imperative if N-MACS is pursued as a sustainable CDR approach.

Governance and societal facets need consideration in macroalgae-based CDR, particularly due to potential spatial competition between macroalgae cultivation and fisheries, especially along the Peruvian coast (Gattuso et al., 2021; Ricart et al., 2022; Merk et al., 2022). A Comprehensive Life Cycle Analysis (LCA) considering energy consumption biomass conversion efficiency, and financial cost is pivotal (Fernand et al., 2017; Melara et al., 2020; Capron et al., 2020; Hughes et al., 2012; Aitken et al., 2014).

5 Open Research

The data files used in this paper are available through GEOMAR at (Wu, 2024).

Acknowledgments

Jiajun Wu acknowledges funding from sea4soCiety (FKZ: 03F0896G) of the German Marine Research Alliance (DAM) research mission "Marine carbon sinks in decarbonization pathways" (CDRmare). Wanxuan Yao acknowledges funding from German Federal Ministry of Education and Research under grant agreement 03F0898E. Jiajun Wu and Wanxuan Yao acknowledge the National Key Research and Development Program of China (No. 2020YFA0608304). Andreas Oschlies and David P. Keller acknowledge funding from the EU Horizon 2020 research and innovation program under grant agreement No.869357 (project OceanNETs).

References

Aitken, D., Bulboa, C., Godoy-Faundez, A., Turrion-Gomez, J. L., & Antizar-Ladislao, B. (2014, July). Life cycle assessment of macroalgae cultivation and processing for biofuel production. *Journal of Cleaner Production*, *75*, 45–56. Retrieved 2023-05-18, from `https://linkinghub.elsevier.com/retrieve/pii/S0959652614003138` doi: 10.1016/j.jclepro.2014.03.080

Anton, A., Hendriks, I. E., Marbà, N., Krause-Jensen, D., Garcias-Bonet, N., & Duarte, C. M. (2018). Iron Deficiency in Seagrasses and Macroalgae in the Red Sea Is Unrelated to Latitude and Physiological Performance. *Frontiers in Marine Science*, *5*. Retrieved 2023-07-11, from `https://www.frontiersin.org/articles/10.3389/fmars.2018.00074`

Arzeno-Soltero, I. B., Saenz, B. T., Frieder, C. A., Long, M. C., DeAngelo, J., Davis, S. J., & Davis, K. A. (2023, June). Large global variations in the carbon dioxide removal potential of seaweed farming due to biophysical constraints. *Communications Earth & Environment*, *4*(1), 1–12. Retrieved 2023-06-21, from `https://www.nature.com/articles/s43247-023-00833-2` (Number: 1 Publisher: Nature Publishing Group) doi: 10.1038/s43247-023-00833-2

Bach, L. T., Gill, S. J., Rickaby, R. E. M., Gore, S., & Renforth, P. (2019, October). CO2 Removal With Enhanced Weathering and Ocean Alkalinity Enhancement: Potential Risks and Co-benefits for Marine Pelagic Ecosystems. *Frontiers in Climate*, *1*, 7. Retrieved 2023-05-18, from `https://www.frontiersin.org/article/10.3389/fclim.2019.00007/full` doi: 10.3389/fclim.2019.00007

Bach, L. T., Tamsitt, V., Gower, J., Hurd, C. L., Raven, J. A., & Boyd, P. W. (2021, May). Testing the climate intervention potential of ocean afforestation using the Great Atlantic Sargassum Belt. *Nature Communications*, *12*(1), 2556. Retrieved 2023-05-18, from `https://www.nature.com/articles/s41467-021-22837-2` doi: 10.1038/s41467-021-22837-2

Baker, J., Sturges, W., Sugier, J., Sunnenberg, G., Lovett, A., Reeves, C., … Penkett, S. (2001, January). Emissions of CH3Br, organochlorines, and organoiodines from temperate macroalgae. *Chemosphere - Global Change Science*, *3*(1), 93–106. Retrieved 2023-05-18, from `https://linkinghub.elsevier.com/retrieve/pii/S1465997200000210` doi: 10.1016/S1465-9972(00)00021-0

Bange, H. W., Arévalo-Martínez, D. L., De La Paz, M., Farías, L., Kaiser, J., Kock, A., … Wilson, S. T. (2019, April). A Harmonized Nitrous Oxide (N2O) Ocean Observation Network for the 21st Century. *Frontiers in Marine Science*, *6*, 157. Retrieved 2023-05-18, from `https://www.frontiersin.org/article/10.3389/fmars.2019.00157/full` doi: 10.3389/fmars.2019.00157

Barrón, C., & Duarte, C. M. (2015, October). Dissolved organic carbon pools and export from the coastal ocean: DOC EXPORT COASTAL OCEAN. *Global Biogeochemical Cycles*, *29*(10), 1725–1738. Retrieved 2023-05-18, from `http://doi.wiley.com/10.1002/2014GB005056` doi: 10.1002/2014GB005056

Berger, M., Kwiatkowski, L., Ho, D. T., & Bopp, L. (2023, February). Ocean dynamics and biological feedbacks limit the potential of macroalgae carbon dioxide removal. *Environmental Research Letters*, *18*(2), 024039. Retrieved 2023-05-18, from `https://iopscience.iop.org/article/10.1088/1748-9326/acb06e` doi: 10.1088/1748-9326/acb06e

Bird, M. I., Wurster, C. M., De Paula Silva, P. H., Bass, A. M., & De Nys, R. (2011, January). Algal biochar – production and properties. *Bioresource Technology*, *102*(2), 1886–1891. Retrieved 2023-05-18, from `https://linkinghub.elsevier.com/retrieve/pii/S0960852410013179` doi: 10.1016/j.biortech.2010.07.106

Bitz, C. M., & Lipscomb, W. H. (1999, July). An energy-conserving thermodynamic model of sea ice. *Journal of Geophysical Research: Oceans*, *104*(C7), 15669–15677. Retrieved 2023-05-20, from http://doi.wiley.com/10.1029/1999JC900100 doi: 10.1029/1999JC900100

Borchers, M., Thrän, D., Chi, Y., Dahmen, N., Dittmeyer, R., Dolch, T., … Yeates, C. (2022, October). Scoping carbon dioxide removal options for Germany–What is their potential contribution to Net-Zero CO2? *Frontiers in Climate*, *4*, 810343. Retrieved 2023-05-18, from https://www.frontiersin.org/articles/10.3389/fclim.2022.810343/full doi: 10.3389/fclim.2022.810343

Boyd, P. W., Bach, L. T., Hurd, C. L., Paine, E., Raven, J. A., & Tamsitt, V. (2022, June). Potential negative effects of ocean afforestation on offshore ecosystems. *Nature Ecology & Evolution*, *6*(6), 675–683. Retrieved 2024-01-24, from https://www.nature.com/articles/s41559-022-01722-1 (Number: 6 Publisher: Nature Publishing Group) doi: 10.1038/s41559-022-01722-1

Broch, O. J., & Slagstad, D. (2012, August). Modelling seasonal growth and composition of the kelp Saccharina latissima. *Journal of Applied Phycology*, *24*(4), 759–776. Retrieved 2023-05-18, from http://link.springer.com/10.1007/s10811-011-9695-y doi: 10.1007/s10811-011-9695-y

Buck, B. H., & Buchholz, C. M. (2004, October). The offshore-ring: A new system design for the open ocean aquaculture of macroalgae. *Journal of Applied Phycology*, *16*(5), 355–368. Retrieved 2023-05-18, from http://link.springer.com/10.1023/B:JAPH.0000047947.96231.ea doi: 10.1023/B:JAPH.0000047947.96231.ea

Buesseler, K. O., Andrews, J. E., Pike, S. M., & Charette, M. A. (2004, April). The Effects of Iron Fertilization on Carbon Sequestration in the Southern Ocean. *Science*, *304*(5669), 414–417. Retrieved 2023-07-15, from https://www.science.org/doi/full/10.1126/science.1086895 (Publisher: American Association for the Advancement of Science) doi: 10.1126/science.1086895

Cai, J., Lovatelli, A., Aguilar-Manjarrez, J., Cornish, L., Dabbadie, L., Desrochers, A., … others (2021). Seaweeds and microalgae: an overview for unlocking their potential in global aquaculture development. *FAO Fisheries and Aquaculture Circular*(1229).

Capron, M. E., Stewart, J. R., De Ramon N'Yeurt, A., Chambers, M. D., Kim, J. K., Yarish, C., … Hasan, M. A. (2020, September). Restoring Pre-Industrial CO2 Levels While Achieving Sustainable Development Goals. *Energies*, *13*(18), 4972. Retrieved 2023-05-18, from https://www.mdpi.com/1996-1073/13/18/4972 doi: 10.3390/en13184972

Chavez, F. P., & Messié, M. (2009, December). A comparison of Eastern Boundary Upwelling Ecosystems. *Progress in Oceanography*, *83*(1-4), 80–96. Retrieved 2023-05-20, from https://linkinghub.elsevier.com/retrieve/pii/S0079661109000998 doi: 10.1016/j.pocean.2009.07.032

Chen, H., Zhou, D., Luo, G., Zhang, S., & Chen, J. (2015, July). Macroalgae for biofuels production: Progress and perspectives. *Renewable and Sustainable Energy Reviews*, *47*, 427–437. Retrieved 2023-05-18, from https://linkinghub.elsevier.com/retrieve/pii/S1364032115002397 doi: 10.1016/j.rser.2015.03.086

Chikaraishi, Y., Kashiyama, Y., Ogawa, N., Kitazato, H., & Ohkouchi, N. (2007, July). Metabolic control of nitrogen isotope composition of amino acids in macroalgae and gastropods: implications for aquatic food web studies. *Marine Ecology Progress Series*, *342*, 85–90. Retrieved 2023-05-18, from http://www.int-res.com/abstracts/meps/v342/p85-90/ doi: 10.3354/meps342085

Duarte, C. M., Bruhn, A., & Krause-Jensen, D. (2021, October). A seaweed aquaculture imperative to meet global sustainability targets. *Nature Sustainability*, *5*(3), 185–193. Retrieved 2023-05-18, from https://www.nature.com/

articles/s41893-021-00773-9 doi: 10.1038/s41893-021-00773-9
Duarte, C. M., Gattuso, J., Hancke, K., Gundersen, H., Filbee-Dexter, K., Pedersen, M. F., … Field, R. (2022, July). Global estimates of the extent and production of macroalgal forests. *Global Ecology and Biogeography*, *31*(7), 1422–1439. Retrieved 2023-05-18, from https://onlinelibrary.wiley.com/doi/10.1111/geb.13515 doi: 10.1111/geb.13515
Duarte, C. M., & Krause-Jensen, D. (2017, January). Export from Seagrass Meadows Contributes to Marine Carbon Sequestration. *Frontiers in Marine Science*, *4*. Retrieved 2023-05-18, from http://journal.frontiersin.org/article/10.3389/fmars.2017.00013/full doi: 10.3389/fmars.2017.00013
Eby, M., Weaver, A. J., Alexander, K., Zickfeld, K., Abe-Ouchi, A., Cimatoribus, A. A., … Zhao, F. (2013, May). Historical and idealized climate model experiments: an intercomparison of Earth system models of intermediate complexity. *Climate of the Past*, *9*(3), 1111–1140. Retrieved 2023-05-18, from https://cp.copernicus.org/articles/9/1111/2013/ doi: 10.5194/cp-9-1111-2013
Eby, M., Zickfeld, K., Montenegro, A., Archer, D., Meissner, K. J., & Weaver, A. J. (2009, May). Lifetime of Anthropogenic Climate Change: Millennial Time Scales of Potential CO2 and Surface Temperature Perturbations. *Journal of Climate*, *22*(10), 2501–2511. Retrieved 2023-05-20, from http://journals.ametsoc.org/doi/10.1175/2008JCLI2554.1 doi: 10.1175/2008JCLI2554.1
Falkowski, P., Scholes, R. J., Boyle, E., Canadell, J., Canfield, D., Elser, J., … Steffen, W. (2000, October). The Global Carbon Cycle: A Test of Our Knowledge of Earth as a System. *Science*, *290*(5490), 291–296. Retrieved 2023-05-29, from https://www.science.org/doi/10.1126/science.290.5490.291 doi: 10.1126/science.290.5490.291
Fanning, A. F., & Weaver, A. J. (1996, June). An atmospheric energy-moisture balance model: Climatology, interpentadal climate change, and coupling to an ocean general circulation model. *Journal of Geophysical Research: Atmospheres*, *101*(D10), 15111–15128. Retrieved 2023-05-20, from http://doi.wiley.com/10.1029/96JD01017 doi: 10.1029/96JD01017
FAO (Ed.). (2018). *Meeting the sustainable development goals* (No. 2018). Rome.
Feng, E. Y., Koeve, W., Keller, D. P., & Oschlies, A. (2017, December). Model-Based Assessment of the CO $_2$ Sequestration Potential of Coastal Ocean Alkalinization. *Earth's Future*, *5*(12), 1252–1266. Retrieved 2023-05-18, from http://doi.wiley.com/10.1002/2017EF000659 doi: 10.1002/2017EF000659
Fernand, F., Israel, A., Skjermo, J., Wichard, T., Timmermans, K. R., & Golberg, A. (2017, August). Offshore macroalgae biomass for bioenergy production: Environmental aspects, technological achievements and challenges. *Renewable and Sustainable Energy Reviews*, *75*, 35–45. Retrieved 2023-05-18, from https://linkinghub.elsevier.com/retrieve/pii/S1364032116307018 doi: 10.1016/j.rser.2016.10.046
Frieder, C. A., Yan, C., Chamecki, M., Dauhajre, D., McWilliams, J. C., Infante, J., … Davis, K. A. (2022, March). A Macroalgal Cultivation Modeling System (MACMODS): Evaluating the Role of Physical-Biological Coupling on Nutrients and Farm Yield. *Frontiers in Marine Science*, *9*, 752951. Retrieved 2023-05-18, from https://www.frontiersin.org/articles/10.3389/fmars.2022.752951/full doi: 10.3389/fmars.2022.752951
Froehlich, H. E., Afflerbach, J. C., Frazier, M., & Halpern, B. S. (2019, September). Blue Growth Potential to Mitigate Climate Change through Seaweed Offsetting. *Current Biology*, *29*(18), 3087–3093.e3. Retrieved 2023-05-18, from https://linkinghub.elsevier.com/retrieve/pii/S0960982219308863 doi: 10.1016/j.cub.2019.07.041

Fréon, P., Barange, M., & Arístegui, J. (2009, December). Eastern Boundary Upwelling Ecosystems: Integrative and comparative approaches. *Progress in Oceanography*, *83*(1-4), 1–14. Retrieved 2023-05-20, from https://linkinghub.elsevier.com/retrieve/pii/S0079661109001323 doi: 10.1016/j.pocean.2009.08.001

Gao, G., Gao, L., Jiang, M., Jian, A., & He, L. (2022, January). The potential of seaweed cultivation to achieve carbon neutrality and mitigate deoxygenation and eutrophication. *Environmental Research Letters*, *17*(1), 014018. Retrieved 2023-05-18, from https://iopscience.iop.org/article/10.1088/1748-9326/ac3fd9 doi: 10.1088/1748-9326/ac3fd9

Gattuso, J.-P., Williamson, P., Duarte, C. M., & Magnan, A. K. (2021, January). The Potential for Ocean-Based Climate Action: Negative Emissions Technologies and Beyond. *Frontiers in Climate*, *2*, 575716. Retrieved 2023-05-18, from https://www.frontiersin.org/articles/10.3389/fclim.2020.575716/full doi: 10.3389/fclim.2020.575716

GESAMP. (2019). High level review of a wide range of proposed marine geoengineering techniques. In P. W. Boyd & C. M. G. Vivian (Eds.), *Rep. stud. gesamp no. 98* (p. 144).

Goecke, F., Klemetsdal, G., & Ergon, . (2020, February). Cultivar Development of Kelps for Commercial Cultivation—Past Lessons and Future Prospects. *Frontiers in Marine Science*, *8*, 110. Retrieved 2023-05-18, from https://www.frontiersin.org/article/10.3389/fmars.2020.00110/full doi: 10.3389/fmars.2020.00110

Hughes, A. D., Black, K. D., Campbell, I., Davidson, K., Kelly, M. S., & Stanley, M. S. (2012, December). Does seaweed offer a solution for bioenergy with biological carbon capture and storage? *Greenhouse Gases: Science and Technology*, *2*(6), 402–407. Retrieved 2023-05-23, from https://onlinelibrary.wiley.com/doi/10.1002/ghg.1319 doi: 10.1002/ghg.1319

IEA. (2023). *Co2 emissions in 2022.* Paris: International Energy Agency. Retrieved from https://www.iea.org/reports/co2-emissions-in-2022 (License: CC BY 4.0)

IPCC. (2022). Summary for Policymakers. In P. Shukla et al. (Eds.), *Climate change 2022: Mitigation of climate change. contribution of working group iii to the sixth assessment report of the intergovernmental panel on climate change.* Cambridge, UK and New York, NY, USA: Cambridge University Press. doi: 10.1017/9781009157926.001

Jacobucci, G. B., Güth, A. Z., & Leite, F. P. P. (2008). Experimental evaluation of amphipod grazing over biomass of Sargassum filipendula (Phaeophyta) and its dominant epiphyte. *Nauplius.*

Jia, Y., Quack, B., Kinley, R. D., Pisso, I., & Tegtmeier, S. (2022, June). Potential environmental impact of bromoform from *Asparagopsis* farming in Australia. *Atmospheric Chemistry and Physics*, *22*(11), 7631–7646. Retrieved 2024-02-27, from https://acp.copernicus.org/articles/22/7631/2022/ (Publisher: Copernicus GmbH) doi: 10.5194/acp-22-7631-2022

Keller, D. P., Brent, K., Bach, L. T., & Rickels, W. (2021, August). Editorial: The Role of Ocean-Based Negative Emission Technologies for Climate Mitigation. *Frontiers in Climate*, *3*, 743816. Retrieved 2023-05-18, from https://www.frontiersin.org/articles/10.3389/fclim.2021.743816/full doi: 10.3389/fclim.2021.743816

Keller, D. P., Feng, E. Y., & Oschlies, A. (2014, February). Potential climate engineering effectiveness and side effects during a high carbon dioxide-emission scenario. *Nature Communications*, *5*(1), 3304. Retrieved 2023-05-20, from https://www.nature.com/articles/ncomms4304 doi: 10.1038/ncomms4304

Keller, D. P., Lenton, A., Littleton, E. W., Oschlies, A., Scott, V., & Vaughan, N. E. (2018, September). The Effects of Carbon Dioxide Removal on the Carbon

Cycle. *Current Climate Change Reports*, *4*(3), 250–265. Retrieved 2023-05-18, from http://link.springer.com/10.1007/s40641-018-0104-3 doi: 10.1007/s40641-018-0104-3

Keller, D. P., Lenton, A., Scott, V., Vaughan, N. E., Bauer, N., Ji, D., … Zickfeld, K. (2018, March). The Carbon Dioxide Removal Model Intercomparison Project (CDRMIP): rationale and experimental protocol for CMIP6. *Geoscientific Model Development*, *11*(3), 1133–1160. Retrieved 2023-05-18, from https://gmd.copernicus.org/articles/11/1133/2018/ doi: 10.5194/gmd-11-1133-2018

Keller, D. P., Oschlies, A., & Eby, M. (2012, September). A new marine ecosystem model for the University of Victoria Earth System Climate Model. *Geoscientific Model Development*, *5*(5), 1195–1220. Retrieved 2024-02-05, from https://gmd.copernicus.org/articles/5/1195/2012/gmd-5-1195-2012.html (Publisher: Copernicus GmbH) doi: 10.5194/gmd-5-1195-2012

Krause-Jensen, D., & Duarte, C. M. (2016, October). Substantial role of macroalgae in marine carbon sequestration. *Nature Geoscience*, *9*(10), 737–742. Retrieved 2024-01-18, from https://www.nature.com/articles/ngeo2790 doi: 10.1038/ngeo2790

Leedham, E. C., Hughes, C., Keng, F. S. L., Phang, S.-M., Malin, G., & Sturges, W. T. (2013, June). Emission of atmospherically significant halocarbons by naturally occurring and farmed tropical macroalgae. *Biogeosciences*, *10*(6), 3615–3633. Retrieved 2023-05-18, from https://bg.copernicus.org/articles/10/3615/2013/ doi: 10.5194/bg-10-3615-2013

Lehahn, Y., Ingle, K. N., & Golberg, A. (2016, July). Global potential of offshore and shallow waters macroalgal biorefineries to provide for food, chemicals and energy: feasibility and sustainability. *Algal Research*, *17*, 150–160. Retrieved 2023-05-18, from https://linkinghub.elsevier.com/retrieve/pii/S2211926416301151 doi: 10.1016/j.algal.2016.03.031

Meinshausen, M., Smith, S. J., Calvin, K., Daniel, J. S., Kainuma, M. L. T., Lamarque, J.-F., … Van Vuuren, D. P. (2011, November). The RCP greenhouse gas concentrations and their extensions from 1765 to 2300. *Climatic Change*, *109*(1-2), 213–241. Retrieved 2023-05-18, from http://link.springer.com/10.1007/s10584-011-0156-z doi: 10.1007/s10584-011-0156-z

Meissner, K. J., Weaver, A. J., Matthews, H. D., & Cox, P. M. (2003, December). The role of land surface dynamics in glacial inception: a study with the UVic Earth System Model. *Climate Dynamics*, *21*(7-8), 515–537. Retrieved 2023-05-18, from http://link.springer.com/10.1007/s00382-003-0352-2 doi: 10.1007/s00382-003-0352-2

Melara, A. J., Singh, U., & Colosi, L. M. (2020, November). Is aquatic bioenergy with carbon capture and storage a sustainable negative emission technology? Insights from a spatially explicit environmental life-cycle assessment. *Energy Conversion and Management*, *224*, 113300. Retrieved 2023-05-18, from https://linkinghub.elsevier.com/retrieve/pii/S0196890420308396 doi: 10.1016/j.enconman.2020.113300

Merk, C., Grunau, J., Riekhof, M.-C., & Rickels, W. (2022, November). The need for local governance of global commons: The example of blue carbon ecosystems. *Ecological Economics*, *201*, 107581. Retrieved 2023-07-19, from https://www.sciencedirect.com/science/article/pii/S0921800922002439 doi: 10.1016/j.ecolecon.2022.107581

N'Yeurt, A. D. R., Chynoweth, D. P., Capron, M. E., Stewart, J. R., & Hasan, M. A. (2012, November). Negative carbon via Ocean Afforestation. *Process Safety and Environmental Protection*, *90*(6), 467–474. Retrieved 2023-05-18, from https://linkinghub.elsevier.com/retrieve/pii/S0957582012001206 doi: 10.1016/j.psep.2012.10.008

Ortega, A., Geraldi, N. R., Alam, I., Kamau, A. A., Acinas, S. G., Logares, R., …

Duarte, C. M. (2019, September). Important contribution of macroalgae to oceanic carbon sequestration. *Nature Geoscience*, *12*(9), 748–754. doi: 10.1038/s41561-019-0421-8

Oschlies, A. (2009, August). Impact of atmospheric and terrestrial CO_2 feedbacks on fertilization-induced marine carbon uptake. *Biogeosciences*, *6*(8), 1603–1613. Retrieved 2023-09-06, from `https://bg.copernicus.org/articles/6/1603/2009/` (Publisher: Copernicus GmbH) doi: 10.5194/bg-6-1603-2009

Oschlies, A., Pahlow, M., Yool, A., & Matear, R. J. (2010, February). Climate engineering by artificial ocean upwelling: Channelling the sorcerer's apprentice: OCEAN PIPE IMPACTS. *Geophysical Research Letters*, *37*(4). Retrieved 2023-05-20, from `http://doi.wiley.com/10.1029/2009GL041961` doi: 10.1029/2009GL041961

Pacanowski, R. C. (1996). Documentation user's guide and reference manual (mom2, version 2). *GFDL Ocean Technical Report 3.2*, *329*.

Paine, E. R., Boyd, P. W., Strzepek, R. F., Ellwood, M., Brewer, E. A., Diaz-Pulido, G., … Hurd, C. L. (2023, June). Iron limitation of kelp growth may prevent ocean afforestation. *Communications Biology*, *6*(1), 1–9. Retrieved 2023-07-11, from `https://www.nature.com/articles/s42003-023-04962-4` (Number: 1 Publisher: Nature Publishing Group) doi: 10.1038/s42003-023-04962-4

Pedersen, M., Filbee-Dexter, K., Frisk, N., Sárossy, Z., & Wernberg, T. (2021, February). Carbon sequestration potential increased by incomplete anaerobic decomposition of kelp detritus. *Marine Ecology Progress Series*, *660*, 53–67. Retrieved 2023-05-18, from `https://www.int-res.com/abstracts/meps/v660/p53-67/` doi: 10.3354/meps13613

Peteiro, C., Sánchez, N., Dueñas-Liaño, C., & Martínez, B. (2014, February). Open-sea cultivation by transplanting young fronds of the kelp Saccharina latissima. *Journal of Applied Phycology*, *26*(1), 519–528. Retrieved 2023-05-18, from `http://link.springer.com/10.1007/s10811-013-0096-2` doi: 10.1007/s10811-013-0096-2

Ravishankara, A. R., Daniel, J. S., & Portmann, R. W. (2009, October). Nitrous Oxide (N_2O): The Dominant Ozone-Depleting Substance Emitted in the 21st Century. *Science*, *326*(5949), 123–125. Retrieved 2023-05-18, from `https://www.science.org/doi/10.1126/science.1176985` doi: 10.1126/science.1176985

Ricart, A. M., Krause-Jensen, D., Hancke, K., Price, N. N., Masqué, P., & Duarte, C. M. (2022, August). Sinking seaweed in the deep ocean for carbon neutrality is ahead of science and beyond the ethics. *Environmental Research Letters*, *17*(8), 081003. Retrieved 2023-05-18, from `https://iopscience.iop.org/article/10.1088/1748-9326/ac82ff` doi: 10.1088/1748-9326/ac82ff

Roberts, D. A., Paul, N. A., Dworjanyn, S. A., Bird, M. I., & De Nys, R. (2015, April). Biochar from commercially cultivated seaweed for soil amelioration. *Scientific Reports*, *5*(1), 9665. Retrieved 2023-05-18, from `https://www.nature.com/articles/srep09665` doi: 10.1038/srep09665

Sarmiento, J. L., & Gruber, N. (2013). *Ocean Biogeochemical Dynamics*. Princeton University Press. Retrieved 2023-05-29, from `http://www.jstor.org/stable/10.2307/j.ctt3fgxqx` doi: 10.2307/j.ctt3fgxqx

Schmittner, A., Oschlies, A., Matthews, H. D., & Galbraith, E. D. (2008). Future changes in climate, ocean circulation, ecosystems, and biogeochemical cycling simulated for a business-as-usual CO2 emission scenario until year 4000 AD. *Global Biogeochemical Cycles*, *22*(1). Retrieved 2023-11-12, from `https://onlinelibrary.wiley.com/doi/abs/10.1029/2007GB002953` (_eprint: https://onlinelibrary.wiley.com/doi/pdf/10.1029/2007GB002953) doi: 10.1029/2007GB002953

Siegel, D. A., DeVries, T., Doney, S. C., & Bell, T. (2021, October). Assessing the sequestration time scales of some ocean-based carbon dioxide reduction strategies. *Environmental Research Letters*, *16*(10), 104003. Retrieved 2023-05-18, from https://iopscience.iop.org/article/10.1088/1748-9326/ac0be0 doi: 10.1088/1748-9326/ac0be0

Thomson, A. M., Calvin, K. V., Smith, S. J., Kyle, G. P., Volke, A., Patel, P., … Edmonds, J. A. (2011, November). RCP4.5: a pathway for stabilization of radiative forcing by 2100. *Climatic Change*, *109*(1-2), 77–94. Retrieved 2023-05-18, from http://link.springer.com/10.1007/s10584-011-0151-4 doi: 10.1007/s10584-011-0151-4

Tivig, M., Keller, D. P., & Oschlies, A. (2021, October). Riverine nitrogen supply to the global ocean and its limited impact on global marine primary production: a feedback study using an Earth system model. *Biogeosciences*, *18*(19), 5327–5350. Retrieved 2023-06-19, from https://bg.copernicus.org/articles/18/5327/2021/ (Publisher: Copernicus GmbH) doi: 10.5194/bg-18-5327-2021

Van Der Molen, J., Ruardij, P., Mooney, K., Kerrison, P., O'Connor, N. E., Gorman, E., … Capuzzo, E. (2018, February). Modelling potential production of macroalgae farms in UK and Dutch coastal waters. *Biogeosciences*, *15*(4), 1123–1147. Retrieved 2023-05-18, from https://bg.copernicus.org/articles/15/1123/2018/ doi: 10.5194/bg-15-1123-2018

Wada, S., & Hama, T. (2013, September). The contribution of macroalgae to the coastal dissolved organic matter pool. *Estuarine, Coastal and Shelf Science*, *129*, 77–85. Retrieved 2023-05-18, from https://linkinghub.elsevier.com/retrieve/pii/S0272771413002722 doi: 10.1016/j.ecss.2013.06.007

Weaver, A. J., Eby, M., Wiebe, E. C., Bitz, C. M., Duffy, P. B., Ewen, T. L., … Yoshimori, M. (2001, December). The UVic earth system climate model: Model description, climatology, and applications to past, present and future climates. *Atmosphere-Ocean*, *39*(4), 361–428. Retrieved 2023-05-18, from https://www.tandfonline.com/doi/full/10.1080/07055900.2001.9649686 doi: 10.1080/07055900.2001.9649686

Wu, J. (2024). *Supplementary data to Wu et al. (2024): Nearshore Macroalgae Cultivation for Carbon Sequestration by Biomass Harvesting: An Evaluation of Potential and Impacts Utilizing an Earth System Model [Data].* GEOMAR Helmholtz Centre for Ocean Research Kiel https://hdl.handle.net/20.500.12085/31ae24e4-98a6-452e-8b55-f27372f9b571.

Wu, J., Keller, D. P., & Oschlies, A. (2023, February). Carbon dioxide removal via macroalgae open-ocean mariculture and sinking: an Earth system modeling study. *Earth System Dynamics*, *14*(1), 185–221. Retrieved 2023-05-18, from https://esd.copernicus.org/articles/14/185/2023/ doi: 10.5194/esd-14-185-2023

Yokoyama, S., Jonouchi, K., & Imou, K. (2007). Energy production from marine biomass: fuel cell power generation driven by methane produced from seaweed. *International Journal of Marine and Environmental Sciences*, *1*(4), 24–27.

Zhang, J., Liu, T., Bian, D., Zhang, L., Li, X., Liu, D., … Xiao, L. (2016, December). Breeding and genetic stability evaluation of the new Saccharina variety "Ailunwan" with high yield. *Journal of Applied Phycology*, *28*(6), 3413–3421. Retrieved 2023-05-18, from http://link.springer.com/10.1007/s10811-016-0810-y doi: 10.1007/s10811-016-0810-y

Zhang, J., Liu, Y., Yu, D., Song, H., Cui, J., & Liu, T. (2011, April). Study on high-temperature-resistant and high-yield Laminaria variety "Rongfu". *Journal of Applied Phycology*, *23*(2), 165–171. Retrieved 2023-05-18, from http://link.springer.com/10.1007/s10811-011-9650-y doi: 10.1007/s10811-011-9650-y

Supporting Information for "Nearshore Macroalgae Cultivation for Carbon Sequestration by Biomass Harvesting: Evaluating Potential and Impacts with An Earth System Model"

Jiajun Wu[1,3], Wanxuan Yao[1], David. P. Keller[1], Andreas Oschlies[1,2]

[1]GEOMAR Helmholtz Centre for Ocean Research Kiel, Wischhofstr. 1-3, 24148 Kiel, Germany

[2]Kiel University, Christian-Albrechts-Platz 4, 24118 Kiel, Germany

[3]Alfred Wegener Institute Helmholtz Center for Marine and Polar Research, Am Handelshafen 12, 27570 Bremerhaven

Contents of this file

1. Figure S1.Global temporal evolution of atmospheric CO_2 concentration and surface averaged temperature (SAT)

2. Figure S2.Annual macroalgae biomass yield (averaged from year 2020 to year 2100) of sensitivity simulation without temperature limiting factor. Dashed red lines outline the initial seeding locations in year 2020. Yellowish areas indicate relatively lower yield ($\leq$100 tonnes DW per km^2 per year)

3. Figure S3.The most limiting growth factor for ordinary phytoplankton in N-MACS simulation from 2020 to 2100

4. Figure S4.Globally averaged vertical profiles of dissolved inorganic carbon (DIC), dissolved phosphate (PO_4), dissolved nitrate (NO_3), and dissolved oxygen (O_2)

5. Figure S5.Yearly averaged variations in global oceanic carbon flux between 2020 and 2100, comparing (a) N-MACS and (b) No_Temp relative to RCP4.5 scenario. Positive values indicate net oceanic carbon uptake from the atmosphere

6. Figure S6.Global profile of air-sea carbon fluxes, N-MACS harvested biomass and oceanic carbon reservoir (GtC yr^{-1})

7. Figure S7.Global profile of air-sea carbon fluxes, No_Temp harvested biomass and oceanic carbon reservoir (GtC yr^{-1})

8. Figure S8.Changes relative to RCP4.5 caused by the deployment of No_Temp (data averaged from year 2020 to 2100, except for **d** which represents data in 2100): **a**: Nitrate distribution in the ocean's surface layer (top 50m); **b**: Alkalinity in the ocean's surface layer; **c**: Phosphate distribution in the surface layer; **d**: Phytoplankton net primary production (PNPP); **e**: Dissolved oxygen concentrations and oxygen minimum zones (OMZs) at a depth of 300m; **f**: Oceanic denitrification rates; Regions within red rectangles (between latitudes 20°S to 0° and longitudes 80°W to 120°W) indicate latitudinal averaged data relative to the Ctrl_RCP4.5: **g**: Phosphate concentrations, **h**: Nitrate concentrations, **i**: Annual denitrification rates

9. Figure S9.Globally integrated diazotroph biomass of N-MACS (bluish line) and No_Temp (greenish line) relative to RCP4.5

10. Figure S10.Variation in global vertically integrated diazotrophs biomass (mmol N m^{-2}): N-MACS vs. RCP4.5 at year 2100 (**a**) and 2200 (**b**); No_Temp vs. RCP4.5 at year 2100 (**c**) and 2200 (**d**)

11. Figure S11.The globally assumed total occupied areas (solid lines) and significant production areas (dashed lines) areas of N-MACS (green tones) and No_Temp (blue tones) simulations

12. Figure S12.Vertical profiles comparing global horizontal averages of (a) alkalinity, (b) phosphate, (c) carbonate export, and (d) dissolved oxygen between N-MACS and RCP4.5 in 2100

13. Table S1.Macroalgae biomass annual productivity (t DW km^{-2} yr^{-1}) in N-MACS regions

Table S1. Macroalgae biomass annual productivity (t DW km^{-2} yr^{-1}) in N-MACS regions.

	N-MACS	**No_Temp**
Mean of all N-MACS areas	97.02	155.10
Significant N-MACS areas	165.25	229.67
Northeast Asia	143.67	214.37
South America	413.46	610.10
Oceania	60.75	77.49
South Africa	196.54	205.14

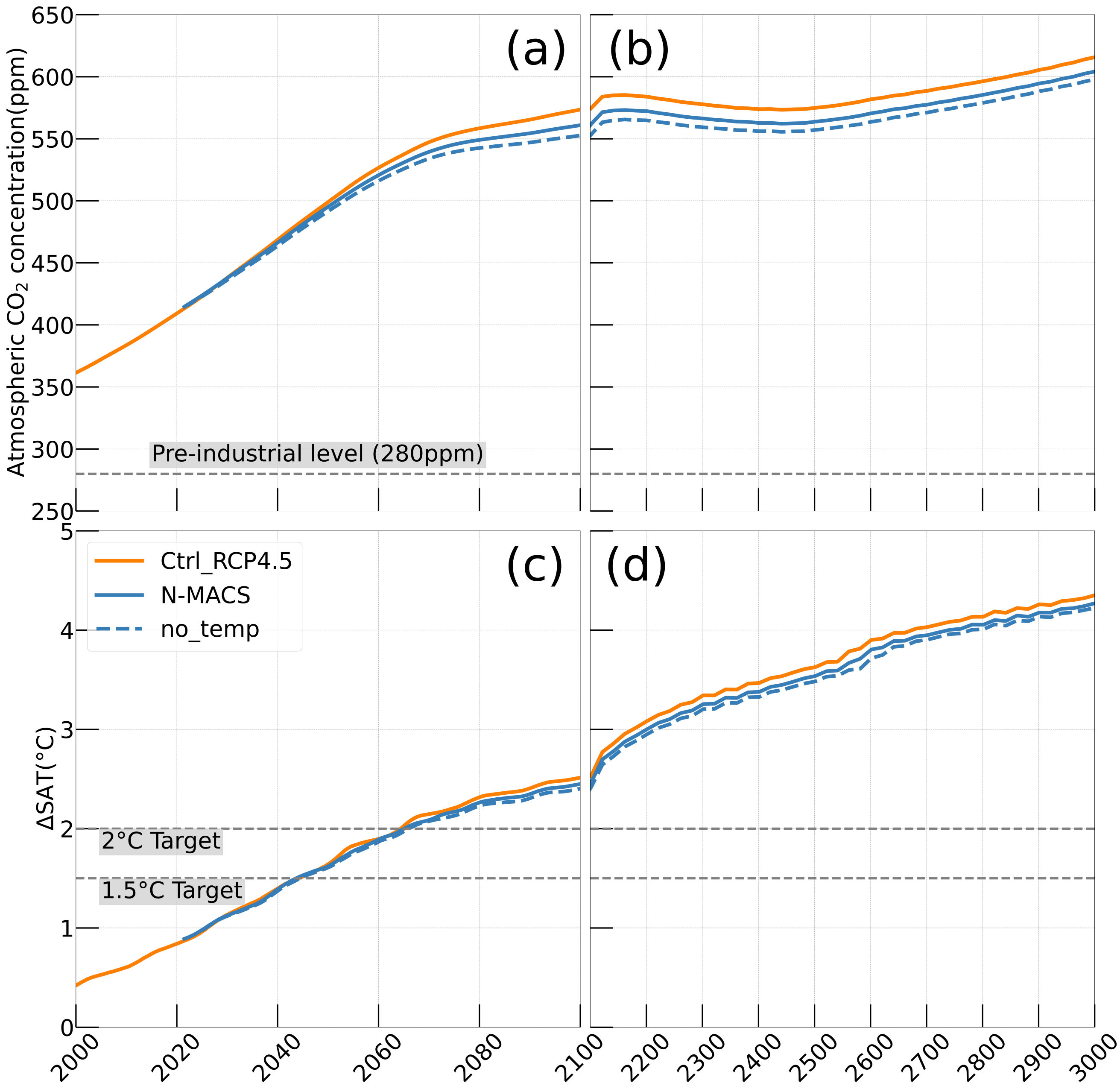

Figure S1. Global temporal evolution of atmospheric CO_2 concentration and surface averaged temperature (SAT)

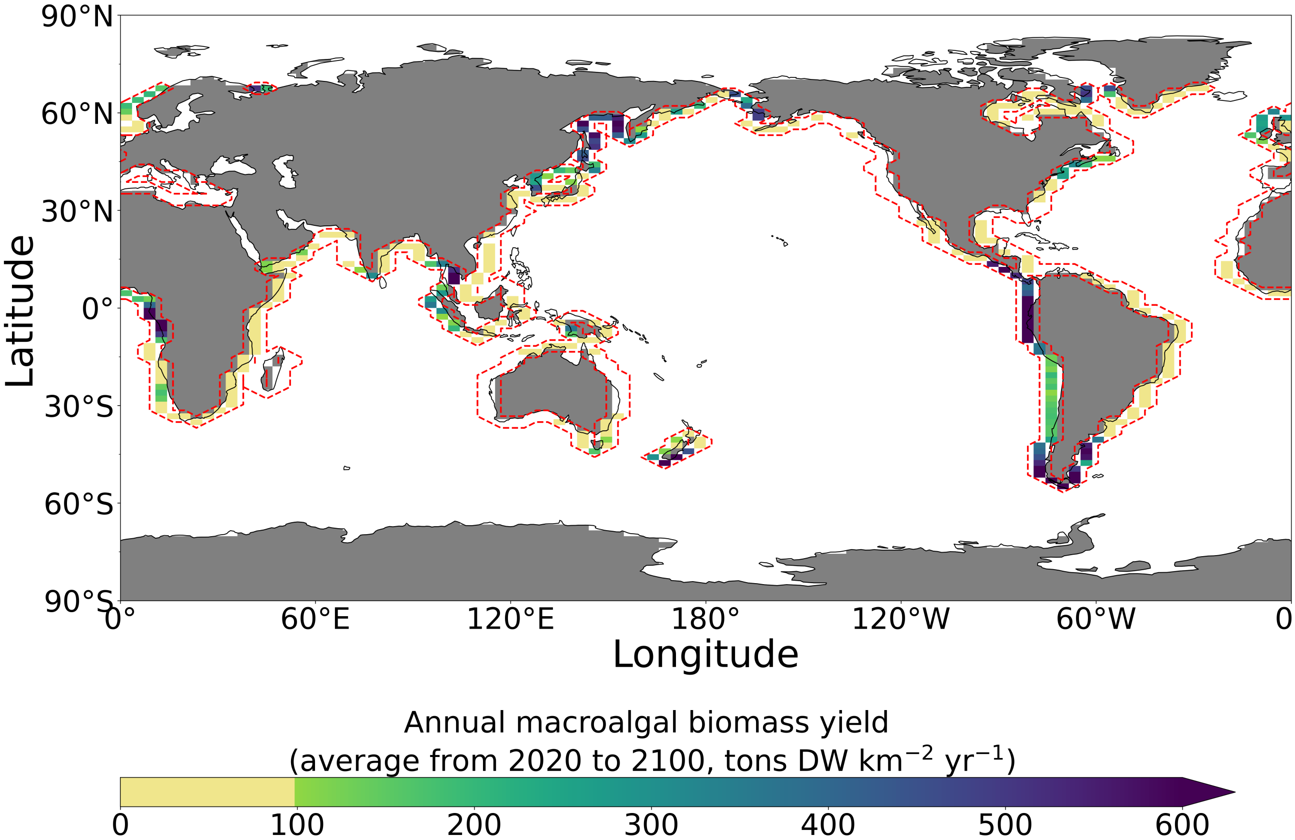

Figure S2. Annual macroalgae biomass yield (averaged from year 2020 to year 2100) of sensitivity simulation without temperature limiting factor. Dashed red lines outline the initial seeding locations in year 2020. Yellowish areas indicate relatively lower yield (≤100 tonnes DW per km^2 per year).

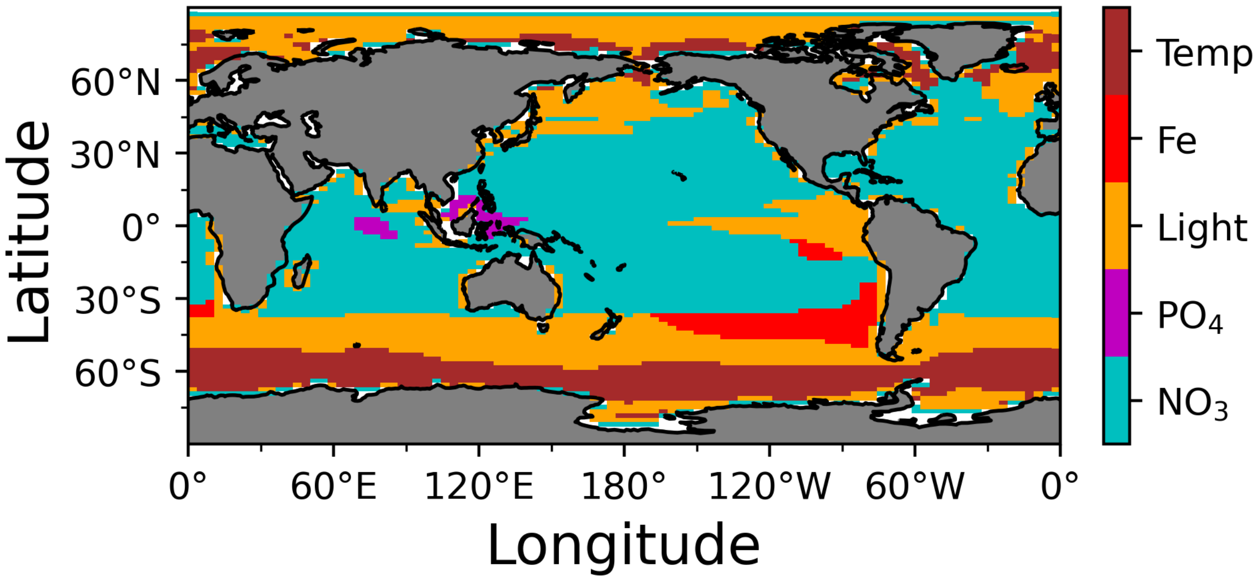

Figure S3. The most limiting growth factor for ordinary phytoplankton in N-MACS simulation from 2020 to 2100.

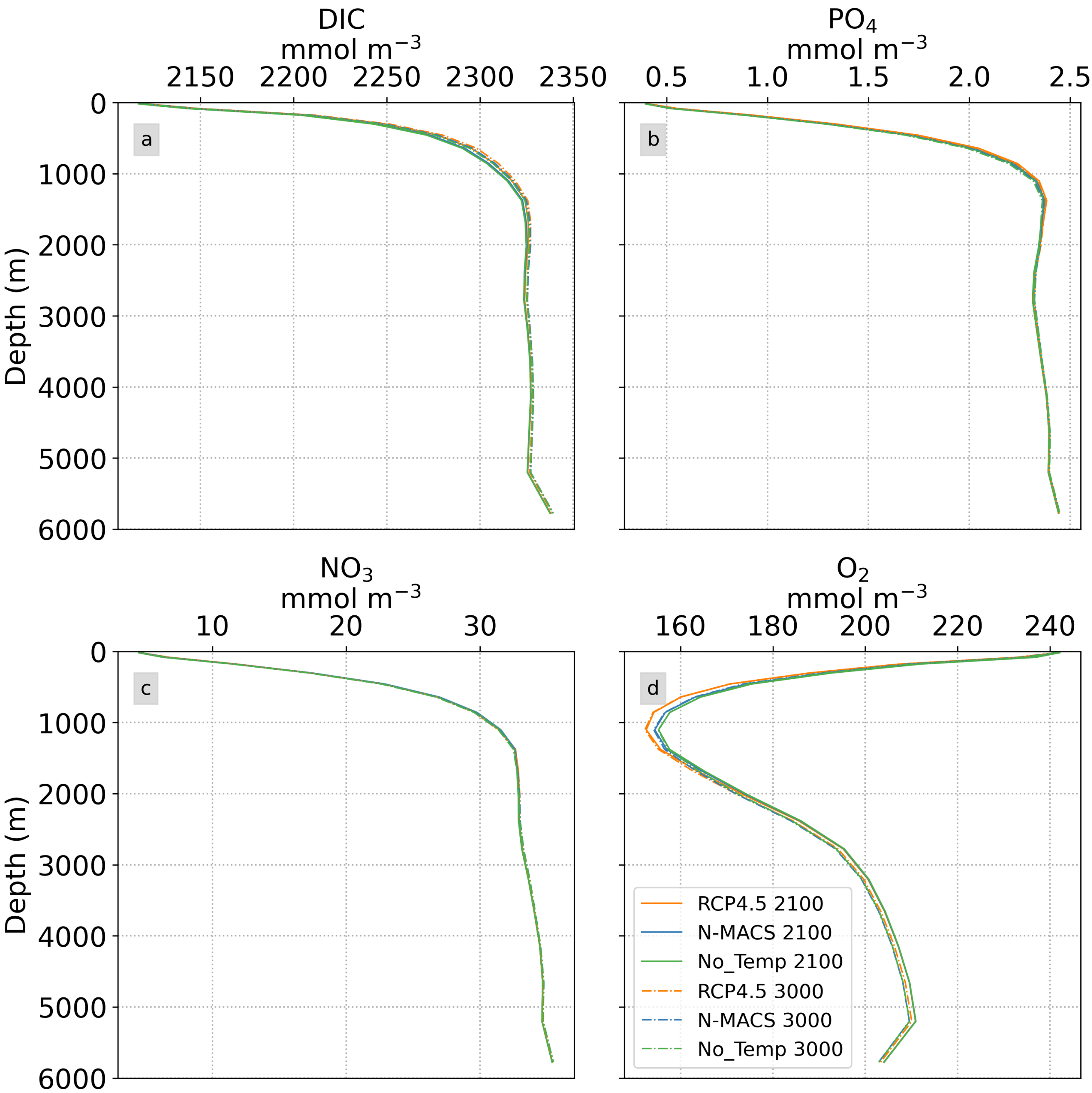

Figure S4. Globally averaged vertical profiles of dissolved inorganic carbon (DIC), dissolved phosphate (PO_4), dissolved nitrate (NO_3), and dissolved oxygen (O_2).

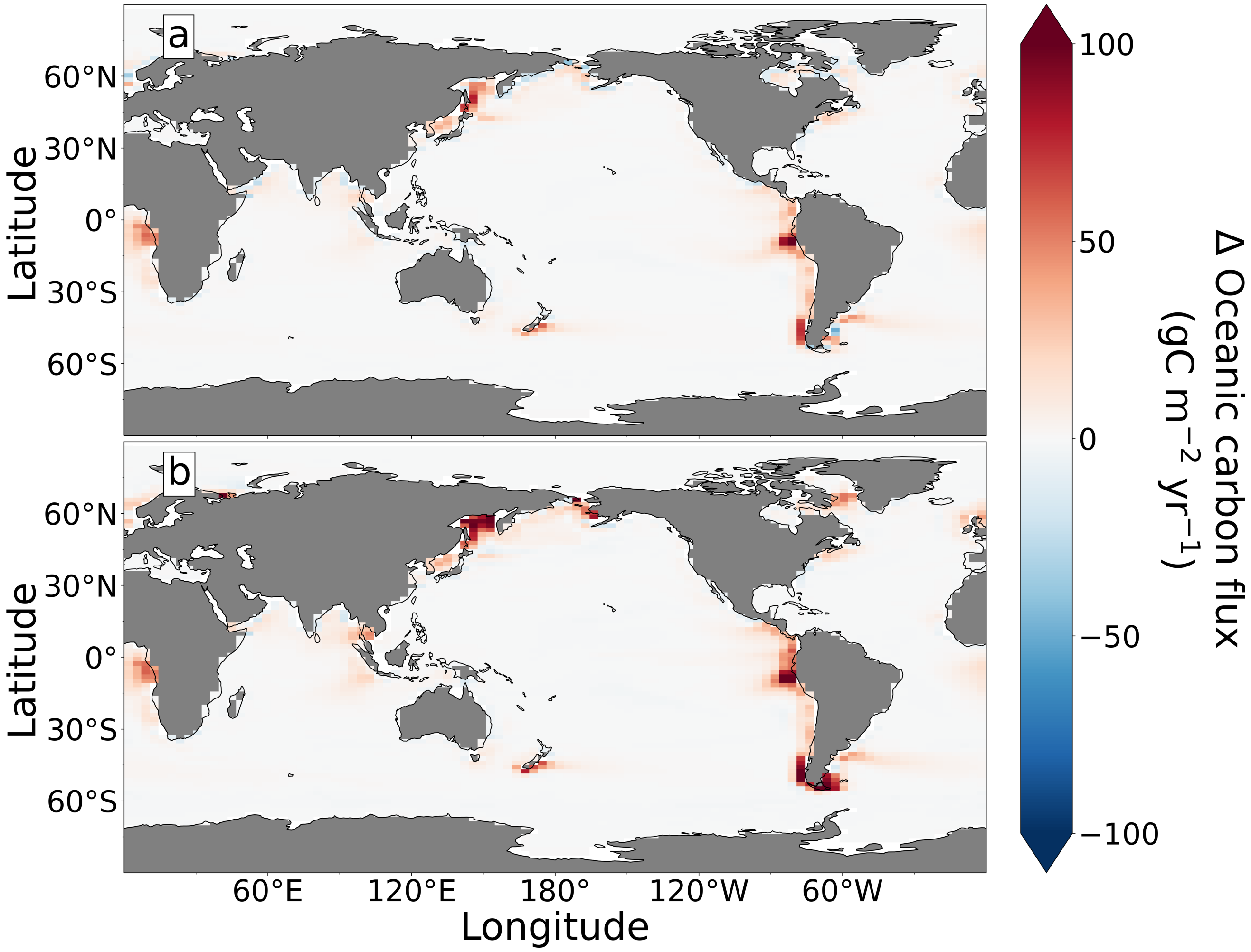

Figure S5. Yearly averaged variations in global oceanic carbon flux between 2020 and 2100, comparing (a) N-MACS and (b) No_Temp relative to RCP4.5 scenario. Positive values indicate net oceanic carbon uptake from the atmosphere.

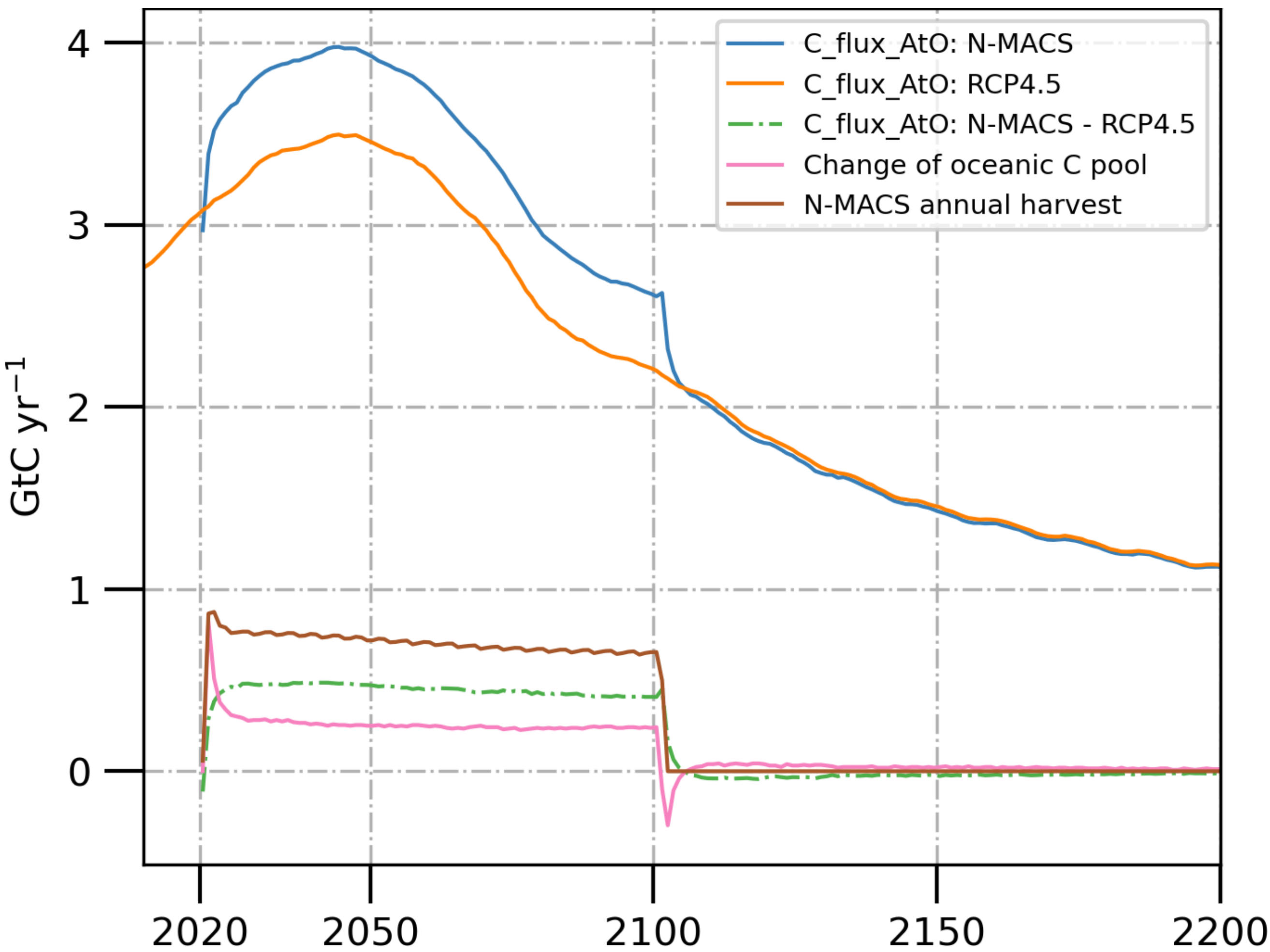

Figure S6. Global profile of air-sea carbon fluxes, N-MACS harvested biomass and oceanic carbon reservoir (GtC yr^{-1}).

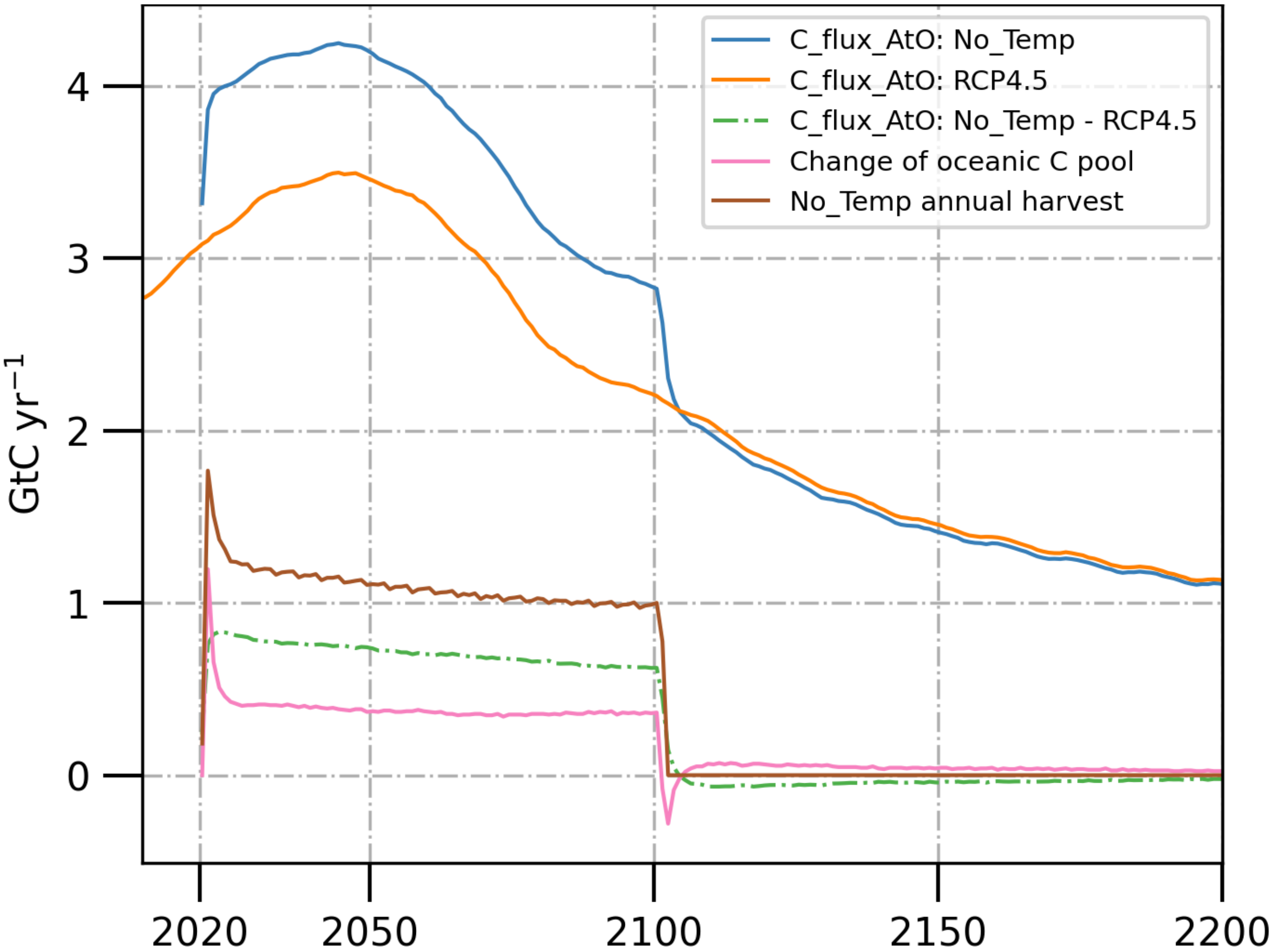

Figure S7. Global profile of air-sea carbon fluxes, No_Temp harvested biomass and oceanic carbon reservoir (GtC yr^{-1}).

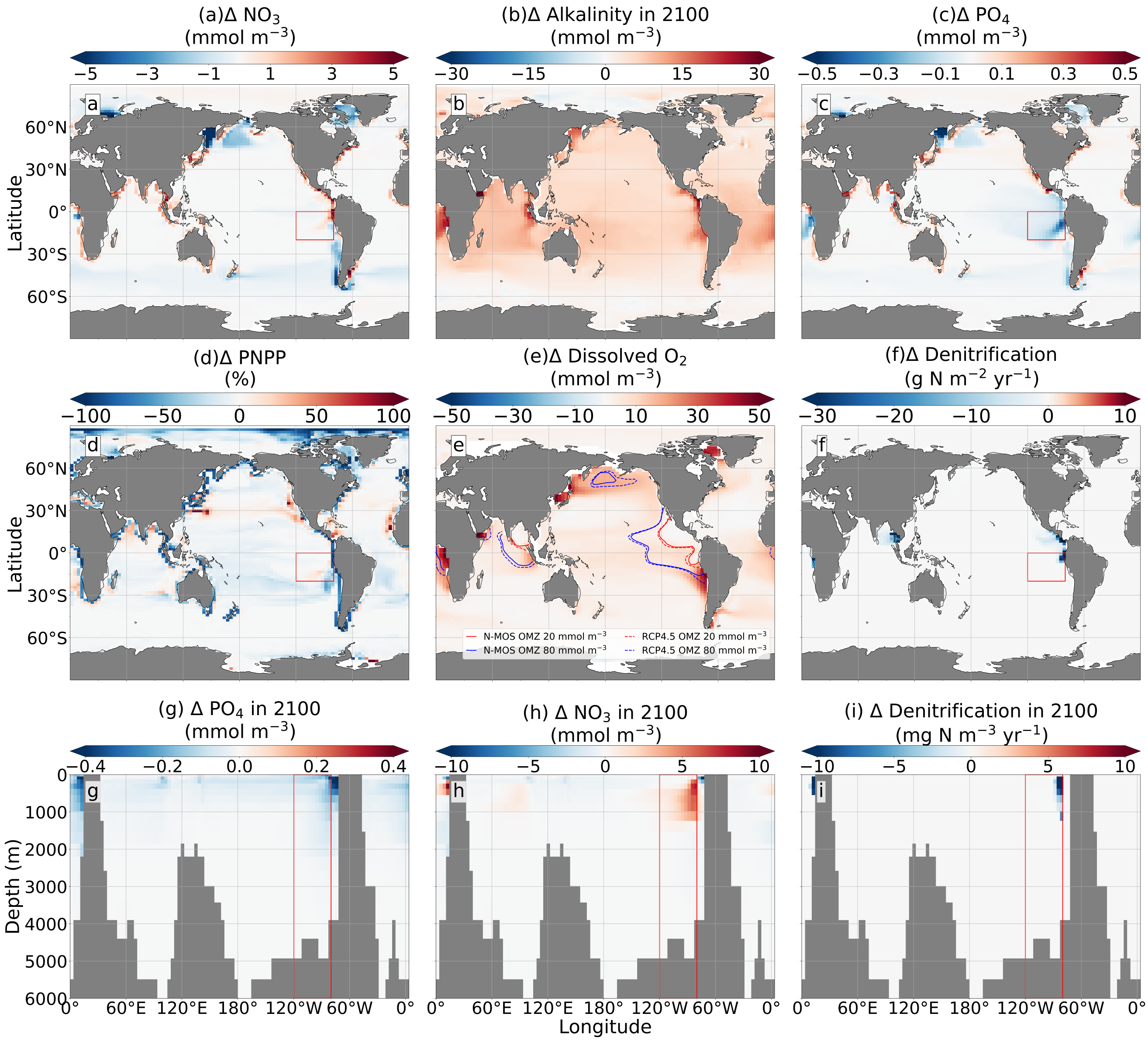

Figure S8. Changes relative to RCP4.5 caused by the deployment of No_Temp (data averaged from year 2020 to 2100, except for **d** which represents data in 2100): **a**: Nitrate distribution in the ocean's surface layer (top 50m); **b**: Alkalinity in the ocean's surface layer; **c**: Phosphate distribution in the surface layer; **d**: Phytoplankton net primary production (PNPP); **e**: Dissolved oxygen concentrations and oxygen minimum zones (OMZs) at a depth of 300m; **f**: Oceanic denitrification rates; Regions within red rectangles (between latitudes 20°S to 0° and longitudes 80°W to 120°W) indicate latitudinal averaged data relative to the Ctrl_RCP4.5: **g**: Phosphate concentrations, **h**: Nitrate concentrations, **i**: Annual denitrification rates.

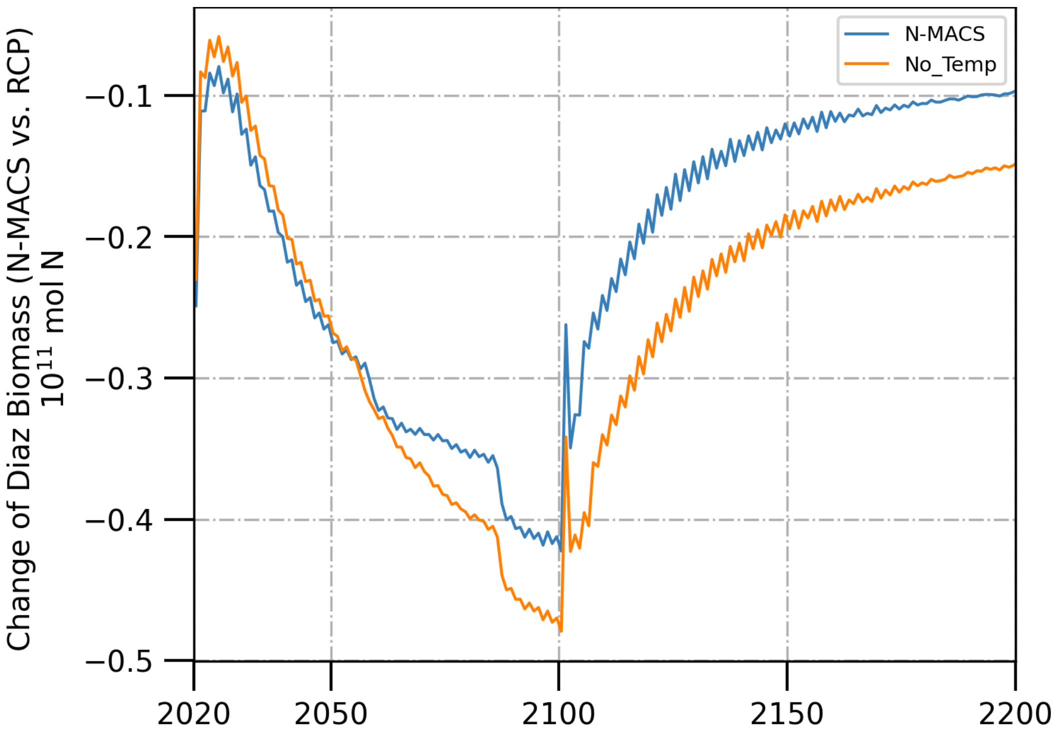

Figure S9. Globally integrated diazotroph biomass of N-MACS (bluish line) and No_Temp (greenish line) relative to RCP4.5.

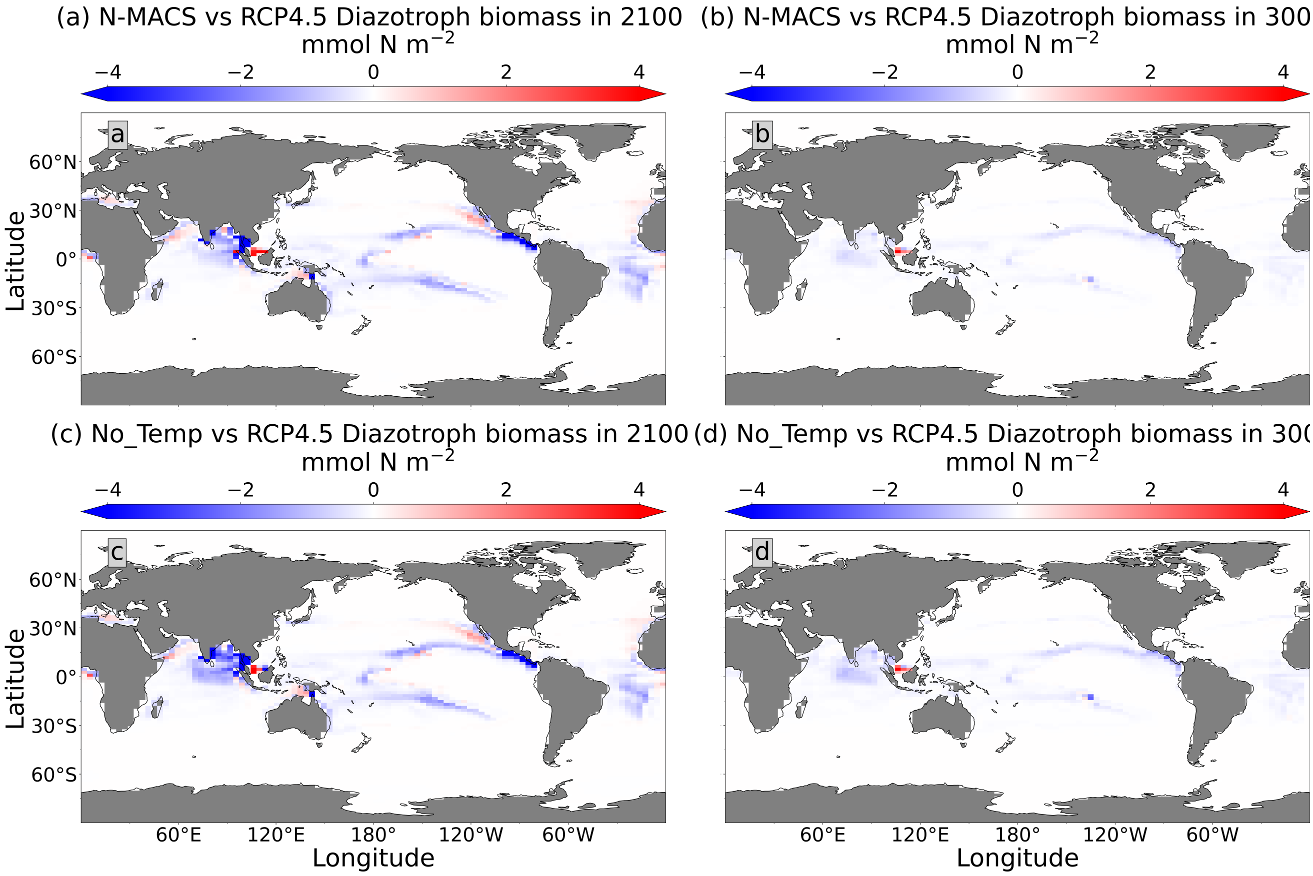

Figure S10. Variation in global vertically integrated diazotrophs biomass (mmol N m^{-2}): N-MACS vs. RCP4.5 at year 2100 (**a**) and 2200 (**b**); No_Temp vs. RCP4.5 at year 2100 (**c**) and 2200 (**d**).

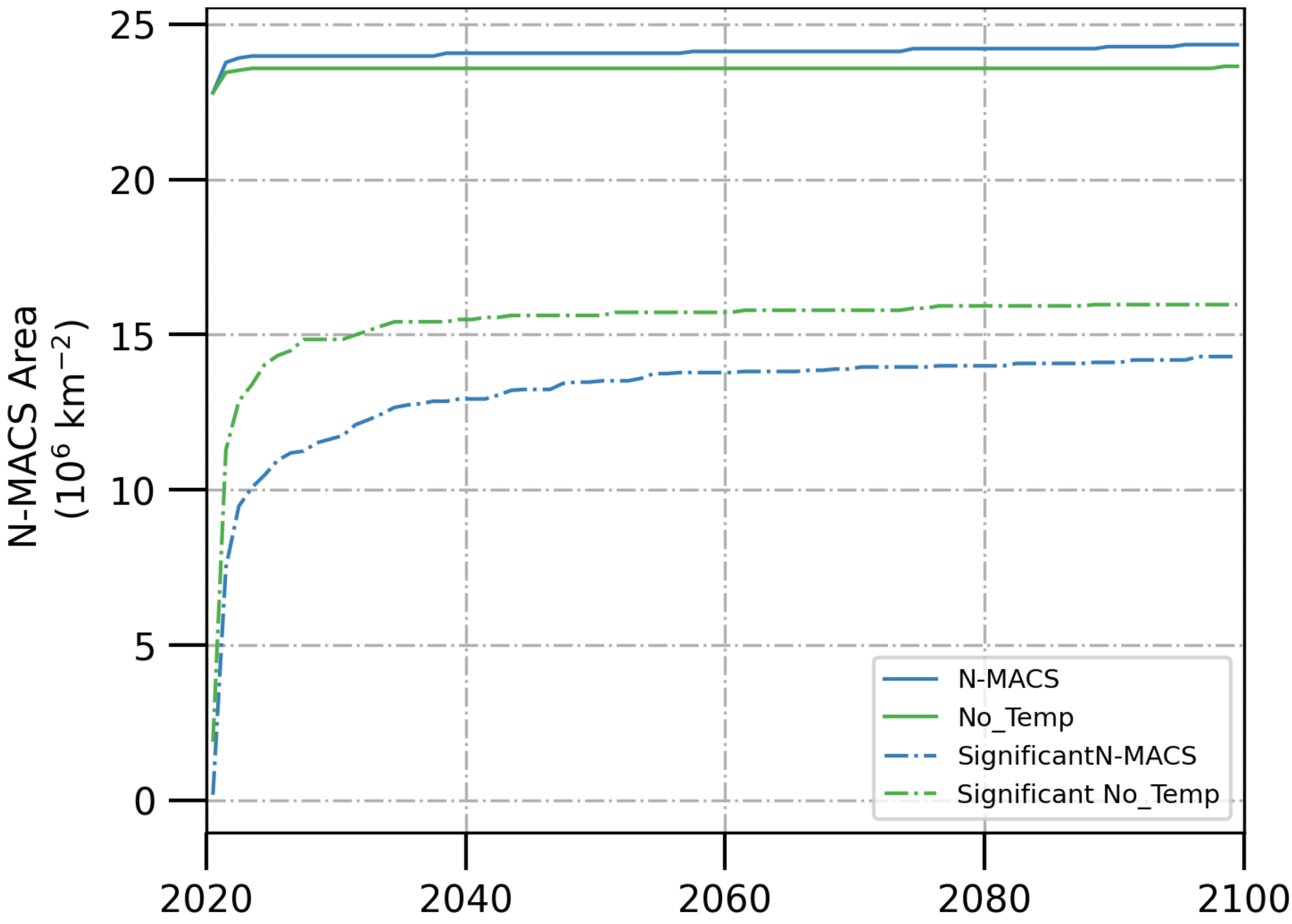

Figure S11. The globally assumed total occupied areas (solid lines) and significant production areas (dashed lines) areas of N-MACS (green tones) and No_Temp (blue tones) simulations.

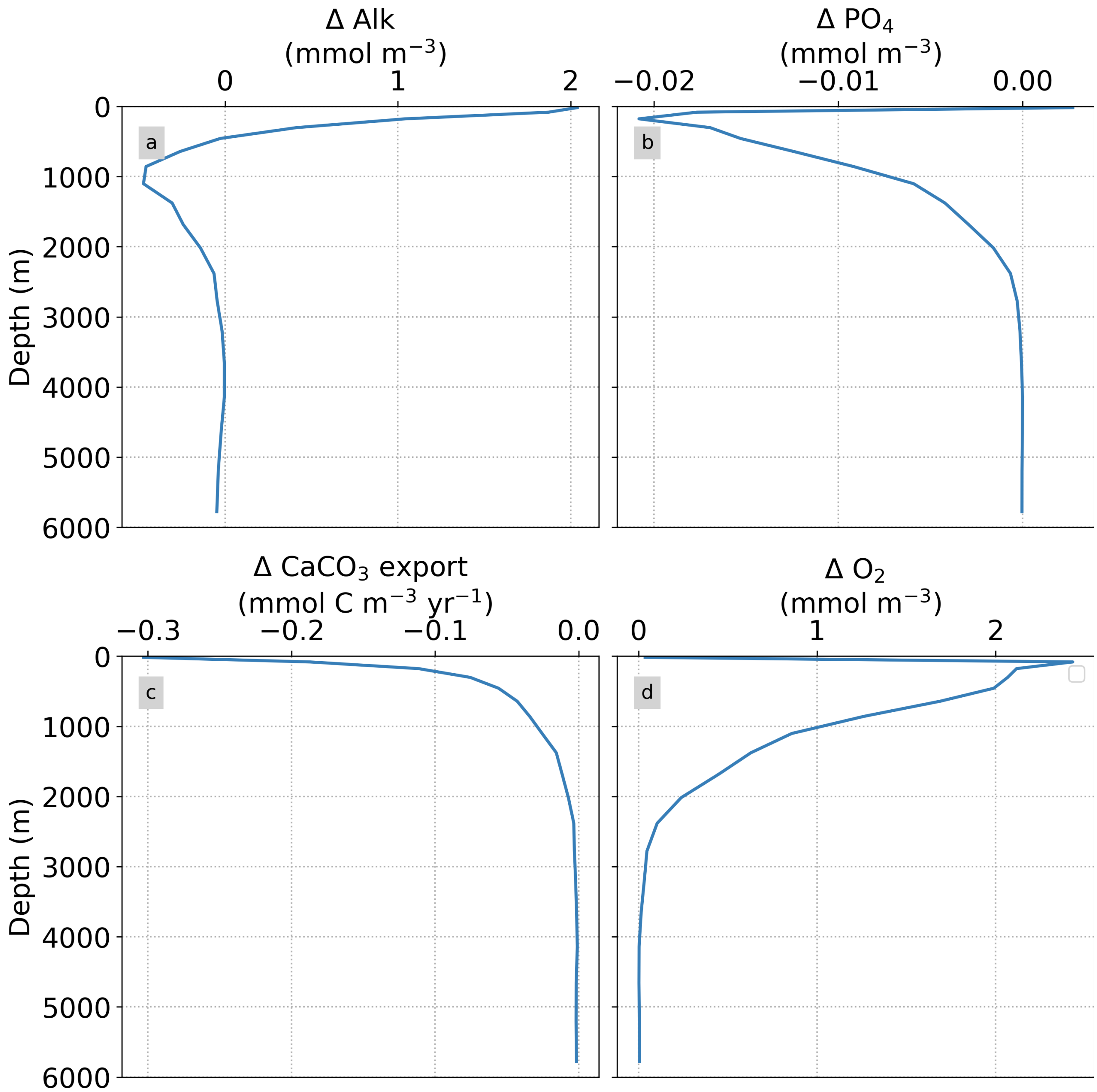

Figure S12. Vertical profiles comparing global horizontal averages of (a) alkalinity, (b) phosphate, (c) carbonate export, and (d) dissolved oxygen between N-MACS and RCP4.5 in 2100.